# THE RELATIONSHIP BETWEEN HIF-1α AND AUTOPHAGY ACTIVITY IN THE HYPOXIC ENVIRONMENT OF BREAST CANCER

by
JUSTIN MILLS

*Thesis presented in fulfilment of the requirements for the degree of Master of Science in the Faculty of Science at Stellenbosch University*

Supervisors: Prof. Anna-Mart Engelbrecht & Dr. Benjamin Loos

March 2013

# DECLARATION

By submitting this thesis/dissertation electronically, I declare that the entirety of the work contained therein is my own, original work, that I am the sole author thereof (save to the extent explicitly otherwise state), that reproduction and publication thereof by Stellenbosch University will not infringe any third party rights and that I have not previously its entirety or in part submitted it for obtaining any qualification.

Date: March, 2013

# ABSTRACT


## Introduction:

Among the cancers that afflict females world-wide, neoplastic disease of breast tissue is the most frequently diagnosed form and the leading cause of cancer-related death. Conventional treatment entails the use of doxorubicin, an anticancer agent belonging to the anthracycline family of chemotherapeutic drugs. Cancer cells are becoming increasingly resistant to doxorubicin therapy. The existence of hypoxic zones, which is a common feature of solid tumours, has been shown to promote the selection of therapy resistant clones in proliferating cancer cells. By modifying cellular homeostasis, neoplastic cells are capable of tolerating the hypoxic insult and thriving within the hostile microenvironment of the tumour. This adaptation is known as 'the hypoxic response' and is mediated through the action of the transcriptional regulator, HIF-1. Its expression in cancer tissue has been associated with a dismal prognosis as it promotes the degree of malignancy to an advanced stage.

## Hypothesis & Aims:

We hypothesized that the targeting of HIF-1α would circumvent the 'protective' hypoxic response conferred upon breast cancer and improve the cytotoxicity of doxorubicin treatment. In this study, the first aim was to identify the hypoxic conditions at which the MCF-7 breast cancer cell line manifests a doxorubicin-resistant phenotype. This was followed by examination of the molecular pathways contributing to the hypoxic resistance by elucidating the potential relationship with the hypoxic regulator HIF-1α. Once the involvement of HIF-1α was established, the next aim was to evaluate whether the attenuation of HIF-1α would terminate the resistant phenotype and sensitize the neoplastic MCF-7 cells to doxorubicin treatment. Finally, the reproducibility of the *in vitro* experiment and efficacy of treatments within an animal model was evaluated.

2-Methoxyestradiol is a naturally occurring metabolite originating from 17β-estradiol. It has recently been exploited as an anticancer agent due to its anti-proliferative and anti-angiogenic properties. Among its various mechanisms of action, this compound has been shown to inhibit the expression of HIF-1α. It is for this reason that this study employed 2-methoxyestradiol in the adjuvant therapeutic treatment, along with doxorubicin.

**Methods:**

The *in vitro* experimental model employed the use of the breast adenocarcinoma estrogen receptor (ER-positive cell line, MCF-7. These neoplastic cells were propagated under standard culture conditions until reaching ~70-80% confluency, after which treatment commenced. The treatment regime comprised a 12 hour exposure to the doxorubicin (1 µM) chemotherapeutic agent, either alone or in combination with HIF-1α inhibitors, 2-methoxyestradiol (10 µM) or siRNA duplex (400 nM), with parallel incubations under normoxic (21%) and hypoxic (~0.1%) conditions. To serve as a positive control for HIF-1α expression, cells were treated with $CoCl_2$ (100 µM). Molecular techniques employed included the Caspase-Glo® 3/7 Assay, western blotting, and the bioreductive MTT Assay. Mitochondrial integrity was assessed by live cell imaging/fluorescent microscopy. Cellular viability was monitored at all times. The experiment was then translated into a pre-clinical *in vivo* model where C57BL/6 mice bearing E0771 xenografts (4 week growth) were allocated into the following treatment groups: (1) control (2) doxorubicin (5 $mg.kg^{-1}$), (3) 2-methoxyestradiol (45 $mg.kg^{-1}$), and (4) the combination of the two previously mentioned groups. Body weight and the rate of tumour growth were monitored throughout the experiment.

**Results:**

Treatment with $CoCl_2$ effectively stabilized HIF-1α under normoxic conditions. 2-Methoxyestradiol was capable of attenuating HIF-1α expression under both normoxia and hypoxia as compared with siRNA transfection, which was only effective under normoxia. HIF-1α stabilization was accompanied by an increase in autophagy along with the morphological transformation of mitochondria from an elongated network to shorter disc-like forms. On the other hand, HIF-1α attenuation caused an induction in the expression of the apoptotic markers, cleaved caspase 3 and cleaved PARP, as well as the restoration of the normoxic morphology. The exposure of MCF-7 cells to 1 µM doxorubicin for 12 hours produced a differential effect in the bioreductive MTT assay between normoxic and hypoxic conditions (42.97 ± 3.095% vs. normoxic dox, $p<0.01$), while stimulating the apoptotic and autophagic pathways. Compared to the control, a significant expression of phospho-AMPK became evident at 21% $O_2$, while the levels remained stable at ~0.1% $O_2$ after doxorubicin exposure. Furthermore, chemotherapeutic treatment caused the morphology of the mitochondria to appear dot-like. Although the combination of the two drugs removed the differential effect witnessed in the MTT assay, there was no significant change when compared to doxorubicin. Levels of apoptotic cell death decreased under both oxygen conditions. While HIF-1α and autophagy decreased under normoxia, they remained elevated under hypoxia.

In the *in vivo* component of the study, the administration of doxorubicin and 2-methoxyestradiol, alone or in combination, did not affect the rate of tumour growth or induce systematic toxicity in any of the experimental mice. When drugs were administered separately, a decrease in apoptosis along with a concomitant increase in autophagy and p-AMPK expression became noticeable while neither

treatment had any significant effect on the expression of HIF-1α. Adjuvant administration, however, was capable of attenuating HIF-1α along with autophagy.

## Discussion:

By inducing ($CoCl_2$) and inhibiting (2-methoxyestradiol; siRNA duplex) HIF-1α, it was established that the autophagic pathway in the *in vitro* experimental setting of this study was dependent on the expression of HIF-1α. The bioreductive MTT assay measures the metabolic state of a cell, which is an indirect indication of cellular viability. Based on this, hypoxia was shown to confer survival to neoplastic MCF-7 cells based on the differential effect witnessed after doxorubicin treatment.

Apart from the induction of apoptosis and its associated mitochondrial fragmentation, the chemotherapeutic drug increased the activation of the metabolic sensor, AMPK, which upregulated autophagy during normoxia. While this autophagic process may assist in the killing mechanism, we speculate that the autophagy upregulated under hypoxia may be responsible for the survival effect and is most likely dependent on HIF-1α.

In contrast to eliciting a synergistic cytotoxic effect, the combination of doxorubicin with 2-methoxyestradiol produced an antagonistic effect on cellular viability instead. We propose that under normoxia, the combined treatment may stimulate the MCF-7 neoplastic cells to enter a state of growth arrest, or senescence, since the results indicate that the decrease in HIF-1α-dependent autophagy did not significantly affect cellular viability. Under hypoxia, despite the incorporation of the pharmacological HIF-1α inhibitor (2-methoxyestradiol), the expression levels of HIF-1α remained unaffected. We speculate that this could be the result of a potentiated stabilization of HIF-1α caused by the build-up of ROS and TCA intermediates which may be the outcome of mitochondrial dysfunction inflicted upon adjuvant therapy under hypoxia. Furthermore, it is also likely that the slight mitogenic effect observed within the MTT assay may be caused by the conversion of 2-methoxyestradiol to a chemically-reactive estrogen derivative, possibly by the action of doxorubicin, and the fact that an ER-positive cancer cell line was employed in this study.

With regards to the *in vivo* experimental model, we speculated that the failure of the molecular changes to manipulate the growth of the tumour could have been the result of an ineffective time- and/or dose regime.

## Conclusion:

We therefore reject our hypothesis based on the fact that an antagonistic rather than synergistic effect was witnessed when the tumorigenic MCF-7 cell line was treated with adjuvant therapy. The results warrant the need for extensive testing on the pharmacodynamics of 2-methoxyestradiol, and more informative techniques to compliment the study.

# OPSOMMING


## Inleiding:

Borskanker is die mees algemeen gediagnoseerde kanker asook die hoof oorsaak van kanker-verwante sterftes in vrouens wêreldwyd. Konvensionele behandeling behels die toediening van doxorubicin, ‘n anti-kankermiddel wat aan die antrasiklien-familie van chemoterapeutiese middels behoort. Kankerselle begin egter toenemend weerstandbiedend raak teen doxorubicin behandeling. Daar is al bewys dat die voorkoms van hipoksiese sones, wat ‘n algemene eienskap van soliede tumore is, die seleksie vir weerstandbiedende klone van prolifererende kankerselle, veroorsaak. Neoplastiese selle kan hierdie hipoksiese toestande weerstaan en in hierdie ongunstige mikro-omgewing floreer deur sellulêre homeostase te modifiseer. Hierdie aanpassing staan bekend as die ‘hipoksiese respons’ en word bemiddel deur die aksies van die transkripsiefaktor reguleerder, HIF-1. Die verhoogde uitdrukking van HIF-1 in kankerweefsel word oor die algemeen geassosieer met ‘n swak prognose omdat dit die maligniteit vehoog.

## Hipotese en Doelwitte:

Die hipotese van hierdie studie behels dus die volgende: Deur HIF-1$\alpha$ te inhibeer, sal die ‘beskermende’ hipoksiese respons wat in borskankerselle voorkom omseil kan word en sodoende die sitotoksisiteit van doxorubicin terapie verhoog. Die eerste doelwit van hierdie studie was dus om die hipoksiese kondisies te identifiseer waar MCF-7 selle ‘n doxorubicin-weerstandbiedende fenotipe vertoon. Daarna is die molekulêre paaie wat bydrae tot hierdie hipoksiese weerstand ondersoek asook hul moontlike verwantskap met die hipoksiese reguleerder, HIF-1$\alpha$. Nadat die rol van HIF-1α bevestig is, was die volgende doelwit om te bepaal of die inhibisie van HIF-1α die weerstandbiedende fenotipe sal onderdruk en neoplastiese MCF-7 selle sal sensitiseer vir doxorubicin behandeling. Laastens is die herhaalbaarheid en effektiwiteit van behandeling in die *in vitro* eksperimente ook in ‘n diermodel getoets.

2-Methoxyestradiol is ‘n metaboliet van 17β-estradiol wat natuurlik in die liggaam voorkom. Dit is ook onlangs as ‘n anti-kanker middel geïdentifiseer as gevolg van die anti-verdelende en anti-angiogeniese eienskappe. Een van die eienskappe van 2-methoxyestradiol is dat dit ook die uitdrukking van HIF-1α kan onderdruk. Dit is dan ook vir hierdie rede dat 2-methoxyestradiol in hierdie studie as bykomende terapie saam met doxorubicin gebruik is.

**Metodes:**

Die *in vitro* eksperimentele model behels die gebruik van 'n borsadenokarsinoom, estrogeenreseptor (ER)- positiewe sellyn, MCF-7. Hierdie neoplastiese selle is onder standaard weefselkultuur omstandighede gekweek totdat konfluensie van ~70-80% bereik is, waarna behandeling begin het. Die behandelingsprosedure behels 'n 12 uur blootstelling aan doxorubicin (1 μM) chemoterapeutiese middel alleen of in kombinasie met die HIF-1α inhibitore, 2-methoxyestradiol (10 μM) of siRNA duplex (400 nM) in normoksiese (21% $O_2$) en hipoksiese (~0.1% $O_2$) toestande. Die selle is ook met $CoCl_2$ behandel wat gedien het as 'n positiewe kontrole vir HIF-1α uitdrukking. Molekulêre tegnieke wat tydens hierdie studie gebruik is, sluit die "Caspase-Glo® 3/7" bepaling in, asook die westelike kladtegniek en die MTT bepaling. Mitochondriale integriteit is bepaal deur middel van lewende sel afbeeldings/fluoresensie mikroskopie. Sellewensvatbaarheid is ten alle tye gemonitor. Hierdie eksperment is verder ook in 'n pre-kliniese *in vivo* model uitgevoer waar C57BL/6 muise met E0771 xenografte (4 weke groei) geïnduseer is en in die volgende behandelingsgroepe verdeel is: (1) kontrole; (2) doxorubicin (5 $mg.kg^{-1}$); (3) 2-methoxyestradiol (45 $mg.kg^{-1}$); en (4) die kombinasie van laasgenoemde twee groepe. Die liggaamsgewig en die tempo van tumorgroei is tydens die hele eksperiment gemonitor.

**Resultate:**

$CoCl_2$ behandeling het HIF-1α effektief gestabiliseer tydens normoksiese omstandighede. 2-Methoxyestradiol het HIF-1α uitdrukking tydens normoksiese en hipoksiese toestande onderdruk wanneer dit vergelyk is met siRNA transfeksie wat slegs tydens normoksiese toestande effektief was. HIF-1α stabilisering het gepaardgegaan met 'n toename in autofagie asook morfologiese veranderinge in die mitochondria vanaf 'n verlengde netwerk tot korter skyfagtige vorme. Aan die ander kant het HIF-1α onderdrukking 'n toename in die apoptotiese merkers, nl kliewing in caspase-3 and PARP veroorsaak wat gepaard gegaan het met die herstel van die tubulêre mitochondriale netwerk. Die blootstelling van die MCF-7 selle aan 1 μM doxorubicin vir 12 ure het 'n differensiële effek in die bioreduktiewe MTT bepaling tot gevolg gehad tussen normoksiese en hipoksiese toestande (42.97 ± 3.095%, $p<0.1$), terwyl die apoptotiese- en autofagiese paaie in beide toestande gestimuleer is. 'n Insiggewende toename in fosfo-AMPK uitdrukking was sigbaar tydens normoksiese toestande van 21% $O_2$, terwyl dit onveranderd gebly het tydens hipoksiese toestande van 0.1% ~$O_2$ na doxorubicin behandeling. Die morfologie van die mitochondria het 'n 'kollerige' voorkoms tydens doxorubicin behandeling gehad. Alhoewel die behandeling van die selle met beide middels gelyktydig, die differensiële effek soos weerspieël in die MTT bepaling ophef, is daar geen insiggewende verandering wanneer met doxorubicin behandeling vergelyk word nie. Apoptotiese seldood verminder met gelyktydige behandeling van biede middels tydens normoksiese en hipoksiese toestande. HIF1-α en autofagie het afgeneem tydens normoksiese toestande, maar bly vehoog tydens hipoksie.

In die *in vivo* model, het die toediening van doxorubicin en 2-methoxyestradiol alleen en in kombinasie nie tumorgroei geaffekteer nie en ook nie sistemiese toksisiteit in enige van die eksperimentele muise tot gevolg gehad nie. Die afsonderlike toediening van die middels het ‘n afname in apoptose in ‘n toename in autofagie en p-AMPK uitdrukking tot gevolg gehad, terwyl afsonderlike toediening van die middels nie ‘n effek op HIF-1$\alpha$ uitdrukking gehad het nie. Die gelyktydige toediening van biede middels het egter ‘n onderdrukking van HIF1-$\alpha$ teweeggebring.

## **Bespreking**:

Deur HIF-1$\alpha$ te induseer ($CoCl_2$) en te inhibeer (2-methoxyestradiol en siRNA) in hierdie *in vitro* eksperimentele omstandighede, bevestig hierdie resultate dat autofagie afhanklik is van die uitdrukking van HIF-1$\alpha$. Die bioreduktiewe MTT bepaling meet die metaboliese staat van die sel wat indirek sellewensvatbaarheid bepaal. Gebasseer op hierdie bepaling is bewys dat hipoksie ‘n weerstandbiedende fenotipe veroorsaak teen doxorubicin behandeling in neoplastiese MCF-7 selle.

Doxorubicin veroorsaak ‘n toename in apoptose met geassosieerde mitochondriale fragmentering asook ‘n aktivering van die metaboliese sensor, AMPK, wat autofagie stimuleer in normoksiese omstandighede. Alhoewel ‘n toename in autofagie seldood kan stimuleer, spekuleer ons dat ‘n toename in autofagie tydens hipoksie verantwoordelik kan wees vir seloorlewing wat heel moontlik ook afhanklik van HIF-1$\alpha$ is.

In kontras met die verwagting dat die kombinasie behandeling ‘n sinergistiese sitotoksiese effek sou teweegbring, dui ons resultate dat daar ‘n antagonistiese effek op sellewensvatbaarheid was. Ons stel voor dat die gekombineerde behandeling tydens normoksiese toestande MCF-7 neoplastiese selle stimuleer om in ‘n toestand van groeistaking in te gaan aangesien die resultate daarop dui dat ‘n afname in HIF-1$\alpha$ afhanklike autofagie nie sellulêre lewensvatbaarheid beïnvloed het nie. Tydens hipoksie, ten spyte van die bykomdende behandeling met die HIF-1$\alpha$ inhibitor (2-methoxyestradiol), het die vlakke van HIF-1$\alpha$ onveranderd gebly. Ons spekuleer dat dat dit die gevolg kan wees van die stabilisering van HIF-1$\alpha$ as gevolg van ‘n toename in ROS en TCA intermediate wat die gevolg van mitochondriale wanfunksie kan wees tydens bykomende terapie onder hipoksiese toestande. Dit is ook moontlik dat die mitogeniese effek wat waargeneem is met die MTT bepaling die gevolg kan wees van die omsetting van 2-methoxyestradiol na ‘n chemiese-reaktiewe estrogeen derivaat; moontlik as gevolg van die aksie van doxorubicin en die feit dat die sellyn wat in hierdie studie gebruik is, ‘n ER-positiewe kankersellyn is.

Met verwysing na die *in vivo* eksperimentele model, spekuleer ons dat die molekulêre veranderinge wat nie in die tumorgroei weerspieël word nie, die resultaat van oneffektiewe tyds- en dosis behandelingswyses is, of foutiewe toediening van die middel kan wees.

**Gevolgtrekking:**

Ons verwerp dus ons hipotese gebaseer op die feit dat bykomende (adjuvante) behandeling eerder ‘n antogonistiese effek as ‘n sinergistiese effek op seldood in MCF-7 selle het. Hierdie resultate regverdig die nodigheid van intensiewe toetsing op die farmakodinamika van 2-methoxyestradiol asook die gebruik van meer informatiewe tegnieke om hierdie studie te komplimenteer.

# ACKNOWLEDGEMENTS

I would like to extend my sincerest gratitude to the following persons:

My guardians, Brian, Melanie, Lauren, Louise, Skyla, and Victor, for their love and light in times of darkness, and providing the strength, heart and faith that allowed me to persevere through the chaos of the past two years.

My supervisors, Prof. Anna-Mart Engelbrecht & Dr. Benjamin Loos, for considering my application and giving me the opportunity to expand my intellectual capacity by providing me with a stimulating, yet challenging research project. Furthermore, I am immensely grateful for their exceptional insight and wisdom, the constructive feedback I received, and the countless hours they devoted to assist me with the structure my thesis.

Gina Leisching, for her passionate and confident approach to the field which inspired me to become a stronger academic, and for her constant guidance and patience throughout the study that enabled me to grasp difficult concepts and regard her not only as a dedicated mentor, but as a dear friend.

Dr. Balindwe Sishi, for her sophisticated, yet sincere character and good-humoured nature which provided a pleasant escape, and for her persistent encouragement that kept me grounded and motivated.

Lize Engelbrecht, Danzil Joseph, Kathleen Reyskens, and Rudo Mapanga, for their contributions, both academic and non-academic, all of which made the journey more manageable and enjoyable.

Theodore Gray & Jacob Kirchner, for their emotional availability, reliability and great efforts in making me feel as comfortable and liberated as possible, allowing me to gain ground amongst all the mayhem.

Lydia Lacerda, for the pain-staking effort of editing my thesis in the most meticulous and concise manner.

CANSA and Marie Stander for providing the financial support that allowed me to devote myself to this study.

# LIST OF TABLES

## CHAPTER 2



## CHAPTER 3

# LIST OF FIGURES

## CHAPTER 1



## CHAPTER 2



## CHAPTER 3

# LIST OF ABBREVIATIONS

| | |
|---|---|
| **%** | Percentage |
| **°C** | degree Celsius |
| **µL** | Microliter |
| **µM** | Micromolar |
| **µm** | Micrometer |
| **A** | Ampere |
| **AU** | arbitrary units |
| **cm** | Centimetre |
| **g** | Gram |
| **Hg** | Mercury |
| **kDa** | kiloDalton |
| **kg** | Kilogram |
| **M** | Molar |
| **mA** | Milliampere |
| **mg** | Milligram |
| **mL** | Millilitre |
| **mM** | Millimolar |
| **mm** | Millimetre |
| **nM** | Nanomolar |
| **nm** | Nanometer |
| **nm** | Nanometer |
| **rpm** | revolutions per minute |
| **V** | Voltage |

| | |
|---|---|
| **MTT** | [3-(4,5-dimethylthiazol-2-yl)-2,5-diphenyltetrazolium bromide] |
| **2-ME** | 2-Methoxyestradiol |
| **ADP** | Adenosine Diphosphate |
| **AMP** | Adenosine Monophosphate |
| **ATP** | Adenosine Triphosphate |
| **APS** | Ammonium Persulfate |
| **AMPK** | AMP-activated protein kinase |
| **AIF** | Apoptosis-Inducing Factor |
| **Apaf-1** | Apoptotic Protease-Activating Factor-1 |

| | |
|---|---|
| **ARNT** | Aryl Hydrocarbon Receptor Nuclear Translocator |
| **bHLH** | basic Helix-Loop-Helix |
| **BH** | Bcl2-Homology |
| **BSA** | Bovine Serum Albumin |
| **CMC** | Carboxymethylcellulose |
| **JNK** | c-Jun N-terminal Kinase |
| **$CoCl_2$** | Cobalt Chloride |
| **$IC_{50}$** | Concentration inducing half-maximal response |
| **CBP** | Creb-Binding Protein |
| **DD** | Death Domain |
| **DED** | Death Effector Domain |
| **DISC** | Death-Inducing Signalling Complex |
| **DNA** | Deoxyribonucleic Acid |
| **DMSO** | Dimethyl Sulfoxide |
| **DIABLO** | Direct IAP Binding Protein with Low pI |
| **DMEM** | Dulbecco's Modification of Eagle's medium |
| **DRP** | Dynamin-Related Protein |
| **ETC** | Electron Transport Chain |
| **ERt** | Endoplasmic Reticulum |
| **ER** | Estrogen Receptor |
| **EDTA** | Ethyelene-Diamine-Tetracetic Acid |
| **FIH** | Factor Inhibiting HIF-1 |
| **FBS** | Fetal Bovine Serum |
| **GLUT** | Glucose Transporter |
| **GFP** | Green Fluorescent Protein |
| **HDI** | Human Development Index |
| **HER2** | Human Epidermal Growth Factor-2 |
| **HCL** | Hydrochloric Acid |
| **HRE** | Hypoxia Response Element |
| **HIF** | Hypoxia-Inducible Factor |
| **LDH-5** | Lactate Dehydrogenase-5 |
| **LC3** | Light Chain 3 |
| **mTOR** | mammalian Target of Rapamycin |
| **MMP-2** | Matrix Metalloprotease 2 |
| **MCF-7** | Michigan Cancer Foundation-7 |
| **MMR** | Mismatch Repair System |

| | |
|---|---|
| **MOMP** | Mitochondrial Outer Membrane Permeabilization |
| **Mfn** | Mitofusion |
| **MAPK** | Mitogen-Activated Protein Kinase |
| **MCT-4** | Monocarboxylate co-transporter-4 |
| **MEF** | Mouse Embryonic Fibroblast |
| **MDR** | Multi-Drug Resistance |
| **TEMED** | N,N,N',N'-Tetramethylethylenediamine |
| **NADH** | Nicotinamide Adenine Dinucleotide |
| **OPA** | Optic Atrophy |
| **ODDD** | Oxygen-Dependant Degradation Domain |
| **$PO_2$** | Partial pressure of oxygen |
| **PAS** | PER-ARNT-SIM |
| **PMSF** | Phenylmethylsulfonyl Fluoride |
| **PTEN** | Phosphatase and Tensin Homolog |
| **PI3K** | Phosphatidylinositol 3-Kinase |
| **PS** | Phosphatidylserine |
| **PAGE** | Polyacrylmide Gel Electrophoresis |
| **PARP** | Poly-ADP-Ribose-Polymerase |
| **PVDF** | Polyvinylidene Fluoride |
| **PHD** | Prolyl Hydroxylases |
| **PDK1** | Pyruvate Dehydrogenase 1 |
| **ROS** | Reactive Oxygen Species |
| **RNA** | Ribonucleic Acid |
| **SERM** | Selective Estrogen Receptor Modulator |
| **siRNA** | small interfering RNA |
| **SDS** | Sodium Dodecyl Sulfate |
| **SDS-PAGE** | Sodium Dodecyl Sulphate Polyacrylamide Gel Electrophoresis |
| **SEM** | Standard Error of Mean |
| **TMRE** | Tetramethylrhodamine Ethyl Ester |
| **TCA** | Tricarboxylic Acid |
| **TSC** | Tubersclerosis Complex |
| **UV** | UltraViolet |
| **ULK1** | UNC 51-like Kinase |
| **VEGF** | Vascular Endothelial Growth Factor |
| **VEGF** | Vascular Endothelial Growth Factor |
| **pVHL** | Von Hippel Lindau protein |

# TABLE OF CONTENTS

# CHAPTER 1: LITERATURE REVIEW

## 1.1 BREAST CANCER

### 1.1.1 Incidence

According to the Globocan population-based registry of 2008, neoplastic disease of the breast is the most frequently diagnosed form (22.9%) and principal cause of death (13.7%) among all cancers in women (Globocan, 2010). Based on this registry, the mortality rate of women in South Africa was predicted to increase by 56.9% in the year 2030. The Human Development Index (HDI) is a calculation that ranks countries into 'high', 'medium' and 'low' human development based on the quality of life (Morse, 2003). From trends seen in the incidence rate of breast cancer world-wide, it was predicted that 'low' and 'medium' HDI regions are bound to follow the incidence patterns of the 'high' HDI regions where the rates in breast cancer are elevated (Cancer Research UK, 2012). This is primarily due to 'westernized' risk factors such as lifestyle (diet, alcohol consumption and lack of exercise) and hormonal therapy. Among the etiological risk factors, a strong positive correlation exists between the threat of breast cancer development and age, familial history, and genetic mutations.

Breast cancer, in terms of incidence and mortality, is considered to increase with age (Surveillance Research, 2012). The lifetime risk in the USA is larger in the age groups 40-59 years (1 in every 27 women) and 60-69 years (1 in every 28 women), than related to the generation younger than 39 years (1 in every 203 women). The chances of developing breast cancer are amplified if a patient has a family history of the disease, rising with the diagnosis of one-degree relatives (Washbrook, 2006). Inheritance of mutations in the susceptibility genes predisposes a patient to the disease. For example, individuals possessing genetic mutations in the breast cancer genes, BRCA1 and BRCA2, are 40-80% more likely to develop breast cancer (Wang *et al.*, 2012).

The clinical detectable forms of a breast neoplasm are heterogeneous, each with a distinct profile (Oakman *et al.*, 2011). Despite the use of mammography screening for earlier detection, and multimodality treatment (chemotherapy, radiotherapy, and surgical resection) for management, the mortality rate is increasing and highlights the requirement for novel therapeutic approaches.

### 1.1.2 Chemotherapeutic Treatment

The abrogation of neoplastic cells without affecting normal non-transformed cells is the primary goal of chemotherapy. Cancerous breast tissue that possesses estrogen receptors is generally responsive to the steroid hormone estrogen (Wang *et al*., 2011). To counteract the potential stimulation of cancerous cell growth and hyperplasia by this ligand, hormonal therapy is beneficial for control. The selective estrogen receptor modulator (SERM) termed Tamoxifen has frequently been prescribed as part of adjuvant therapy to treat breast cancer patients that are positive for estrogen receptors (Yamamoto *et al*., 2001). This hormone antagonist blocks the action of estrogen by inducing the

formation of a co-repressor complex, and thus preventing transcriptional activation of target genes. The use of Tamoxifen, however, is frequently limited due to metastatic relapse with the development of endometrial carcinoma (Singh *et al*., 2007). An alternative antineoplastic drug that is used conventionally to treat a broad spectrum of cancers including soft tissues sarcomas, breast cancers, haematological cancers, and neuroblastoma in children is Doxorubicin, also known as Adriamycin® (Sessa *et al.*, 2008; Cheung *et al.*, 2001; Levy *et al.*, 2001; Minotti *et al.*, 2004). Discovered in the 1960s, it originates as a secondary metabolite which is biosynthesized by the soil bacterium *Streptomyces peucetious* variant *caesius*. This compound belongs to a family of chemotherapeutic agents called the anthracyclines which also include Daunorubicin and Epirubicin (Minotti *et al.*, 2004). Doxorubicin is used either as a single treatment agent or, in an attempt to either compliment a mechanism or produce a synergistic effect, in various combinations with other drugs such as cyclophosphamide, vincristine, 5-fluorouracil, and/or mitomycin C (Koo *et al.*, 2007; Hatam *et al.*, 2011; Cheung *et al.*, 2001).

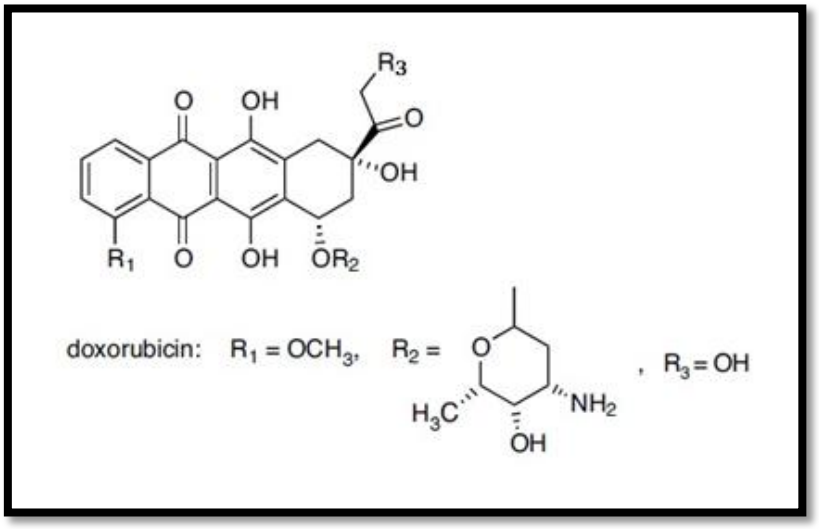


**Figure 1.1 The molecular structure of Doxorubicin.** The antineoplastic antibiotic is composed of an algycone and a sugar moiety. The four-ring quinone structure is shared amongst the anthracyclines and is involved in biotransformation reactions (Airley, 2009a).

### 1.1.3 Pharmacodynamics of Doxorubicin

This anti-tumour antibiotic exerts its cytotoxic effects by several molecular mechanisms:

(1) The anthracycline intercalates between adjacent DNA bases of the double helix chain consequently inhibiting the replication of nucleic acids (Gewirtz, 1999).

(2) The tension generated by the unwinding of the parental double helix during DNA replication and transcription is typically relieved with the aid of Topoisomerase-II. This enzyme makes transient double-stranded cuts which maintain the structure and sequence of the genetic material as its form is changed to remove the supercoils (Minotti *et al.,* 2004). Doxorubicin targets this process

by stabilizing enzyme-DNA intermediates, thus preventing the religation of the strands and forming double-stranded breaks (Airley, 2009a).

(3) The formation of covalent Doxorubicin-DNA adducts which precede the formation of non-covalent DNA interstrand cross links (Cutts *et al.*, 2001; Swift *et al.,* 2006).

(4) The four-ringed quinone structure that is shared among the anthracyclines allows them to accept an electron and become reduced to a free radical, termed semiquinone, which acts as an alkylating agent (Raschi *et al.*, 2010). This unstable intermediate may further react with molecular oxygen to generate other reactive oxygen species including hydroxyl radicals, peroxides, and superoxides, all of which induce oxidative damage within DNA as well as lipid peroxidation of plasma membranes (Gewirtz, 1999).

(5) All these upstream events may culminate in the initiation of a cellular death pathway, termed apoptosis (Swift *et al.*, 2006; Lüpertz *et al.*, 2010).

## 1.2 APOPTOSIS

Apoptosis, or type I cell death, is a self-destructive, energy-consuming process that is genetically regulated by the cell (Maiuri *et al*., 2007; Edinger & Thompson, 2004). In multicellular organisms, under normal physiological conditions, apoptosis is important during embryological development of the central nervous system and immune system, as well as in general tissue remodelling. It maintains homeostasis by controlling the balance between the growth and death rate of cells (Airley, 2009b; Clayton & Hardwick, 2008). Furthermore, it serves as a crucial defence mechanism which can be triggered in response to numerous extracellular or intracellular stimuli to eradicate potentially malignant cells. The importance of apoptosis is evident from the numerous pathological diseases that manifest from a dysfunctional/mutated apoptotic pathway which includes neurodegenerative diseases, viral infections and cancer (Anlar *et al.*, 2003; Lowe & Lin, 2000).

### 1.2.1 Morphological Characterization

Apoptosis (type I cell death) is characterized by distinct morphological changes. The physical process begins with the detachment and shrinkage of the apoptotic-competent cell (Lawen, 2003). This is followed by the nuclear chromatin condensation (pyknosis) and its degeneration into internucleosomal fragments (karyorrhexis) by endonucleases to produce the classic DNA-laddering pattern. Subsequently, permeabilization and blebbing of the plasma membrane gives rise to discrete apoptotic bodies. A membrane phospholipid termed phosphatidylserine (PS), typically contained within the inner plasma membrane, becomes exposed to the outer membrane surface during the morphological transformation (Botto, 2004). The process culminates in the recognition of these apoptotic-competent cells by phagocytes which proceed to engulf the apoptotic bodies in a rapid, yet irreversible manner (Steinbach & Weller, 2006). The externalized PS lipids aid in the recognition of the apoptotic bodies and its subsequent phagocytosis (Hoffmann & Ogden 2001). Clearance occurs without invoking an inflammatory response (Edinger & Thompson, 2004).

### 1.2.2 Molecular Regulation

Central to this mode of programmed cell death are the caspases, a subfamily of cysteine proteases responsible for the degradation of vital components within the cell upon execution (Maiuri *et al.,* 2007). Activation of these catabolic enzymes can occur through either of two pathways, namely the intrinsic or extrinsic pathway and culminate in the demise of the cell.

#### 1.2.2.1 The Extrinsic Pathway

The extrinsic pathway, also known as the death receptor-mediated pathway, is induced by extracellular damage signals leading to the recognition and ligation of a ligand to its corresponding death receptor (e.g. FasL/CD95L to Fas/CD95 receptor; TRAIL/Apo2L to DR4 and DR5 receptor; TNF-α to TNFR1 receptor) (Clayton & Hardwick, 2008). These receptors are transmembrane proteins present on the surface of the cell and are responsible for the initiation of the caspase cascade. The intracellular portion of these receptors contains a 'death domain' (DD) which associates with an adapter molecule. This adapter molecule itself contains a 'death effector domain' (DED) which recruits the pro-caspase-8 zymogen (inactive precursor) forming a complex called the death inducing signalling complex (DISC) (Kumar *et al.*, 2005). Oligomerization of zymogen aggregates at this complex transactivates the initiator protease (caspase 8) by the process of autocatalysis (Degterev *et al.*, 2003). In turn, caspase 8 proteolytically cleaves and activates procaspase-3 and procaspase-7. These executioner caspases mediate the apoptotic process in a systematic manner.

#### 1.2.2.2 The Intrinsic Pathway

The intrinsic pathway, also known as the mitochondrial-mediated pathway, is controlled by the Bcl-2 family of proteins, all of which share one or more Bcl-2 homology (BH) domains (Levine *et al.*, 2008). This family can be divided into the 'BH3-only' pro-apoptotic members (Nox; Puma; Bad; Bim) containing a single BH domain, the multi-domain pro-apoptotic members (Bax; Bak) containing three BH domains, and the multi-domain anti-apoptotic members (Bcl-2; Bcl-$x_L$) containing four BH domains. The balance between pro- and anti-apoptotic key members regulates the mitochondrial outer membrane permeabilization (MOMP) (Lawen, 2003). The function of the pro-apoptotic members is generally inhibited by those belonging to the anti-apoptotic family in the absence of apoptotic stimuli. The intrinsic pathway is stimulated by genotoxic stress (radiation and/or chemotherapy), hypoxia and growth factor deprivation, causing a shift in the relative levels of these Bcl-2 family proteins. Under these stress conditions, there is an excess of pro-apoptotic signals. Typically the specific 'BH3-only' members of the Bcl-2 family target the hydrophobic groove of their cognate anti-apoptotic partners, disrupting the inhibitory association of the latter on multi-domain apoptosis-promoting members and stimulating the oligomerization of the downstream Bax and Bak in the outer mitochondrial membrane (Levine *et al.*, 2008). The MOMP which results promotes the mitochondrion-cytosolic release of apoptogenic factors (cytochrome c, Smac/Diablo, and apoptosis-inducing factor (AIF) from the intermembrane space (Steinbach & Weller, 2006). Upon release of cytochrome c from

the mitochondria, a complex termed the apoptosome is formed together with the apoptotic protease-activating factor-1 (Apaf-1) under the utilization of adenosine triphosphate (ATP). This is the caspase-activating complex which recruits and oligomerizes procaspase-9, followed by its autocatalytic activation (Degterev *et al.*, 2003). Caspase-9 subsequently activates the downstream executioner caspases-3 and -7 by cleavage of their inactive forms. The anti-caspase activity of the inhibitor of apoptosis proteins (IAPs) is neutralized by the release of another apoptogenic factor, called Smac/Diablo, upon Bax/Bak homodimerization (Jiang & Wang, 2004). Executioner caspases then target substrates to dismantle the cellular structure.

Poly-ADP-ribose-polymerase (PARP) is a 113 kDa protein which is constitutively expressed in multicellular organisms (Alvarez-Gonzalez *et al.,* 1999). It plays a role in sensing the genotoxic damage inflicted upon DNA and maintaining the stability of the genome. If the damage is mild, PARP initiates a DNA repair mechanism by base excision. Beyond a critical point when the damage is too severe, PARP will instead signal the release and translocation of AIF from the mitochondrial intermembrane space to the nucleus (Zhang *et al.*, 2007; Nguewa *et al.*, 2005). AIF is another liberated apoptogenic factor that induces DNA fragmentation and thus apoptosis, but in a caspase-independent manner. PARP contains a caspase-cleavage site in the DNA binding domain which is proteolytically cleaved by caspase-3 into two polypeptide fragments, the 89 kDA carboxy terminus and the 24 kDa amino terminus (Nguewa *et al.*, 2005).

The extrinsic pathway is linked to the intrinsic pathway by the 'BH3-only' protein, Bid (Lowe & Lin, 2000). The cleavage of Bid by receptor-mediated activation of caspase-8 produces a truncated form which transclocates to the mitochondria and encourages cytochrome c release, followed by the caspase cascade. The intrinsic pathway may serve as an amplified signalling route which is cross-activated by the extrinsic pathway (Michalak *et al.*, 2005).

The transcription factor, p53, functions as a critical cell cycle checkpoint (Lowe & Lin, 2000). Cellular stress, including DNA damage and hypoxia, stabilizes this tumour suppressor causing it to accumulate in the nucleus where it regulates the balance between cellular proliferation and death. There is evidence linking p53 to cell cycle arrest and apoptosis (Michalak *et al.*, 2005). Studies have revealed that this factor is able to trigger type I cell death by transactivating distinct p53-responsive genes which include the 'BH3-only' pro-apoptotic members of the Bcl-2 family, namely Bax, Noxa and Puma. Similarly, genes that encode for death receptors (Fas/CD95; DR4; DR5) can be also be transcribed. In addition, studies show a transcription-independent mechanism where p53 directly associates directly with Bcl-$x_L$ leading to Bax oligomerization and the activation of the caspase cascade (Steinbach & Weller, 2006).

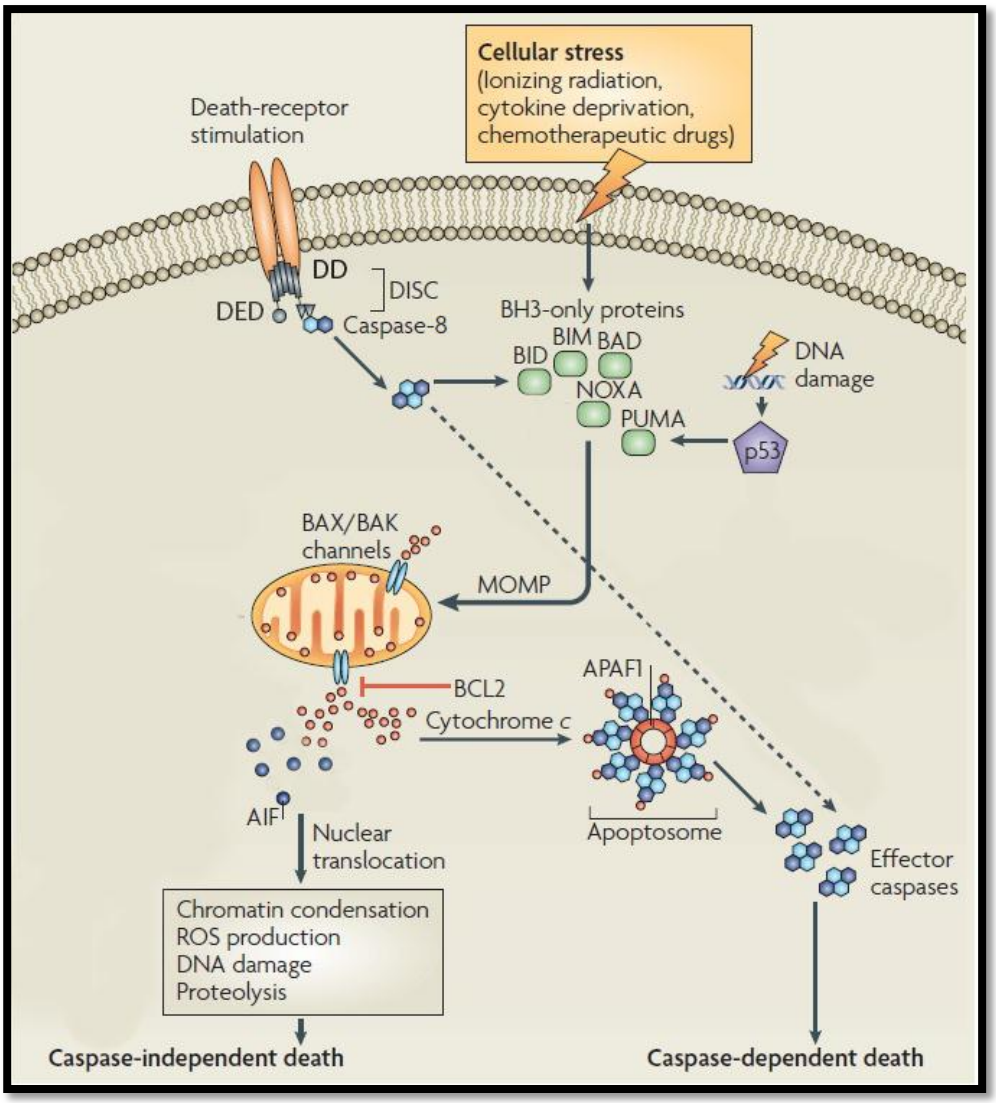


**Fig. 1.3 The extrinsic and intrinsic molecular regulation of the apoptotic cellular death pathway.** The extrinsic 'death receptor-mediated' pathway involves the recognition and ligation of a ligand to its corresponding death receptor. The "death-domain" (DD) of the receptor associates with the "death-effector-domain" of an adaptor molecule. This is followed by the incorporation of the inactive caspase 8 precursor to form the "death-inducing signalling complex" (DISC). Upon caspase 8 activation, it either directly activates the downstream effector caspases, or cleaves the BH3-only protein, BID, which translocates to the mitochondrion and initiates mitochondrial outer membrane permeabilization (MOMP). For the initiation of the intrinsic 'mitochondrial-mediated' pathway, a stressor causes the BH3-only proteins to disrupt the inhibitory interaction between pro- and anti-apoptotic family members. The released pro-apoptotic members, Bax and Bak, translocate to the mitochondria where they form channels in the outer membrane and stimulates MOMP. This leads to the release of apoptogenic factors: apoptosis inducing factor (AIF), which initiates a caspase-independent form of apoptosis; while cytochrome C activates the initiator caspase 9 protease via the formation of the apoptosome. Caspase 9 subsequently activates downstream effector caspases. Illustration adapted from Maiuri *et al*. (2007).

### 1.2.3 Apoptotic Resistance

Although a myriad of chemotherapeutic drugs, including Doxorubicin, act by inducing apoptosis, several studies have revealed a link between drug resistance and an inactivated pathway and/or mutations in key regulatory proteins. This could arise either from an increased expression of anti-apoptotic genes or the diminished expression of pro-apoptotic genes (both multi-domain and BH3-only members) (Mathiasen & Jäättelä, 2002).

Drug-resistant-selected subclones of human leukemia were shown to have a significant overexpression of the Bcl-2 death suppressor protein when compared to their drug-susceptible cancerous counterpart (Su *et al.*, 2007). This resistance could be antagonized by the use of the Bcl-2 inhibitor, HA14-I. Another experimental study found lower levels of the BH3-only pro-apoptotic protein, Bik, is a common characteristic in renal cell carcinoma tissues and cell lines (Sturm *et al.*, 2006).

Mutations in many other oncogenes/tumour suppressor genes related to this cell death pathway are also common including caspase 8, APAF-1, DR4/DR5, and p53 [as reviewed in (Steinbach & Weller, 2006)]. Genetic mutations of the p53 gene are a frequently encountered disturbance in more than 50% of manifested cancers (Airley, 2009c).

The appearance of apoptotic-resistance promotes tumorigenesis as chemotherapeutic drugs, specifically relying on this tumour suppressing pathways for treatment, become ineffective. Apoptosis incompetence is a hallmark of a broad variety of cancers (Hanahan & Weinberg, 2011).

## 1.3 PATHOPHYSIOLOGY OF SOLID TUMOURS

During tumorigenesis, an unfavourable environment develops due to the rapid proliferation of neoplastic cells coupled with the chaotic architecture of the vascular network which is morphologically and functionally inept (Rademakers *et al.*, 2008). This impairs the delivery of nutrients and oxygen to the tumour and the outcome is an imbalance between supply and utilization. The common attributes witnessed in the microenvironment of solid tumours are hypoxia, acidosis, and nutrient deprivation.

The oxygenation status of a tumour is dependent on two factors. Firstly, when the distance between the neoplastic cell and the perfusing tumour-associated vessels exceeds the diffusion distance of oxygen, a chronic form of hypoxia develops which is termed diffusion-limited hypoxia (Airley, 2009d). The second factor, termed 'acute hypoxia' is dependent on the tumour-associated microvasculature which is stimulated by hypoxic conditions to fuel neoplastic growth (Magagnin *et al.*, 2006; Rademakers *et al.*, 2008). The stimulation of new vessel formation, or angiogenesis, gives rise to an abnormally structured and unorganized vascular architecture which frequently experiences temporal fluctuations in the flow of blood (Fukumura & Jain, 2007). This could lead to the development of transient regions of low oxygen tension known as perfusion-limited hypoxia.

The depleted energy sources, as well as the ROS generated during the cyclic pattern of tumour hypoxia-reoxygenation, could be detrimental to the cancerous cells by compromising essential physiological functions (Gogvadze *et al.*, 2010). If events that restore homeostasis are activated before this stress reaches a critical point, survival of the cells may be maintained.

### 1.3.1 Regulation of the Hypoxic Response through HIF-1α

To circumvent these disturbances, a myriad of molecular pathways, collectively known as the hypoxic response, is initiated in normal and transformed cells when oxygen tension is low (Roudier & Perrin, 2009). The pathways are mediated by a family of transcriptional factors termed HIF-1. HIF-1 regulates the expression of genes that promote the adaptation and survival of transformed cells to the hostile microenvironment of a tumour to restore oxygen and nutrient homeostasis. Therefore, in this scenario, HIF-1 acts as an oncogene. This master regulator is a heterodimer composed of two subunits: the constitutively expressed HIF-1β (80 kDa) subunit, also known as the aryl hydrocarbon receptor nuclear translocator (ARNT), and the oxygen-regulated HIF-1α (120 kDa) subunit which is ubiquitously expressed in many tissues (Rohwer & Cramer, 2011). These are helix-loop-helix proteins belonging to the PER-ARNT-SIM (PAS) family and contain two transactivation domains (N-terminal and C-terminal) along with a central oxygen-dependent degradation (ODD) domain (O'Donnell *et al.*, 2006). Two other isoforms of the alpha subunit exist, namely HIF-2α and HIF-3α, the expression of which is limited to specific cell types (Keith *et al.*, 2011).

#### 1.3.1.1 Normoxic Conditions

Under normoxic conditions, HIF-1α protein becomes hydroxylated by prolyl hydroxylases using $O_2$ and α-ketoglutarate as co-substrates, and ferrous iron ($Fe^{2+}$) as a cofactor (Hansen *et al.*, 2011). Hydroxyl groups are added to proline residues (P402 and P564) within the ODDD (Keith *et al.*, 2011). These modified sites are recognized by the von Hippel-Lindau (VHL) tumour suppressor which recruits the E3 ubiquitin complex to subsequently polyubiquitinate the protein, directing it to the proteasome for degradation (Rohwer & Cramer, 2011). Therefore the presence of oxygen confers a very short half-life to this protein. Beyond regulation of HIF-1α stability by the post-translational activity of prolyl hydroxylases, this subunit is also regulated at the transcriptional level by an asparaginyl hydroxylase called the factor-inhibiting-HIF-1 (FIH) (Hansen *et al.*, 2011). FIH hydroxylation of an asparagine residue (803) present in the carboxy-terminal transactivation domain (C-TAD) hinders the interaction of HIF-1α with its transcriptional co-activators, CBP and P300, when oxygen is present (Magagnin *et al.*, 2006).

#### 1.3.1.2 Hypoxic Conditions

During hypoxic conditions, when the relative level of oxygenation is inadequate (below ~5%), the oxygen-dependent hydroxylases (PHD and FIH) become inactive and hydroxylation of proline and asparagine residues ceases (Hansen *et al.*, 2011). Inactivated PHD allows the HIF-1α protein to avoid proteasomal degradation and become stabilized. The stabilized HIF-α translocates to the nucleus where it dimerizes with HIF-1β to form the activated HIF-1 complex. The inactivated FIH stimulates the assembly of a robust HIF-1α-CBP/P300 transcription-initiation complex to the hypoxia responsive elements (HRE) in the promoter regions of downstream hypoxia-inducible genes and transactivation proceeds (O'Donnell *et al.*, 2006). Adaptation occurs through changes in the physiological characteristics of the neoplastic cells and its microenvironment.

### 1.3.2 Oxygen-independent HIF-1α Stabilization

Despite oxygen-regulation, HIF-1α expression can be triggered due to mutations in signalling pathways that switch on oncogenes, turn off tumour suppressors, and/or stimulate the PI3K-Akt-mTOR pathway when growth factors bind to receptors belonging to the tyrosine kinase family (Ferreira, 2010; Yeo *et al.*, 2004). Studies have also implicated complex III-generated ROS in upregulated expression of HIF-1α (Klimova & Chandel, 2008; Chandel *et al.*, 2000). HIF-1α may be stabilized by hypoxia-mimicking agents such as the iron-chelating desferrioxamine and cobalt chloride (O'Donnell *et al.*, 2006; Al Okail, 2010). Cobalt chloride was shown to inhibit prolyl hydroxylases by competing with ferrous iron ($Fe^{2+}$), the essential co-factor regulating the activity of these enzymes (Epstein *et al.*, 2001).

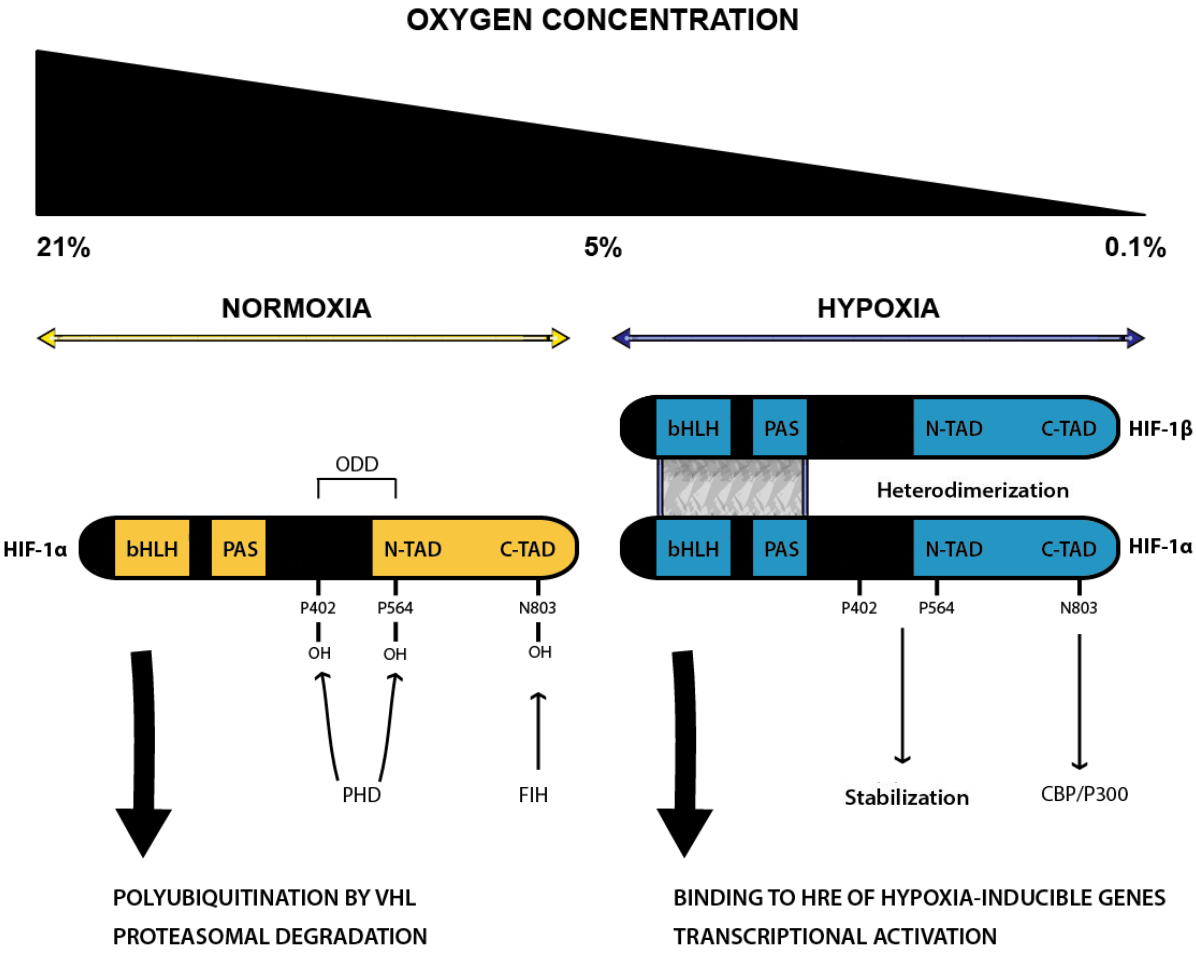


**Figure 1.3 Oxygen-dependent regulation of HIF-1 stabilization and degradation.** The HIF-1 subunits are basic helix-loop-helix (bHLH) proteins of the PER-ARNT-SIM (PAS) family. When adequate $O_2$ is available, the HIF-1α regulatory subunit is modified by the hydroxylation of proline residues (P402; P564), present in the central oxygen dependent degradation (ODD) domain, and the hydroxylation of the asparagine reside (N803), present in the carboxy-terminal transactivation domain (C-TAD). These reactions are catalysed by the 'prolyl hydroxylase domain' (PHD) proteins and the factor-inhibiting HIF (FIH), respectively. This proline hydroxylation modification is recognized by the von-Hippel Lindau (VHL) tumour suppressor which ubiquitinates HIF-1α, targeting it for degradation via the proteasome. Under hypoxic conditions (<5%), HIF-1α becomes stabilized due to the inactivation of prolyl hydroxylases. HIF-1α heterodimerises with the constitutively-expressed HIF-1β subunit. In the absence of FIH activity, the co-activator CBP-P300 is recruited, stimulating the assembly of a transcription-initiation complex at hypoxia-response elements (HRE) of hypoxia-inducible genes, mediating transactivation.

### 1.3.3 Adaptive Pathways

Adaptation to the hypoxic microenvironment of solid tumours has been shown to stimulate the progression of transformed cells to a more aggressive phenotype. It confers resistance in cancers response to radiotherapy (Kessler *et al.*, 2010), chemotherapeutic agents such as Adriamycin, Cisplatin, Palitaxel, and Etoposide [as reviewed in (Rohwer & Cramer, 2011)], and predisposes the neoplastic cells to metastasis (Dai *et al.*, 2011). Hypoxia has therefore been associated negatively with clinical outcome and may be used as a biomarker for poor prognosis (Rohwer & Cramer, 2011).

#### 1.3.3.1 The Metabolic Switch

One of the first compensatory alterations of the hypoxic response is the remodelling of oxidative metabolism to anaerobic glycolysis. In non-transformed cells, glucose is completely oxidized to $CO_2$ and $H_2O$ (Ferreira, 2010). The bulk of energy, in the form of ATP, is produced within the mitochondria primarily through the Krebs cycle and oxidative phosphorylation. The conversion of pyruvate to lactate (anaerobic glycolysis) is inhibited by the presence of oxygen, this phenomenon being termed the 'Pasteur' effect (Solaini *et al.*, 2010).

In contrast, under aerobic conditions, transformed cells adjust their metabolism and preferentially produce the majority of their energy via aerobic glycolysis in spite of the presence of oxygen (Ferreira, 2010). This process is termed the 'Warburg' effect. While certain studies have suggested that this phenomenon could be accounted for by the impairment or alteration of normal mitochondrial respiration (Chandel *et al.*, 2000; Kroemer & Pouyssegur, 2008), others have shown that mitochondria of cancer cells have functional oxidative capacity (Gogvadze *et al.*, 2010). In the latter case, the selection of aerobic glycolysis over oxidative phosphorylation may possibly be attributed to the increased glucose demand in highly proliferating cancer for anabolic reactions (synthesis of ribose-5 phosphate, phospholipids and triacylglycerides, and alanine and malate) to sustain the growth and proliferation of the cells (Solaini *et al.*, 2011; Weljie & Jirik, 2011; Roudier & Perrin, 2009). This may provide a selective proliferation advantage.

When oxygen is not available as the terminal electron acceptor, production of ATP by mitochondrial oxidative phosphorylation is compromised and transformed cells become solely dependent on glycolysis (Weljie & Jirik, 2011). In anaerobic glycolysis, energy is extracted from glucose by substrate-level phosphorylation where the yield of ATP is significantly lower. To compensate, there is an increased demand for glucose. The HIF-1α-mediated switch to anaerobic glycolysis involves the upregulation of glucose transporters (GLUT-1; GLUT-3), to augment the uptake of glucose, as well as hexokinases (I; II), which are responsible for the 'priming' step of glycolysis (Kroemer & Pouyssegur 2008). This facilitates the increased glycolytic rate often witnessed in hypoxic cancer cells to support the biomass.

HIF-1α was also shown to shunt pyruvate away from mitochondrial oxidative respiration by the expression of two key enzymes that enhance its metabolism (Solaini *et al.*, 2010): (1) pyruvate dehydrogenase kinase 1 (PDK1); which inhibits the oxidative activity of pyruvate dehydrogenase (PDH), preventing the conversion of pyruvate to acetyl CoA, a carbon substrate for the tricarboxylic acid cycle and subsequently the electron transport chain during oxidative phosphorylation; and (2) lactate dehydrogenase-5 (LDH-5); which stimulates the reduction of pyruvate to lactate.

### 1.3.3.2 Acidosis and pH Regulation

The appearance of high acidity within the tumour microenvironment stems from the excessive lactate produced by anaerobic glycolysis. Interstitial acidosis has been linked to an increased risk of invasiveness (Semenza, 2009). In 2001, Brizel *et al.* analysed biopsies of head-and-neck cancer which revealed a significant correlation between the metastatic potential of the primary tumours and their lactate concentration levels (Brizel *et al.*, 2001). Metastatic relapse was significantly higher in patients with elevated tumour lactate concentrations.

As indicated by Robey *et* al., the aggressively metastatic breast cell lines MDA-mb-435 and MDA-mb-231 had elevated HIF-1α-induced expressions of GLUT-1 and GLUT-2 with a concomitant elevation in their glycolytic rates under normoxic oxygen tension compared to the non-metastatic cell line MCF7 (Robey *et al.*, 2005). Lactate levels were also higher in the metastatic cell lines compared to the non-metastatic cell line. Upon hypoxic stimulation, HIF-1α became stabilized and lactate levels within MCF-7 were raised.

Maintenance of the intracellular and extracellular pH is achieved by transporters/exchangers. Carbonic anhydrase IX (CAIX) is the tumour-specific, membrane-associated enzyme that is transcriptionally activated by HIF-1 and responsible for the extracellular hydration of $CO_2$ to $HCO_3^-$ and $H^+$ (Solaini *et al.*, 2010; Rademakers *et al.*, 2008). The carbonate ion is imported into the cell to buffer the excess $H^+$. The expression of monocarboxylate co-transporter 4 (MCT-4) is also induced in glycolytic cells under hypoxia and catalyse the efflux of lactate and $H^+$, potentiating interstitial acidosis (Kroemer & Pouyssegur, 2008).

### 1.3.3.3 Angiogenesis

Among the genes upregulated during the hypoxic response are the pro-angiogenic factors. The expression of vascular endothelial growth factor (VEGF) is necessary to initiate the formation of a new micro-vascular network, a process known as angiogenesis (Rademakers *et al.*, 2008). This angiogenic switch aims to re-establish a local supply of nutrients and oxygen to the demanding tumour, allowing it to maintain growth and expand. Other angiogenesis-stimulating factors include erythropoietin (EPO), which stimulates the production and differentiation of endothelial progenitor cells into mature red blood cells, and matrix metalloproteases 2 (MMP-2), which degrades the

extracellular matrix and may contribute to metastasis (Dome *et al.*, 2009; Rapisarda & Melillo, 2009; Fujita *et al.*, 2002).

#### 1.3.3.4 Resistance to Radio- & Chemotherapy

Evidence exists where hypoxia promotes the selection of therapy-resistant clones in proliferating cancer cells. Graeber *et al.* (1996) found that the *in vitro* selection of transformed cells, which are apoptosis-incompetent due to a mutation in the p53 tumour suppressor gene, is encouraged in the presence of hypoxia which thus confers a survival advantage (Graeber *et al.*, 1996). Furthermore, a human colon carcinoma clone that harbours a deficiency in the DNA mismatch repair system (MMR) was selectively expanded when subjected to anaerobic conditions as compared to the MMR-proficient clones (Kondo *et al.*, 2001). The expanded population of MMR-deficient clones showed resistance to cisplatin- and 6-thioguanine-therapeautic treatments.

In 2006, Kim *et al.* showed that the ROS produced under hypoxic conditions stabilized the HIF-1α-induced expression of PDK1, and this rescues cells from ROS-induced apoptosis (Kim *et al.*, 2006).

In addition, it was discovered that, within the promoter region of the multi-drug resistance (MDR) P-glycoprotein in both normal and cancerous cells, there exists a hypoxic response element which may be regulated by HIF-1α (Comerford *et al.*, 2002). To simulate the hypoxic environment of a tumour, Doublier *et al.* grew 3-dimensional MCF-7 spheroid clusters and discovered that HIF-1α-induced expression of P-glycoprotein was associated with resistance to doxorubicin as indicated by lower caspase 9 activity (Doublier *et al.*, 2012).

All of the above evidence supports the idea that the hypoxic response increases the tolerance of cancer cells to the adverse microenvironment of a tumour. Recently, another cellular pathway that has been shown to be upregulated under these unfavourable conditions is autophagy.

## 1.4 AUTOPHAGY

Autophagy is defined as a cellular process of self-degradation that is evolutionary conserved amongst species (Maiuri *et al.*, 2007). It occurs constitutively at base-line levels within the cell to ensure homeostasis by removing aged, damaged or accumulated proteins and/or organelles. Beyond its quality control function, the autophagic process can also be massively augmented in response to various intracellular and extracellular stress stimuli (Chen & Karantza-Wadsworth, 2009). These include nutrient and growth factor deprivation (metabolic stress), radiation and chemotherapy (DNA damage), endoplasmic reticulum (ERt) stress, hypoxia, and viral invasion. During starvation conditions, cellular metabolism and biosynthesis can be sustained from the recycled pool of cytosolic biomolecules generated during autophagy (Morselli *et al.*, 2009). Elimination of excessive reactive oxygen species produced by mitochondria under hypoxia, as well as unfolded or aggregated proteins

may prevent these forms of 'cellular garbage' from potentially inducing carcinogenesis. While short-lived proteins are degraded by the ubiquitin proteasome pathway, long-lived proteins are mitigated by autophagy (Mathew & White, 2011).

Depending on the mechanism by which the cytosolic cargo is delivered to lysosomes for degradation, three different types of autophagy exist. Chaperone-mediated autophagy mediates the direct translocation of a single cytosolic protein, possessing a specific sequence motif, to the lysosome for degradation (Majeski & Dice, 2004). This form of autophagy lacks the characteristic vesicular formation and rather employs the use of cytosolic chaperones which selectively recognize and translocate proteins. Micro-autophagy and macro-autophagy (referred to generally as autophagy) are the other two forms of autophagy characterized by the formation of vesicles which allow for the degradation of cystol, proteins, and/or organelles (Todde *et al.*, 2009). While the former entails the direct sequestration and degradation of cargo by lysosomal membrane invaginations, the latter necessitates the vacuolization of cargo within double-membraned structures, termed the autophagosomes, prior to fusion with the lysosome.

### 1.4.1 Morphological Characterization

The execution process of autophagy begins within the cytoplasm with the formation of crescent-like membranous structures termed phagophores, or isolation membranes (Eskelinen & Saftig, 2009). This is the initiation stage of the autophagic process. During the elongation stage that follows, these specialized structures expand into double- or multi-membraned autophagosomes, also known as early autophagic vesicles, which sequester cytosol or cellular components for 'bulk' degradation. The cargo may be targeted selectively or non-selectively (Mathew & White, 2011).

The outer autophagosomal membrane first fuses with an endosomal vesicle to form an amphisome (Eskelinen & Saftig, 2009). This is followed by fusion with a lysosome to form an autophagolysosome, also known as a late autophagic vesicle. Acid hydrolases within the lysosome digest the inner membrane of the autophagosome along with its encapsulated luminal cargo. These hydrolases include nucleases, proteases, glycosidases, and lipases, enabling a broad range of macromolecules to be degraded simultaneously (Maiuri *et al.*, 2007; Kuma & Mizushima, 2010).

### 1.4.2 Molecular Mechanism

The autophagic signalling pathways are strictly regulated by a group of autophagy-related genes (Atgs) that were first identified and characterized in the yeast genome (Chen & Debnath, 2010). The entire complement of mammalian homologues has yet to be fully identified, but the mechanisms that exist have remained highly conserved.

The *induction* of the autophagic process involves the activation of the ULK1 (the mammalian homologue of Atg1) kinase (Jung *et al.*, 2010). This activation depends on the phosphorylation status of Atg 13 (mammalian homolog yet to be identified), a substrate of mTOR.

Once mTOR kinase activity becomes inactivated, the Atg13 protein is dephosphorylated and subsequently becomes associated with the scaffold protein, Atg17 (Mizushima, 2010). This promotes the formation of a complex with ULK1, stimulating its kinase activity. The complex then localizes to the isolation membrane where *nucleation* proceeds (Levy & Thorburn, 2011).

*Vesicle nucleation* begins when Beclin 1 (the mammalian homolog of the yeast Atg6) associates with the cofactor UV irradiation resistance-associated gene (UVRAG) (Morselli *et al.*, 2009). This stimulates the activity of the lipid kinase class III phosphatidylinositol 3-kinase (PI3-K) named Vps34 to promote the activation of the elongation process and autophagosome biogenesis (Levy & Thorburn, 2011; Chen & Debnath, 2010).

*Elongation* entails the use of two conjugation systems, namely the Atg12-Atg5 and the phosphatidylethanolamine-Atg8 systems (Meijer & Codogno, 2004). Both systems resemble the ubiquitin-proteasomal pathways. The first system entails the conjugation of Atg12 to Atg5 which is catalysed by E1-like Atg7 and E2-like Atg10 enzymes (Notte *et al.*, 2011). This conjugate localizes onto an isolation membrane where it becomes associated with Atg16L (mammalian homolog). The second conjugation system involves the mammalian homologue of the yeast Atg8, called the microtubule-associated protein 1 light chain 3 (LC3) (Levy & Thorburn, 2011). The nascent unprocessed form is cleaved by the Atg4 protease, producing soluble cytosolic LC3-I with an exposed glycine terminal. A phosphatidylethanolamine (PE) moiety is then conjugated to this terminal with the aid of the E1-like Atg7 enzyme and the E2-like Atg3 enzyme, producing the lipidated form, LC3-II, which is incorporated into the pre-autophagosomal membrane. The site of LC3-II anchorage is dependent on Atg16L which recruits the soluble LC3-I polypeptide to the vicinity of PE in the membrane (Fujita *et al.*, 2008). Modification and localization of cytosolic LC3-I to autophagosomal LC3-II is used as a marker for autophagosome formation (Zakeri *et al.*, 2008).

Upon closure of the phagophore, *maturation* proceeds by fusion with the endosomal or lysosomal vesicles. Sequestosome (P62/SQSTM1) is a cargo receptor protein that recognizes polyubiquitinated targets via their C terminal domains and delivers them to autophagosomes, thus playing a role in

cargo selectivity (Levy & Thorburn, 2011). The P62 protein is cleared along with the cargo and is been used as a biomarker of the autophagic process (Mathew & White, 2011; Mathew *et al.*, 2009).

### 1.4.3 Signalling Pathways Regulating Autophagy

#### 1.4.3.1 The PI3K-Akt-mTOR axis

A serine/threonine kinase termed the mammalian target of rapamycin (mTOR) has been implicated as holding the central position in multiple signalling cascades regulating transcription, translation and metabolism (Jung *et al.*, 2010). It balances cell growth and proliferation with the autophagic pathway. The mTOR kinase operates as a negative regulator of autophagy and is controlled by the signalling of the upstream class I PI3K-Akt pathway which senses nutrient availability, particularly amino acids and glucose (Meijer & Codogno, 2004). An ample supply of nutrients activates the PI3K-Akt-mTOR axis inducing cell growth and proliferation while simultaneously inhibiting autophagy (Chen & Karantza-Wadsworth, 2009).

#### 1.4.3.2 LKB1-AMPK –Autophagy-Axis

Under bioenergetic stress conditions, the depletion in cellular ATP causes an elevation in the AMP: ATP ratio (Hardie, 2004). This parameter is sensed by the AMP-activated protein kinase (AMPK), a heterotrimeric complex (catalytic α-subunit; regulatory β- and γ- subunits) responsible for monitoring intracellular energy status and controlling glucose, lipid and protein metabolism (Xiao *et al.*, 2011). The activity of mTOR is inversely correlated with activated AMPK (Chen *et al.*, 2010). AMP has been shown to allosterically activate AMPK (Sanders *et al.*, 2007). However, major AMPK activation is dependent on an upstream tumour suppressor, termed LKB1, which phosphorylates AMPK-α at the Thr172 residue. This occurs by binding of AMP to the γ-regulatory subunit, which prevents the dephosphorylation at the Thr172 site. Activated AMPK responds by promoting catabolic, energy-producing pathways while limiting anabolic, energy-consuming pathways.

Since autophagy is an energy-producing pathway, AMPK has been shown to induce this lysosomal process by phosphorylation of the tuberous sclerosis complexes -1 (TSC-1) and -2 (TSC-2) which is a negative mTOR regulator (Maiuri *et al.*, 2010). Activation of TSC-1 and -2 suppresses mTOR activity. An alternative pathway is by the direct phosphorylation and activation of ULK1, the kinase involved in autophagosome formation (Egan *et al.*, 2011).

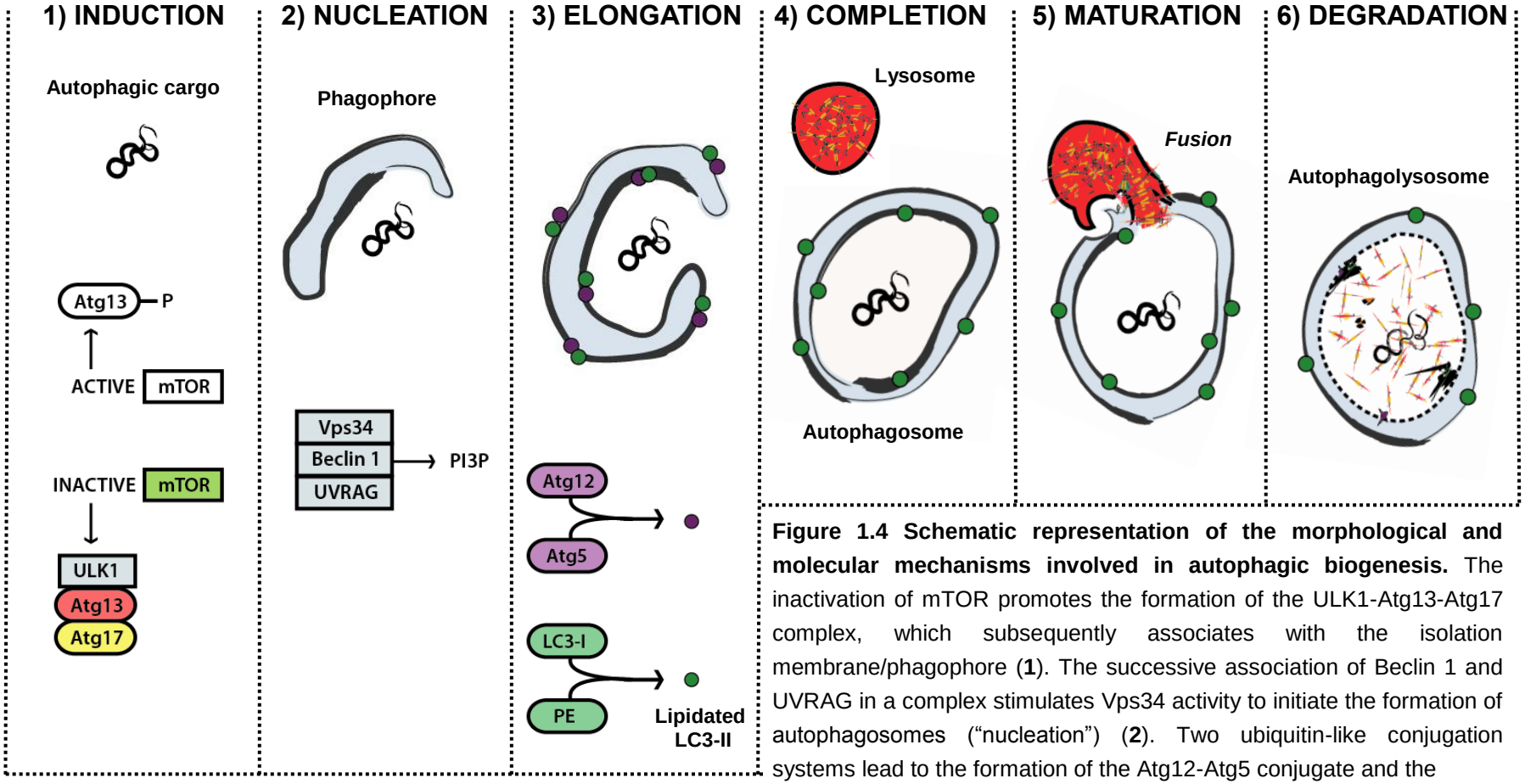


**Figure 1.4 Schematic representation of the morphological and molecular mechanisms involved in autophagic biogenesis.** The inactivation of mTOR promotes the formation of the ULK1-Atg13-Atg17 complex, which subsequently associates with the isolation membrane/phagophore (**1**). The successive association of Beclin 1 and UVRAG in a complex stimulates Vps34 activity to initiate the formation of autophagosomes ("nucleation") (**2**). Two ubiquitin-like conjugation systems lead to the formation of the Atg12-Atg5 conjugate and the lipidated phosphatidylethanolamine (PE)-associated LC3-II conjugate, both of which promote elongation (**3**). The LC3-II conjugate becomes incorporated into the membranes of the developing autophagosome. Upon completion (**4**), the maturation phase follows with the fusion of the autophagosome with a lysosome to form an autophagolysosome (**5**). The encapsulated cargo, as well as the inner limiting membrane, becomes degraded by acid lysosomal hydrolyases (**6**).

### 1.4.4 Relationship between Autophagy & Apoptosis

A link between the molecular mechanisms controlling autophagy and apoptosis was suggested when the conserved tumour suppressor factor, Beclin 1, was identified as a Bcl-2-interacting protein (Levine *et al.*, 2008). In 2007, a study entailing the use of *in vitro* pull down assay demonstrated that Beclin 1 directly interacts with several anti-apoptotic proteins, each through different binding efficiencies (Erlich *et al.*, 2007). Furthermore they showed that, although multidomain pro-apoptotic proteins are unable to interact with Beclin 1, the BH3-only proteins indirectly interfere by disrupting its inhibitory association with anti-apoptotic Bcl-2 members. Using sequence alignment and molecular modelling, they elucidated that Beclin 1 possessed a putative BH3-like domain which interacts with the hydrophobic BH3 receptor domains present on anti-apoptotic members of the Bcl-2 family. This was supported by studies carried out by Oberstein *et al*. identifying Beclin 1 as a novel BH3-only member (Oberstein *et al.*, 2007). Therefore autophagy is capable of being modulated by the family of Bcl-2 apoptotic regulators, suggesting a mechanism of cross-talk between the two pathways (Levine *et al.*, 2008). The physical interaction between Beclin 1 and Bcl-2 or Bcl-$x_L$ forms an inhibitory complex that prevents the autophagic tumour suppressor from allosterically activating Vps34, the lipid kinase responsible for autophagosome formation (Levy & Thorburn, 2011). Competitive disruption by BH3 only proteins liberates the Beclin 1 allowing it to activate autophagy.

Since similar stimuli can initiate apoptosis and autophagy, the relationship between the two is puzzling in terms of the pathway that is preferentially selected (Maiuri *et al.*, 2007). González-Polo *et al*. (2005) performed a study on HeLa cells and mouse embryonic fibroblasts where they showed that the protective mechanism of autophagy, which is upregulated under starvation conditions, eventually succumbs to apoptosis when autophagy is inhibited. RNA interference was used to deplete two lysosome proteins, LAMP1 and LAMP2, thus blocking the fusion of autophagosomes with lysosomes during autophagy (Maiuri *et al.*, 2007; González-Polo *et al.*, 2005). Vice versa, the survival of apoptotic-deficient bone marrow cells, with a double-knockout of pro-apoptotic Bak and Bax proteins, was sustained using autophagy as an alternative source of ATP upon withdrawal of the IL-3 growth factor (Lum *et al.*, 2005).

While autophagy may contribute to the survival of cells, in other scenarios it constitutes as an alternative form of demise (type II cell death), particularly in apoptotic-incompetent cells (Eskelinen & Saftig, 2009). A study by Shimizu *et al.* (2004) revealed that the loss of cell viability in $Bax^-/Bak^-$ apoptosis-deficient mouse embryonic fibroblasts was mediated by the generation of autophagosomes/autolysosomes in response to treatment with the topoisomerase inhibitor, Etoposide (Shimizu *et al.*, 2004). Another study showed that the selective elimination of mitochondria from neurons and HeLa cells occurred through autophagy when the caspases were inhibited (Xue *et al.*, 2001). The decision of whether BH3-only proteins target pro-apoptotic proteins to induce apoptosis or anti-apoptotic proteins to induce autophagy is yet to be elucidated. Certain studies hypothesize that the BH3-only members may have variable sensitivities to stimuli (Levine *et al.*, 2008).

### 1.4.5 Autophagy in Tumorigenesis

The abnormal regulation of the autophagy signalling cascade has been implicated in numerous pathological diseases including myopathy, neurodegeneration and cancer (Meijer & Codogno, 2004). In the context of tumorigenesis, autophagy has been documented as having both a cellular death as well as a pro-survival function (Chen & Karantza-Wadsworth, 2009).

#### 1.4.5.1 Suppression of Tumorigenesis

The frequent mutations of several genes in the autophagic pathway have suggested a cytoprotective role against tumorigenesis. This is either due to the activation/deregulation of oncogenes or inactivation of tumour suppressor genes. For instance, Beclin 1 is considered a tumour suppressor and is frequently expressed at lower levels in prostate, ovarian, and breast cancers due to its monoallelic deletion (Liang *et al.*, 1999).

An *in vivo* study involving the transgenic expression of GFP-LC3 in mice that harboured a heterozygous disruption in Beclin 1 revealed a more diffuse pattern of LC3 as compared to transgenic GFP-LC3 Beclin 1 $^{+}/^{+}$ which produced punctuate regions under starvation conditions (Qu *et al.*, 2003). This disruption in autophagy was shown to correlate with the generation of spontaneous tumours in various organs of the Beclin $^{+}/^{-}$ mice.

Multiple lines of evidence support the notion that mutations in other regulators, including the monoallelic deletion of UVRAG, the over-expression of Bcl-2 and Bcl-$x_L$ autophagy repressors, and the diminished expression of BH3-only Bcl-2 family (as reviewed in (Morselli *et al.*, 2009)), can act as the driving force for cancer development.

#### 1.4.5.2 Promotion of Tumorigenesis

Conversely, autophagy may also be upregulated in response to radiation or anticancer drugs to eradicate the resulting genotoxic damage imposed, thus contributing to survival (Chen & Karantza-Wadsworth, 2009). Treatment of malignant U251 glioma cells with the DNA-damaging agent, Temozolomide, was shown induce autophagy allowing these cancerous cells to evade cell death by micro-nucleation (Katayama *et al.*, 2007).

Carew & Medina provided insight into the survival mechanism of autophagy when they inhibited the pathway in HT29 and HCT8 colon tumour cells using a pharmacological inhibitor of lysosomal fusion, termed Chloroquine (Carew & Medina, 2010). In this autophagy-deficient setting, cell death via apoptosis was augmented during treatment of these cells with the histone deacetylase inhibitor, Vorinostat. Cell death was attributed to the increased accumulation of protein aggregates that are typically removed by autophagy.

The process of autophagy represents a survival response during metabolic stress by the catabolic breakdown of macromolecules for nutrient supply under energy limiting conditions (Maiuri *et al.*, 2007). The development of a solid tumour is typically accompanied by the deprivation of nutrients (glucose; amino acids) due to the abnormal vascular network that is associated with the tumour (Trédan *et al.*, 2007). The dependency of cancer cells on autophagy during metabolic insult is supported by Degenhardt *et al*., whose research revealed that apoptotic-defective HeLa cells (forced Bcl-2 or Bcl-$x_L$ expression) thrived under ischaemic conditions (incubation in glucose-free medium under 1% oxygen) (Degenhardt *et al.*, 2010). This survival was attributed to the autophagic mechanism as the pattern of EGFP-LC3 was converted from diffuse to punctuate when subjected to the metabolically stressful conditions. HeLa cells exhibited necrotic cell death upon the knock-down of Beclin-1 by RNA interference.

## 1.5 RELATIONSHIP BETWEEN AUTOPHAGY AND HYPOXIA

Besides damage by chemo- and radiotherapy, a limited supply of nutrients and oxygen in the microenvironment of the tumour can also constitute a stressful insult. As mentioned previously, autophagy serves as a protective mechanism in nutrient-limiting conditions and would therefore be expected to generate the necessary supplies that fuel the metabolism for neoplastic proliferation (Nan Chen & Debnath, 2010). Therefore, disruption of this pathway would lead to a metabolic catastrophe and cell death, limiting the growth of the tumour (González-Polo *et al.*, 2005).

A recent *in vitro* study on human cervical (HeLa) and ovarian (OVCAR-8) cancer cell lines revealed that the apoptosis that arises under normoxic conditions in response to treatment with Fenretinide, an anticancer agent known to induce apoptosis by generation of reactive oxygen species, is replaced by autophagy when oxygen is depleted (Liu *et al.*, 2010). Disruption of the autophagic process with 3-Methyladenine or Chloroquine sensitized the cells to Fenretinide treatment indicating that autophagy upregulated under hypoxia is protective. Furthermore, HIF-1α knockdown with short hairpin RNA (shRNA) abrogated the autophagic response indicating that this process acts downstream of the transcription factor.

The hypoxic-inducible gene, BNIP3, has been implicated as the factor responsible for autophagy upregulation (Rohwer & Cramer, 2011). Zhang *et al.* showed that the potential cytotoxicity due to the reactive oxygen species generated during hypoxic stress was mitigated by mitochondrial autophagy, or mitophagy, in mouse embryo fibroblasts (Zhang *et al.*, 2008). This autophagy was shown to be dependent on BNIP3 expression, which was induced by HIF-1α stabilization during hypoxia. BNIP3 is a BH3-only member of the Bcl-2 family which is also responsible for antagonizing the pro-survival effects of Bcl-2 and Bcl-$x_L$, further providing evidence for potential cross-talk between autophagy and apoptosis (Levine *et al.*, 2008).

## 1.6 TARGETING THE HYPOXIC ENVIRONMENT OF TUMOURS

2-Methoxyestradiol is an endogenous metabolite derived from 17β-estradiol by an oxidative biotransformation process occurring naturally under physiological conditions in both males and females (Sutherland *et al.*, 2007). Under normal physiological conditions, plasma concentrations of 2-methoxyestradiol are relatively low (within the pico-molar range) (Mueck & Seeger, 2010). Recent interest in the exploitation of 2-methoxyestradiol as an anticancer agent has arisen as it has been shown to possess anti-carcinogenic properties. This compound possesses a weak estrogenic activity and its mode of action is believed to be independent of the estrogen receptor status of cells (Sutherland *et al.*, 2007; LaVallee *et al.*, 2002).

### 1.6.1 Mechanism of Action of 2-Methoxyestradiol

The universal mode of action exhibited by 2-methoxyestradiol has yet to be elucidated, but a variety of possible mechanisms have been suggested. Its anti-proliferative properties have been demonstrated on both endothelial cells and several cancer cell lines [as reviewed in (Mooberry, 2003; Dubey & Jackson, 2009)]. These properties may arise from interference of the estradiol metabolite with the progression of the cell cycle leading to accumulation of cells in the $G_2$/M phase (Stander *et al.*, 2010; Kumar *et al.*, 2001). An alternative mechanism is the induction of the extrinsic and intrinsic apoptotic pathways, where studies have shown 2-ME to upregulate the death receptor 5 (LaVallee *et al.*, 2003), generate a surge in the production of free radicals due to inhibition of superoxide dismutase (Huang *et al.*, 2000), and/or the activation of the stress c-Jun N-terminal kinase (JNK), which subsequently inactivates the anti-apoptotic Bcl-2 proteins by phosphorylation (Bu *et al.*, 2002). The mechanism of action chosen appears to be dependent on the cell line. Apart from this direct effect on endothelial cells, this compound has also been demonstrated to indirectly inhibit neo-angiogenesis via HIF-1α-dependent down-regulation of VEGF (Stander *et al.*, 2010). Mabjeesh *et al.* noted that the decrease of HIF-1α protein expression in human breast (MDA-MB-231) and prostate (PC-3) cancer cell lines upon 2-methoxyestradiol treatment occurred through a translational-dependent mechanism (Mabjeesh *et al.*, 2003). Not only was VEGF mRNA attenuated, but the decreased HIF-1α expression correlated with the depolymerisation of microtubules. Furthermore, these researchers proceeded with an *in vivo* approach where the microvascular density of tumours, obtained from an orthotopic breast cancer model, was quantified. A significant decrease in vascularization was seen in response to 2-methoxyestradiol exposure.

Its appeal as an anticancer drug was further emphasized by its ability to selectively target proliferating tumorigenic and endothelial cells, while its effect on normal epithelial cells appears to be negligible (Parks *et al.*, 2011; Kato *et al.*, 2008). This selective toxicity was observed by Van Zijl *et al*. (2008) who showed that the capability of 2-methoxyestradiol to induce apoptosis, multipolar spindles and mitotic blockage, thereby inhibiting cellular proliferation, was weaker in the epithelial non-tumorigenic MCF-12A cell line compared to tumorigenic MCF-7 cells (Van Zijl *et al*., 2008).

### 1.6.2 Adjuvant Therapy & Clinical Trials of 2-Methoxyestradiol

Previous studies using xenograft murine models have revealed 2-methoxyestradiol to be proficient at synergistically enhancing the cytotoxic effects of anticancer agents while maintaining a low systemic toxicity profile. For example, Han *et al*. (2005) showed that by combining 2-methoxestradiol with the anticancer drugs, paclitaxel or vinorelbine, a more pronounced growth inhibitory effect on the MDA-MB-231 xenografts compared to either drug treatment alone (Han *et al.*, 2005).

These preclinical results have transcended the 2-methoxyestradiol compound to Phase I and II clinical trials where evaluation of its efficacy have been carried out on patients inflicted with epithelial ovarian cancer (Matei *et al.*, 2009), metastatic breast cancer (James *et al.*, 2006) and solid tumours (Dahut & Lakhani, 2006). Different formulations of this drug, currently registered as Panzem® by EntreMed (Rockville, USA), have evolved in order to improve its delivery and stability, including the NanoCrystal® Dispersion (NCD) delivery system (Harrison *et al.*, 2011).

## 1.7 PROBLEM STATEMENT

Despite the manifestation of the pathology of cancer throughout different tissues of the body, that of the breast seems to be the prime site of occurrence and the most fatalistic form in women.

Although breast cancer exhibits a heterogeneous phenotype, the most effective antineoplastic drug used for treatment is doxorubicin, belonging to the anthracycline class of antibiotics. This anticancer drug debilitates cancer cells by multiple mechanisms, most of which culminate in the apoptotic cell death pathway. The responsiveness to chemotherapeutic treatment is frequently hindered within solid tumours. This has been attributed to the adverse microenvironment existing within the tumour, often featuring regions of hypoxia. An endogenous biomarker of hypoxia is the HIF-1α transcription factor, with its expression in hypoxic environments capable of inducing survival advantages that simultaneously select for a more aggressive phenotype in terms of malignancy and chemo-resistance. Autophagy is an evolutionary conserved process that is active at basal levels within almost all cells to maintain homeostasis of a cell by eliminating potentially hazardous proteins and organelles. Studies have indicated that the autophagic process is capable of promoting tumorigenesis and survival despite multi-modality treatment. Furthermore, hypoxia is also a potent stimulus for autophagy.

Therefore, to counteract the chemotherapeutic resistance that impedes the success of doxorubicin, a strategy that manipulates autophagy in the context of a hypoxic environment represents an appealing approach. To target the hypoxic response, which has been shown to include the autophagic pathway, would be by inhibiting the master regulator, HIF-1. Through the posttranslational disruption of the HIF-1α protein (pharmacological intervention; 2-methoxyestradiol), or alternatively, the silencing of the HIF-1α mRNA transcript (transcriptional intervention; siRNA duplex), the cytotoxic pharmacodynamic profile of doxorubicin on breast cancer (MCF-7; E0771) may be improved by antagonizing the chemotherapeutic-resistant response. The combination of therapies exhibiting different modes of action not only allow for the maximum mitigation of tumorigenic cells, but simultaneously enable the therapies to be used at sub-toxic doses that would otherwise target and potentially destroy non-malignant cells. In the context of this study, the full potential of the antineoplastic drug, doxorubicin, could thus be exploited by inhibition of the hypoxic response.

### 1.7.1 Hypothesis

Abrogation of the ‘protective’ hypoxic response by pharmacological (2-methoxyestradiol) or genetic (siRNA transfection) disruption of the HIF-1α master regulator will sensitize MCF-7 neoplastic cells to the chemotherapeutic drug, doxorubicin.

### 1.7.2 Aims

1. To determine the conditions at which hypoxia confers a survival advantage to the MCF-7 tumorigenic cells in response to doxorubicin treatment.

2. To characterize the molecular events responsible for this selective advantage under hypoxia.
3. To link these molecular events to the expression levels of the HIF-1 master regulator.
4. To assess whether the disruption of the 'protective' hypoxic response by HIF-1 inhibition can sensitize the tumorigenic cell line to doxorubicin treatment, therefore producing a synergistic effect.
5. To show reproducibility of the *in vitro* experiment in a pre-clinical animal model.

# CHAPTER 2 - MATERIALS & METHODS

***IN VITRO***

## 2.1 STUDY DESIGN

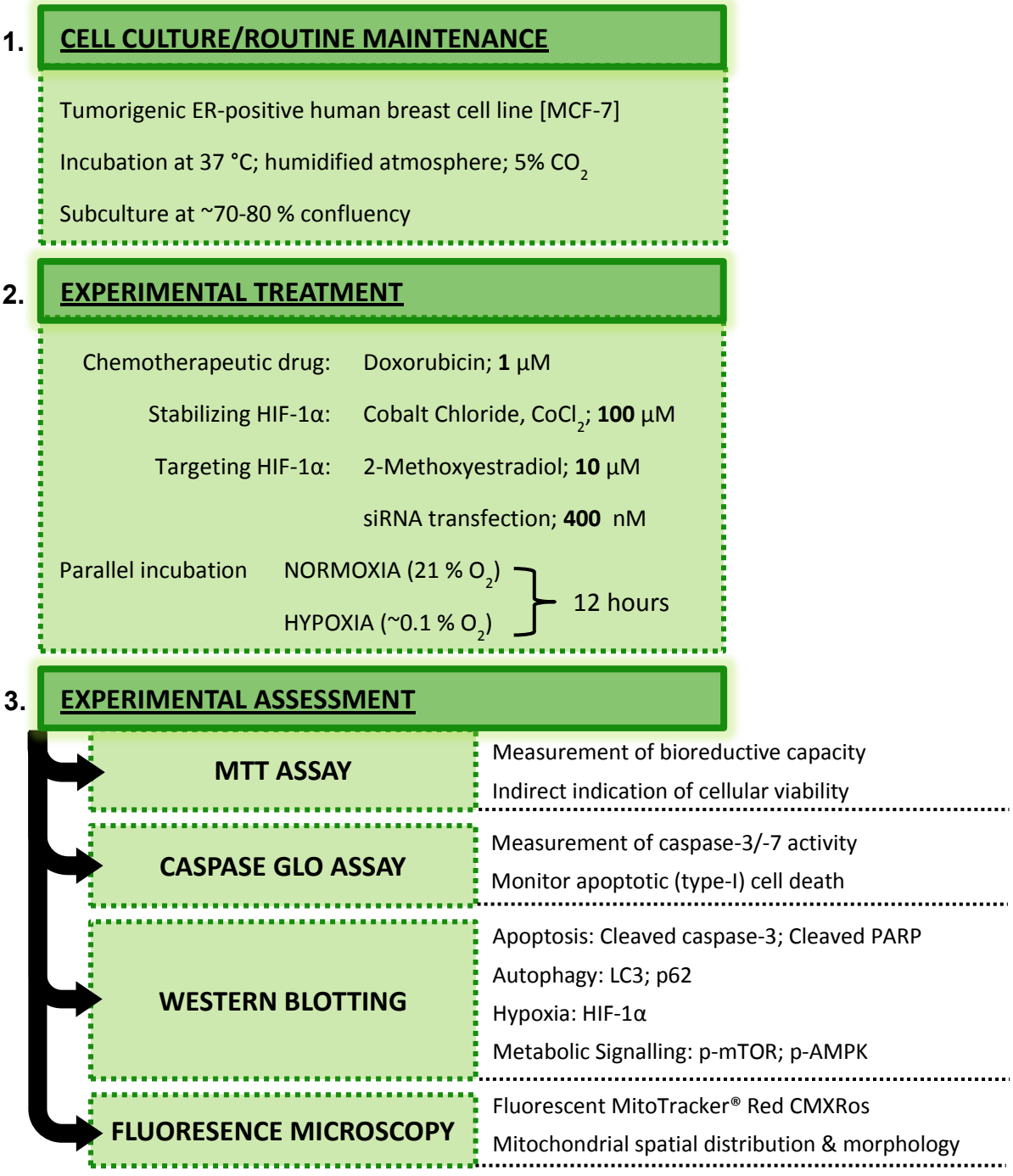


**Figure 2.1 *In vitro* study design.** Human breast cancer epithelial cells (MCF-7) were treated with doxorubicin, either alone or in combination with HIF-1α disruption, and incubated in parallel under either normoxic (21% $O_2$) or hypoxic (~0.1% $O_2$) conditions for 12 hours. Experiments were assessed based on bioreductive capacity (MTT Assay), metabolic pathways (Western blotting), and cellular death pathways (Caspase-Glo Assay, Western Blotting, and Live Cell Imaging).

## 2.2 CHEMICALS & REAGENTS

The growth medium constituents: Dulbecco's Modified Eagle Medium (DMEM; #10564-037), heat-inactivated Fetal Bovine Serum (FBS; #10082), and Penicillin-Streptomycin-Glutamine (100X liquid, #10378-016) were all obtained from Invitrogen, Life Technologies (Johannesburg, South Africa). Doxorubicin Hydrochloride (#D1515) was purchased from Sigma-Aldrich (Johannesburg, South Africa), 2-Methoxyestradiol (#13021) from Cayman Chemical (Michigan, USA), and Cobalt (II) Chloride Hexahydrate (#102539) from Merck (Darmstadt, Germany). The HIF-1α siRNA transfection kit (#35561) was obtained from Santa Cruz Biotechnology (California, USA). The MTT reagent, Thiazolyl Blue Tetrazolium Bromide (#M2128), was acquired from Sigma-Aldrich (Johannesburg, South Africa). Promega (Madison, USA) provided the Caspase-Glo® 3/7 Assay (#G809) kit. For western blotting, following primary antibodies: rabbit anti-Cleaved Caspase-3 (Asp175), #9661; rabbit anti-Cleaved PARP (Asp214), #9541; rabbit anti-LC3B, #2775; rabbit anti-SQSTM1/p62, #5114; rabbit anti-HIF-1α, #3716; rabbit anti-Phospho-mTOR (Ser2448), #2971; rabbit anti-Phospho-AMPK (Thr172), #2531; and the secondary antibody: HRP-linked goat anti-rabbit, #7074; were all purchased from Cell Signaling (MA, USA). Invitrogen, Life Technologies (Johannesburg, South Africa) supplied the MitoTracker® Red CMXRos required for live cell imaging/fluorescent microscopy.

## 2.3 CELL LINES

The MCF-7 tumorigenic cell line is an adherent, estrogen-receptor positive cell line where the primary culture originated from the pleural effusion obtained from a woman with malignant adenocarcinoma of the mammary gland. The MCF-7 cell line was utilized in this study and obtained from the American Type Culture Collection (catalogue no# HTB-22; Rockville, MD, USA).

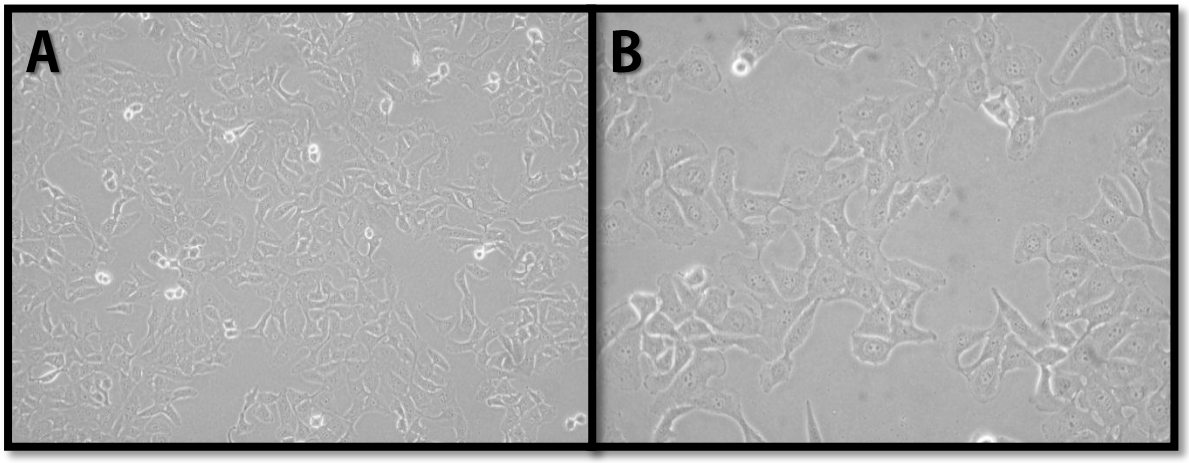


**Figure 2.2 Images of the MCF-7 cell line obtained with an inverted microscope.** (**A**) 100x and (**B**) 400x magnification.

## 2.4 CELL CULTURE

For routine maintenance, the MCF-7 cell line was propagated in tissue culture flasks at a seeding density of 5000 cells/$cm^2$. Cells were incubated under a humidified atmosphere containing 5% $CO_2$/95% $O_2$ at 37°C. The growth medium employed was Dulbecco's Modification of Eagle's Medium (DMEM) supplemented with 10% Fetal Bovine Serum (FBS) and 1% Penicillin-Streptomycin. Growth of the cultures was monitored using an inverted phase microscope (Olympus CKX4SF; Tokyo, Japan). Once a confluency of approximately 70-80% was reached, new cultures were established by subculture/passage. Cells were never passaged more than 10 times. Strict aseptic control was applied at all times.

## 2.5 EXPERIMENTAL PROTOCOL

### 2.5.1 Seeding Densities for Experimental Purposes

**Table 2.1 Guide for recommended seeding densities of MCF-7 cells based on the surface area of culture vessels.** The recommended seeding densities are based on both the doubling time of tumorigenic MCF-7 cell line (~29 hours) and the requirement of at least ~24 hours for reverse transfection in HIF siRNA groups. The treatment regime commenced once a confluency of ~70-80% is reached.

| TECHNIQUE | CULTURE VESSEL | SURFACE AREA ($cm^2$) | SEEDING DENSITY (cells/$cm^2$) |
|---|---|---|---|
| WESTERN BLOTTING | 6-Multiwell Plate | 9.5 | ~5.0 x $10^4$ |
| LIVE CELL IMAGING | 8-Chamber Slide | 0.8 | ~4.0 x $10^3$ |
| BIOREDUCTIVE MTT ASSAY | 12-Multiwell Plate | 3.8 | ~2.0 x $10^4$ |
| CASPASE-GLO® 3/7 ASSAY | 96-Multiwell Plate | 0.32 | ~2.0 x $10^3$ |

### 2.5.2 Reverse Transfection

Knock-down of HIF-1α gene expression was performed using a reverse transfection approach. The HIF-1α siRNA duplex was combined with 6 µL transfection reagent, FuGENE®6 (Fugent, L.L.C, USA), and diluted in siRNA transfection medium (excluding serum and antibiotics) such that the final concentration of the siRNA duplex was 400 nM. The siRNA-FuGENE®6 mixture was added to the culture dishes and incubated for a minimum of 45 minutes. MCF-7 cells that had been resuspended in growth medium (containing serum for cell growth, but excluding antibiotics) were then seeded at the appropriate density into the culture dishes containing the siRNA-FuGENE®6 preparation. Cells were

then incubated at 37°C until reaching a confluency of 80% (~24 hours) after which the drug treatment proceeded.

### 2.5.3 Drug Treatments

The following stocks were made: 3.4 mM doxorubicin solution using growth medium as the solvent, 33 mM 2-methoxyestradiol solution using DMSO, and 25 mM $CoCl_2$ solution using $dH_2O$. Aliquots of both doxorubicin and 2-methoxyestradiol were prepared so as to avoid freeze-thaw cycles and stored at -20°C while the $CoCl_2$ solution was stored at room temperature. Immediately prior to each experimental treatment, these chemicals were diluted in growth medium to a final concentration of 1 µM, 10 µM, and 100 µM for doxorubicin, 2-methoxyestradiol and $CoCl_2$, respectively.

### 2.5.4 Treatment Conditions

Following the treatment regime, cells were then subjected to either normoxic (21% $O_2$) or hypoxic (~0.1% $O_2$) conditions for a period of 12 hours in parallel. Cultures were incubated in Perspex sub-chambers within an incubator and conditions were rendered hypoxic with the aid of the ProOx C21 (BioSpherix, New York, USA) oxygen controller unit by infusion with Nitrogen gas (Afro, South Africa).

## 2.6 THE MTT BIOREDUCTIVE ASSAY

The MTT bioreductive assay is a method used to quantify the metabolically active cells in a population, thus giving an indication of cellular viability. This colorimetric assay is based on the bioreductive capacity of cells. Metabolically active cells are able to reduce the water-soluble yellow tetrazolium salt 3-(4,5-dimethylthiazol-2-yl)-2,5-diphenyl tetrazolium bromide (MTT) to water-insoluble purple formazan crystals of which the absorbance can be detected spectrophotometrically. The amount of the formazan product generated is directly proportional to the number of metabolically viable cells. This rapid test is widely used to evaluate and compare the *in vitro* responses to the cytotoxic effects of anti-tumour candidates.

Cells in their exponential growth phase were seeded in 12-well tissue culture plates at a density of 2.0 X $10^4$ MCF-7 cells/1000 µL/well and allowed to adhere under standard culture conditions (37°C; 5% $CO_2$). The groups that required transfection were simultaneously reverse transfected during plating. Once a confluency of ~80% was reached, treatment was initiated as described previously in the experimental protocol. On completion of the treatment, the medium was aspirated from the adherent cells and a prewarmed PBS/1% MTT (0.01 g MTT/1 mL PBS) reagent mixture was gently added to each well in a 3:1 ratio. Culture plates were maintained in the dark at 37°C in a humidified 5% $CO_2$ atmosphere for 60 minutes. Solubilisation of the purple formazan product was achieved using an acidified isopropanol:triton-x mixture (50:1). The absorbance values were monitored on a spectrophotometer at 540 nm using the acidified isopropanol: triton-x mixture as a blank. Experiments

were performed in quadruplicate and repeated a minimum of three times. Data was expressed as a percentage compared to untreated control samples (100%).

## 2.7 THE CASPASE-GLO® 3/7 ASSAY

Caspase 3- and 7- are the executioners of the apoptotic cellular death pathway and their activities can be measured by the addition of a luminogenic reagent that, in combination with the enzyme luciferase, produce a light signal proportional to the amount of caspase activity present. Cells in their exponential growth phase were seeded in 96-well tissue culture plates at a density of 2000 MCF-7 cells/100 µL/well and allowed to adhere under standard culture conditions (37°C; 5% $CO_2$). A reverse transfection approach was simultaneously followed during plating in the necessary groups. Once a confluency of ~80% was reached, treatment was initiated as described previously in the experimental protocol. At the end of treatment, 50 µL of the treatment medium was transferred to the wells of a white-walled 96-well plate and an equal volume of the Caspase-Glo® Reagent was added. The contents were mixed gently and incubated in the dark for 60 minutes. The luminescence was measured in a luminometer (GloMax™ 96 Microplate Luminometer, Promega). Data was expressed as a percentage (relative light units, RLU) compared to untreated control samples.

## 2.8. WESTERN BLOTTING

### 2.8.1 Protein Extraction

All the procedures involved in the extraction of total protein from cells were performed on ice (4°C) or in a walk-in fridge. Upon completion of treatment, cells were harvested as follows: The medium containing the detached cells was transferred directly to conical tubes. After the addition of ice-cold PBS to each well, the adherent cells were mechanically harvested by gentle scraping with the aid of a rubber cell scraper. The cell suspension was then transferred to its respective conical tube containing the medium. MCF-7 cells were pelleted by centrifugation (1500 rpm; 3 minutes; 4°C) and resuspended in ~200 uL of RIPA buffer (50 mM Tris-HCl, 150 mM NaCl, 1% NP-40, 0.25% Na Deoxycholate, 1mM PMSF, 1 mM Benzamidine, 1 mM EDTA, 1 µg/1 mL Leupeptin, 2 µg/1 mL Aprotonin, 1 µg/1 mL Pepstatin, 4 µg/1 mL SBTI-1, 1 mM $Na_3VO_4$, 1 mM NaF) per 9.5 $cm^2$ and maintained for a duration of 10 minutes. Cells were disrupted by multiple short bursts (~3 seconds) of sonication using the ultrasonic liquid processor (Misonix Sonicator 4000, Connecticut, USA). Lysates were clarified by centrifugation (8000 rpm for 10 minutes; 4°C) which removed the insoluble cellular debris, and final supernatants collected.

### 2.8.2 Determination of Protein Concentration

All the procedures involved in the determination of protein content in lysates, as well as sample preparation were performed on ice (4°C). Protein quantification was performed using the Bradford colorimetric assay (Bradford, 1976) from a bovine serum albumin (BSA) standard curve. The

absorbance values were measured with a spectrophotometer (Cecil 2000, type CE 2021 UV/VIS, Cambridge, England) at a wavelength of 595 nm.

### 2.8.3 SDS-PAGE & Electrotransfer

For high molecular weight proteins (phospho-mTOR, 298 kDa; HIF-1α, 120 kDa; Cleaved PARP, 89kDa; phospho-AMPK, 62 kDa; p62, 62 kDa), lysates were separated on a 6% polyacrylamide gel, whereas for low molecular weight proteins (β-actin, 42 kDa; LC3, 14 kDa, 16 kDa; Cleaved Caspase 3, 17 kDa, 19 kDa), a 12% polyacrylamide gel was used. Equivalent amounts of protein (50 µg) were loaded per lane with a molecular marker being loaded in the first lane to assist with orientation and sizing of separated proteins. Proteins were fractionated by sodium dodecyl sulphate polyacrylamide gel electrophoresis (SDS-PAGE; Mini-PROTEAN® Tetra cell, Biorad) at a constant voltage of 100 V and current of 200 mA (Biorad Power Pac 1000) until the migration front reached the bottom of the gel.

Resolved proteins were then electro-transferred onto polyvinylidene fluoride membrane (PVDF; Immobilon, Millipore, USA) using a horizontal semi-dry electrotransfer system (Biorad Trans-blot® SD, USA) at voltage of 15 V and constant current of 0.5 A (Biorad Power Pac 1000). Alternatively, a vertical wet transfer system (Mini- Trans blot cell, Italy) was used when electrotransfer was performed using a voltage of 200 V and constant current of 200 mA (Biorad Power Pac™ HC).

### 2.8.4 Immuno-detection

Non-specific hydrophobic binding sites were blocked with incubation in 5% non-fat milk. For the phosphorylated proteins, 3% bovine albumin serum was used as a blocking solution as non-fat milk contains the phosphorylated protein casein which would bind antibody and therefore nonspecific proteins. Blots were then incubated overnight at 4°C in primary antibody. The protein of interest was detected using recommended dilutions of the primary antibodies: LC3-II and p62 (autophagy), cleaved caspase 3 and cleaved PARP (apoptosis), HIF-1α (hypoxia), and p-mTOR and p-AMPK (metabolism). The blots were then incubated in anti-rabbit horseradish peroxidase-conjugated secondary antibody. Membranes were then exposed to ECL Western Blotting Substrate (BioVision, USA, San Francisco) and the light emission produced was detected by exposure to photographic film in a dark room. Alternatively, chemiluminescent signals were captured with the Chemidoc MP Imager System (Biorad). To control for protein loading, all blots were probed for the representative protein β-actin. The images were refined in terms of their display using the Image Lab™ Software (version 4.0 build 17). Densitometric analysis was performed using the Quantity One 1-D Analysis Software (Biorad) and normalized against its respective loading control. Three independent experiments were performed.

## 2.9 LIVE CELL IMAGING

### 2.9.1 Staining the Mitochondria

To assess the spatial distribution and morphology of intracellular mitochondria, a qualitative approach using a mitochondrion-selective dye, MitoTracker® Red CMXRos, was employed. This cell-permeable probe becomes oxidized on entry into an actively respiring cell and concentrates in the mitochondria, which then fluoresce.

Cells were seeded into an 8-chamber slide (Nunc) at a density of 4.0 x $10^3$ MCF-7 cells/300 µL/well and allowed to adhere under standard culture conditions (37°C; 5% $CO_2$). Reverse transfection was simultaneously carried out on the necessary groups. Treatment commenced once cells reached 80% confluency. At the end of the desired treatment period, cells were loaded with a 1 mM working solution of MitoTracker® Red. This specific fluorescent probe has an excitation/emission maximum of 579 nm/599 nm. Nuclei were counter-stained using Hoechst 33342 (1:200). The cells were observed using an Olympus IX81 inverted fluorescent microscope equipped with a 100x oil immersion objective and a Xenon-Arc burner (Olympus Biosystems GMBH) as the light source. To minimize photobleaching of the mitochondrion-specific dyes, the focal plane was set using the Hoechst-excitation parameter. Samples were excited with the 360 nm (DAPI) and 572 nm (TxRed) excitation filter. The emission was acquired using a UBG triple-bandpass emission filter cube (Chroma). For the z-stack image frame acquisition, an Olympus Plan Apo N 60x/1.4 Oil objective and the Cell^$^R$ imaging software have been used. Increments between the separate image frames in z were 0.4 µm.

### 2.9.2 Processing the Fluorescent Images

The raw fluorescent images were processed and non-specific background subtracted using the Cell^$^R$ imaging software. Finally, the image stacks were projected as a maximum intensity projection.

## 2.10 STATISTICAL ANALYSIS

Data from at least three independent experiments (each conducted in three replicates) were analysed. Significant differences were assessed by one-way analysis of variance (ANOVA) using the Bonferroni post-hoc test. The GraphPad Prism version 5 software was employed to conduct all statistical analysis.

*IN VIVO*

## 2.11 STUDY DESIGN

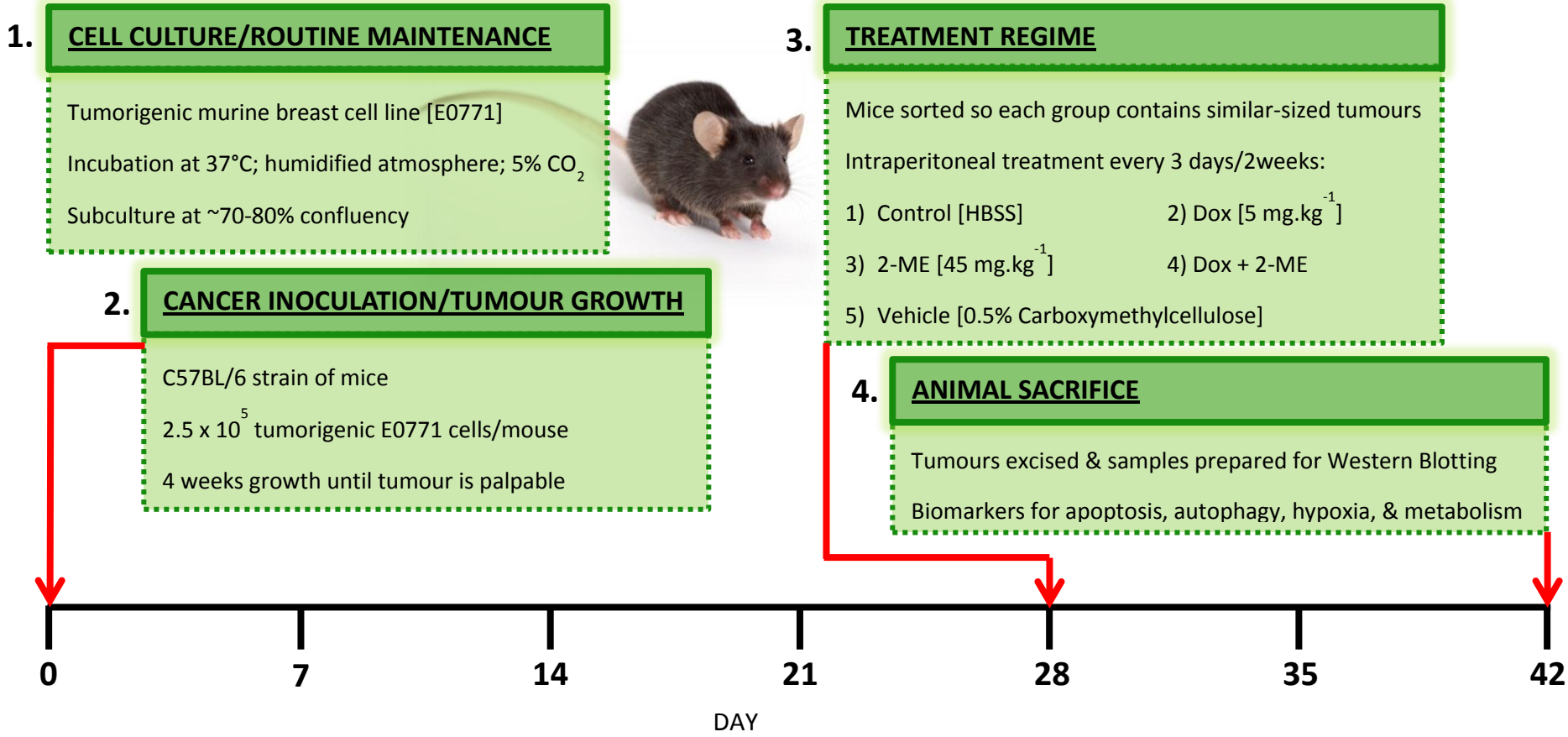


**Figure 2.3 *In vivo* study design.** C57BL/6 mice were inoculated with murine adenocarcinoma mammary cells (E0771). Treatment began at 28 days post-inoculation once the tumours became palpable and the mice were then randomly sorted into 5 different treatment groups. Mice received treatment every 3 days for 2 weeks. On day 42, they were sacrificed and resected tumours were analysed for biomarkers using western blotting.

## 2.12 ANIMALS

The *in vivo* study employed the use of the C57BL/6 mouse strain. Mice were maintained in the animal facility at the University of Stellenbosch and provided with standard chow feed and tap water *ad libitum*. Mice were housed in sterilized cages with filtered air. Animal research was ethically approved (clearance no# 2009B02004) and experiments were performed under conditions that complied with the requirements of the institution.

## 2.13 CELL LINES

The cell line used in this study was the tumorigenic E0771 cell line which originated from a tumour that developed by spontaneous mutation in a C57BL/6 mouse. This cell line was generously provided by Fengshi Li (Roswell Park Cancer Institure, Buffalo, New York, USA).

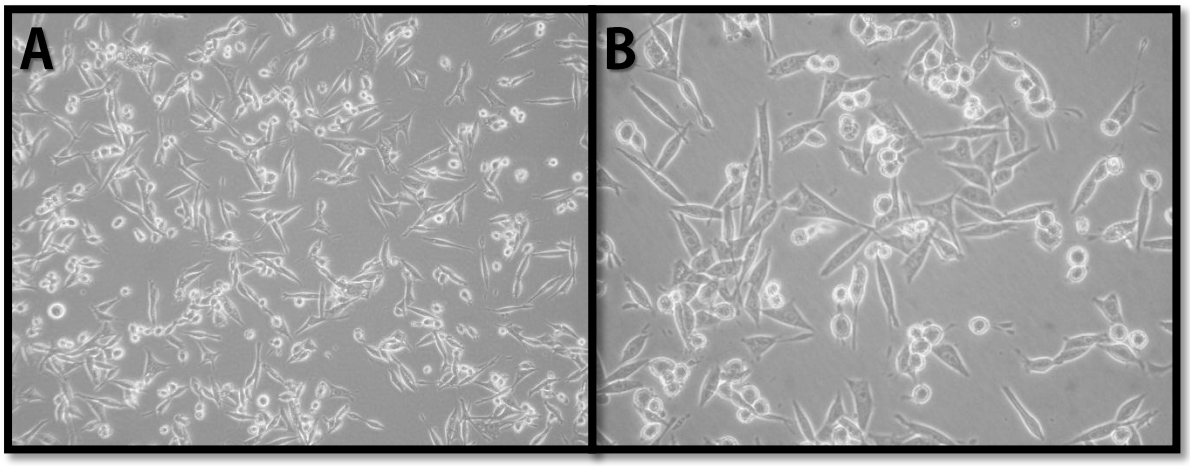


**Figure 2.4 Images of the E0771 cell line obtained with an inverted microscope.** (**A**) 100X and (**B**) 400X magnifications.

## 2.14 EXPERIMENTAL PROTOCOL

### 2.14.1 Cell Culture

For routine maintenance, the E0771 cell line was propagated in tissue culture flasks under a humidified atmosphere containing 5% $CO_2$/95% $O_2$ at 37°C. The growth medium employed was DMEM supplemented with 10% Fetal Bovine Serum and 1% Penicillin-Streptomycin. Growth of the cultures was monitored using an inverted phase microscope (Olympus CKX4SF; Tokyo, Japan). Cultures were established once the confluency reached approximately 70-80%. Cells were examined on a daily basis for changes in cell morphology and growth. Cells were not passaged more than 10 times. Strict aseptic control was applied at all times. A master stock of the cell line at a specific passage was made.

### 2.14.2 Inoculation of Cancer

Female 8-week old C57BL/6 mice with an average weight of ~22.5 g were inoculated subcutaneously into the left fourth mammary fat pad with 2.5 x $10^5$ E0771 cells/200 µL Hanks Balanced Salt Solution (HBSS; Sigma H8264, St Louis, USA). The day of inoculation was designated as day 0.

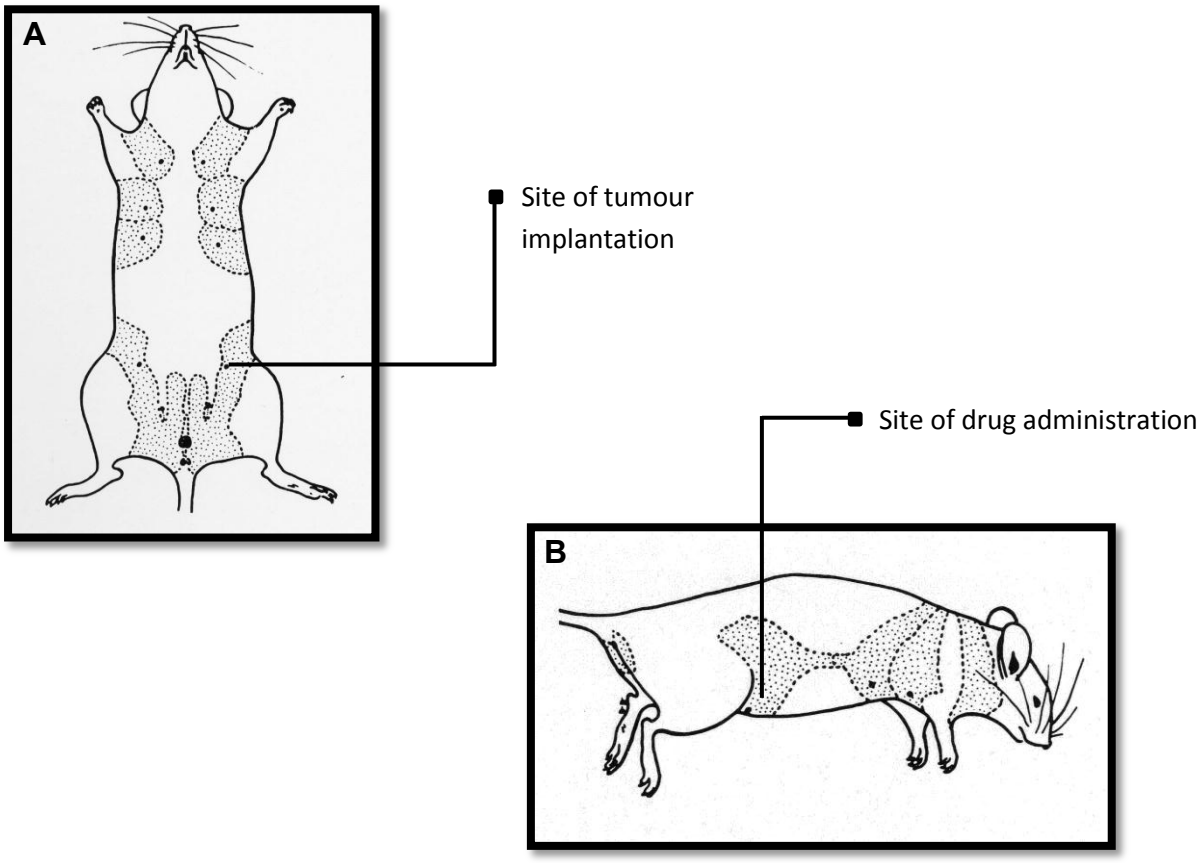


**Figure 2.5 Modified illustration indicating site of tumour implantation and drug administration.** Mammary glands of the experimental mouse indicating (**A**) the site of E0771 cancer cell inoculation and (**B**) the site of drug administration. Illustration was adapted from (Murphy, 1966).

### 2.14.3 Drug Administration, Tumour Excision, and Experimental Evaluation

The following stocks were made: 10 mg/3 mL doxorubicin solution using growth medium as the solvent and a 50 mg/1 mL 2-Methoxyestradiol solution using 0.5% carboxymethylcellulose (CMS) as the solvent. Immediately prior to each drug injection, these chemicals were diluted in HBSS (Sigma H8264, St Louis, USA) such that the final volume of each treatment administered was 100 µL. When the tumours became palpable on day 28, tumour-bearing mice were randomly sorted into 5 different treatment groups: (1) control (HBSS), (2) doxorubicin-treated (5 $mg.kg^{-1}$), (3) 2-methoxyestradiol-treated (45 $mg.kg^{-1}$), (4) mice treated with the combination of doxorubicin and 2-methoxyestradiol, and (5) vehicle (0.5% CMS). Mice were restrained and drugs administered intraperitoneally every 3 days for a duration of two weeks.

Each mouse was tagged in the ear and monitored individually. The body mass of control and treated animals was measured every three days. Simultaneously, tumour volume was monitored by recording the perpendicular length and width of the tumours using a slide calliper. The volume of tumours was calculated using the following formula: 0.52 x (shortest diameter)$^2$ x (longest diameter).

Experimental mice were sacrificed at the end of the treatment period (day 42) and tumours were excised as rapidly as possible and placed on ice. Tumour tissue was dissected into pieces and placed in ~1 mL of RIPA buffer per 1 $mm^3$. Tissue was then disrupted with the aid of a homogeniser. Lysates were centrifuged (8000 rpm for 10 minutes; 4°C), which removed the insoluble cellular debris, and final supernatants collected. Western blot sample preparation and analysis of tumours was approached in the same manner as the *in vitro* component of this study.

# CHAPTER 3: RESULTS

## *IN VITRO*

### 3.1 CONCENTRATION-RESPONSE CURVES

The MTT bioreductive assay was employed to assess the sensitivity of the tumorigenic MCF-7 cell line exposed to various concentrations of the chemotherapeutic drug, doxorubicin, and the pharmacological HIF-1α-inhibitor, 2-methoxyestradiol, for a duration of 24 hours. This allowed us to establish the concentration of the drugs required for the study.

#### 3.1.1 Doxorubicin

The capacity of MCF-7 cells to reduce the MTT tetrazolium salt under normoxic conditions became significantly reduced with increasing concentrations of doxorubicin, from 0.5 – 5 µM (**Fig. 3.1.1A**). At concentrations more potent than 5 µM, this inhibitory effect appeared to plateau. Although a similar inhibitory pattern was witnessed under hypoxic conditions, a significant effect only became noticeable from a concentration of 0.75 µM and higher. A half-maximal response ($IC_{50}$) was elicited at ~1 µM and was therefore chosen as the concentration of doxorubicin to be used throughout this study.

#### 3.1.2 2-Methoxyestradiol

The 24 hour exposure of MCF-7 cells to 2-methoxyestradiol exhibited a similar concentration-dependent inhibitory effect under both normoxia and hypoxia as was seen with the doxorubicin drug (**Fig. 3.1.1B**). Although the capacity of MTT salt reduction decreases with increasing concentrations, the effect is much weaker when compared to that of doxorubicin. The $IC_{50}$ was calculated as ~10 µM.

#### 3.1.3 Cobalt Chloride

Of the serial $CoCl_2$ concentrations, those higher than 300 µM produced a significant decrease in the bioreductive capacity of MCF-7 cells (**Fig. 3.1.2**).

### 3.2 TIME-RESPONSE CURVES

Our next aim was to elucidate the duration of MCF-7 exposure to doxorubicin which would be capable of inducing a differential response between normoxic and hypoxic conditions.

A differential effect was evident in all experimental groups after 6 hours of exposure, where MCF-7 neoplastic cells under hypoxia possessed a greater bioreductive capacity compared to their normoxic

counterparts (**Fig. 3.2.1**). This effect became statistically significant within the control (117.6 ± 3.479% vs normoxic control, $p<0.001$) and doxorubicin-treated (40.39 ± 2.810% vs normoxic dox, $p<0.01$) groups after a treatment duration of 12 hours. After a 24 hour of exposure, this distinct effect had disappeared. Beyond this time point (**Fig. 3.2.2**, 48 hours; **Fig 3.2.3**, 72 hours), a reversal of the differential effect was observed in the control group where MCF-7 cells under hypoxia presented a significant decrease in their capacity to reduce the tetrazolium salt compared to those under normoxia. Therefore, 12 hours was selected as the time point for the study based on the prominent differential effect that manifested within the doxorubicin treated group.

## 3.3 THE EFFECT OF THE TREATMENT REGIME ON APOPTOSIS IN MCF-7 CELLS DURING NORMOXIA AND HYPOXIA

### 3.3.1 The Caspase-Glo® 3/7 Assay

An increase in the luminescent signal was observed in all the doxorubicin-treated groups (**Fig. 3.3**). Within these groups, the activities of the executioner caspases-3 and -7 were significantly greater when HIF-1α was silenced by transfection in MCF-7 cells under both normoxia (16.94 ± 2.749 RLU vs. normoxic dox, $p<0.05$) and hypoxia (17.85 ± 3.059 RLU vs. hypoxic dox, $p<0.05$). There was no noticeable effect when doxorubicin was combined with 2-methoxyestradiol.

### 3.3.2 Western Blotting

To further validate the results obtained from the Caspase-Glo® 3/7 Assay, the expressions of two biomarkers playing a role in the apoptotic pathway were assessed by immunoblotting.

Similar to the pattern witnessed in the Caspase-Glo® 3/7 Assay experiment (section **3.3.1**), the cleavage of caspase 3 became more pronounced in the groups treated with doxorubicin compared to the control. Under normoxic conditions, there was a statistical increase of caspase 3 cleavage in the doxorubicin-HIF-1α siRNA group (16.81 ± 2.602 AU vs. normoxic dox, $p<0.05$) compared to doxorubicin alone (**Fig. 3.4.1**). In contrast, cleavage was significantly diminished when doxorubicin was combined with 2-methoxyestradiol (3.802 ± 0.06586 AU vs. normoxic dox, $p<0.05$). Under hypoxic conditions, the combination of the doxorubicin and 2-methoxyestradiol produced a similar statistical difference (3.239 ± 0.2156 AU vs. hypoxic dox, $p<0.05$) as evident from **Fig. 3.4.2**. However, no significance was detected when HIF-1α was silenced.

The apoptotic trend seen with caspase 3 cleavage was mimicked when another biomarker was employed, namely the cleavage of PARP, which occurs downstream of caspase 3 activation. Under normoxia (**Fig. 3.5.1**) and hypoxia (**Fig. 3.5.2**), doxorubicin combined with 2-methoxyestradiol reduced PARP cleavage significantly (3.824 ± 0.1078 AU vs. normoxic dox, $p<0.05$ for normoxia and

19.15 ± 4.377 AU vs. hypoxic dox, $p<0.0001$ for hypoxia), whereas the treatment of HIF-1α silenced neoplastic cells with doxorubicin did not alter the expression profile significantly.

## 3.4 THE EFFECT OF THE TREATMENT REGIME ON AUTOPHAGY IN MCF-7 CELLS DURING NORMOXIA AND HYPOXIA

### 3.4.1 Western Blotting

To evaluate the autophagic intensity under baseline conditions and possible changes induced in response to experimental treatment conditions, two biomarkers specific for the autophagic pathway were employed.

The conversion of the cytosolic form of the microtubule-associated protein light chain (LC3-I) to the lipidated, autophagosome-associated form (LC3-II) is a marker used to assess the formation of autophagosomes. Under normal oxygen tension, in comparison to the control, the LC3-I to LC3-II conversion detected was considerably higher in groups treated with $CoCl_2$, doxorubicin alone, doxorubicin in the presence of 2-methoxyestradiol, HIF-1α siRNA alone, and the siRNA transfection in combination with doxorubicin (**Fig. 3.6.1**). The accumulation of LC3-II was significantly augmented (2.076 ± 0.05859 AU vs. normoxic dox, $p<0.05$) when doxorubicin was used in combination with 2-methoxyestradiol compared to doxorubicin alone. In relation to the hypoxic control, the treatment of cells with $CoCl_2$, doxorubicin, and the doxorubicin-2-methoxyestradiol combination under hypoxic conditions caused a significant degree of LC3-II expression (**Fig 3.6.2**). In contrast to the doxorubicin treatment of MCF-7 cells expressing functional HIF-1α, the transfection of these cells with HIF-1α siRNA demonstrated a significant decrease in LC3-II accumulation (1.160 ± 0.07788 AU vs. hypoxic dox, $p<0.05$) when 1 µM of doxorubicin was administered for 12 hours.

Another established marker of autophagy is termed sequestosome (p62) which is digested by autophagolysosomes along with the selected cargo. In the normoxic setting, examination of p62 levels revealed significant differences in three treatment groups compared to the control (**Fig. 3.7.1**). While MCF-7 displayed lower p62 expression in the doxorubicin-only group, it was induced when HIF-1α was silenced alone and in combination with doxorubicin treatment. Combination of doxorubicin with either 2-methoxyestradiol (1.044 ± 0.08184 AU vs. normoxic dox, $p<0.05$) or HIF-1α siRNA transfection (1.434 ± 0.1543 AU vs. normoxic dox, $p<0.05$) exhibited elevated p62 protein levels as compared to when doxorubicin was used as a single agent. Compared to the levels present in the control group at ~0.1% $O_2$, p62 was elevated in those groups transfected with HIF-1α siRNA alone and in conjugation with doxorubicin when MCF-7 cells were incubated under hypoxic conditions (**Fig. 3.7.2**).

## 3.5 THE EFFECT OF THE TREATMENT REGIME ON HIF-1 STABILIZATION IN MCF-7 CELLS DURING NORMOXIA AND HYPOXIA

### 3.5.1 Western Blotting

The potential of $CoCl_2$ to serve as a positive control for this study was tested. Upon $CoCl_2$ treatment, there was an increase in the expression of HIF-α compared to the baseline control levels present under normoxia (**Fig. 3.8.1**). The inhibition of HIF-1α by 2-methoxyestradiol and RNA transfection was shown to significantly decrease HIF-1α levels compared to the normoxic control. Furthermore, doxorubicin alone and its combination with 2-methoxyestrediol both decreased the levels of HIF-1α compared to baseline levels. When related to the expression of non-transfected MCF-7 cells that received doxorubicin, a significant expression of HIF-1α became apparent when HIF-1α siRNA transfection was integrated with the chemotherapeutic treatment (1.513 ± 0.1222 AU vs. normoxic dox, $p<0.01$). During hypoxia, HIF-1α expression levels were reduced upon $CoCl_2$ treatment with respect to the hypoxic control (**Fig. 3.8.2**). 2-Methoxyestradiol was significantly effective at mitigating the expression of HIF-1α under these conditions, whereas no change in HIF-1α levels occurred with transfection. As with normoxia, HIF-1α siRNA-transfected MCF-7 cells that were subjected to 12 hours of doxorubicin treatment upregulated HIF-1α levels by a statistically significant degree (1.621 ± 0.007219 AU vs. hypoxic dox, $p<0.01$) compared to un-transfected doxorubicin-treated MCF-7 cells.

## 3.6 THE EFFECT OF THE TREATMENT REGIME ON THE OXYGEN (AMPK) AND NUTRIENT (mTOR) SENSORS IN MCF-7 CELLS DURING NORMOXIA AND HYPOXIA

### 3.6.1 Western Blotting

The incubation of MCF-7 cells under the standard atmospheric oxygen concentration (21%) permitted the activated form of the mammalian target or Rapamycin, designated as p-mTOR, to become more pronounced in two treatment groups compared to the control: the HIF-1α silenced groups, alone and upon treatment with 1 µM doxorubicin for a duration of 12 hours (**Fig. 3.9.1**). The vehicle group which contained dimethyl sulfoxide displayed a reduced level of activated mTOR. When oxygen was flushed out of the chamber, the phosphorylation status of mTOR became significantly reduced compared to the control when MCF-7 cells were treated with $CoCl_2$ or the combination of doxorubicin with 2-methoxyestradiol (**Fig. 3.9.2**). Phospho-mTOR expression within the latter group was shown to be significantly lower (0.3914 ± 0.01285 AU vs. hypoxic dox, $p<0.05$) compared to those within the group treated with doxorubicin alone.

With respect to the AMPK oxygen sensor, besides the groups treated with doxorubicin alone, which led to an increase in AMPK activation (1.307 ± 0.1053 AU vs. normoxic control, $p<0.01$), and 2-methoxyestradiol alone, where p-AMPK expression was attenuated (0.4567 ± 0.07481 AU vs. normoxic control, $p<0.01$), none of the other groups displayed any statistically significant difference

with respect to the control when exposed under normal oxygen tension (**Fig. 3.10.1**). The $CoCl_2$-treated group was able to significantly decrease p-AMPK (0.9356 ± 0.01247 AU vs. hypoxic control, $p<0.01$) in comparison with control when conditions were rendered hypoxic (**Fig. 3.10.2**).

## 3.7 THE EFFECT OF THE TREATMENT REGIME ON THE MITOCHONDRIAL INTEGRITY OF MCF-7 CELLS DURING NORMOXIA AND HYPOXIA

### 3.7.1 Live Cell Imaging/Fluorescent Microscopy

With the aid of the mitochondrion-specific dye, MitoTracker® Red CMXRos, imaging by fluorescence microscopy allowed for the qualitative characterization of mitochondrial integrity, in terms of structure and distribution. Exposure of tumorigenic MCF-7 cells to the low oxygen tension (~0.1%) displayed alterations in the structure of their mitochondria. The tubular-network of elongated mitochondria which are usually present under normoxic conditions transformed into compact disc-like forms, yet remained distributed throughout the cytoplasm (**Fig. 3.11.1A**). This morphological change was reproduced when cells were treated with $CoCl_2$ under both normoxia and hypoxia (**Fig. 3.11.1B**).

Under normoxia and hypoxia, the treatment with doxorubicin caused the structure of the mitochondria to be completely disrupted and assume a peri-nuclear distribution within the cell, regardless of whether it was applied alone (**Fig. 3.11.1C**), or in combination with 2-methoxyestradiol (**Fig 3.11.2E**) or HIF-1α siRNA transfection (**Fig. 3.11.3G**). Furthermore, the nuclei which were counter-stained with Hoechst 33342 displayed condensation of chromatin. The focal plane of the cells shifted suggesting detachment from the growth surface.

2-methoxyestradiol alone also seemed to give rise to detached cells presenting nuclear chromatin condensation, or pyknosis (**Fig. 3.11.2D**).

## 3.7 THE EFFECT OF THE TREATMENT REGIME ON THE BIOREDUCTIVE CAPACITY OF MCF-7 CELLS DURING NORMOXIA AND HYPOXIA

### 3.7.1 The Bioreductive MTT Assay

The formation of formazan crystals by the reduction of tetrazolium salt became significantly lower when MCF-7 cells were exposed to doxorubicin, 2-methoxyestradiol, and the combination of these two drugs (**Fig. 3.12**). Furthermore, the silencing of HIF-1α by transfection produced a similar decline when treated with doxorubicin. These effects were noticeable under both normoxia and hypoxic conditions. While there was a prominent difference between the normoxic and hypoxic doxorubicin-treated cells (42.97 ± 3.095%, $p<0.01$), no other oxygen-dependent differential effects were observed in any of the other treatment groups.

## *IN VIVO*

### 3.8 THE EFFECT OF THE TREATMENT REGIME ON THE RATE OF TUMOUR GROWTH

The size of the tumours present within all the treatment groups increased over the 42 day period (**Figure 3.13**). However, variance in the size between tumours within groups was large and no significance difference in the rate of tumour growth was evident between groups. Despite this, we were able to demonstrate changes within groups on a molecular level from tumour tissue lysates with the aid of the western blotting technique.

### 3.9 THE EFFECT OF THE TREATMENT REGIME ON APOPTOSIS WITHIN TUMOUR TISSUE

#### 3.9.1 Western Blotting

Relative to the group treated with doxorubicin, a significantly larger amount of PARP became cleaved when mice were treated with both doxorubicin and 2-methoxyestradiol (1.217 ± 0.1854 AU vs. dox, $p<0.05$) (**Fig. 3.14**). No significant changes in cleaved caspase 3 became evident.

### 3.10 THE EFFECT OF THE TREATMENT REGIME ON AUTOPHAGY WITHIN TUMOUR TISSUE

#### 3.10.1 Western Blotting

The expression of LC3-II became less detectable in tumour tissue when simultaneously treated with doxorubicin and 2-methoxyestradiol (0.6163 ± 0.1251 AU vs. dox, $p<0.05$) compared to doxorubicin treatment alone (**Fig. 3.15**). No significant changes in p62 became evident.

### 3.11 THE EFFECT OF THE TREATMENT REGIME ON HIF-1α STABILIZATION WITHIN TUMOUR TISSUE

#### 3.11.1 Western Blotting

HIF-1α within tumour tissue excised from the mice that were simultaneously treated with both doxorubicin and 2-methoxyestradiol produced a significantly diminished amount of expression compared to the amounts existing in the doxorubicin treated group (0.6514 ± 0.1168 AU vs. dox, $p< 0.05$) (**Fig. 3.16**).

## 3.12 THE EFFECT OF THE TREATMENT REGIME ON THE NUTRIENT (mTOR) and OXYGEN (AMPK) SENSORS WITHIN TUMOUR TISSUE

### 3.12.1 Western Blotting

Compared to the levels present in the doxorubicin group, significantly lower p-mTOR (0.1887 ± 0.02781 AU vs. dox, $p<0.01$) and p-AMPK (1.045 ± 0.1018 AU vs. dox, $p<0.05$) levels were evident when this drug was used in conjunction with 2-methoxyestradiol (**Fig. 3.17**).

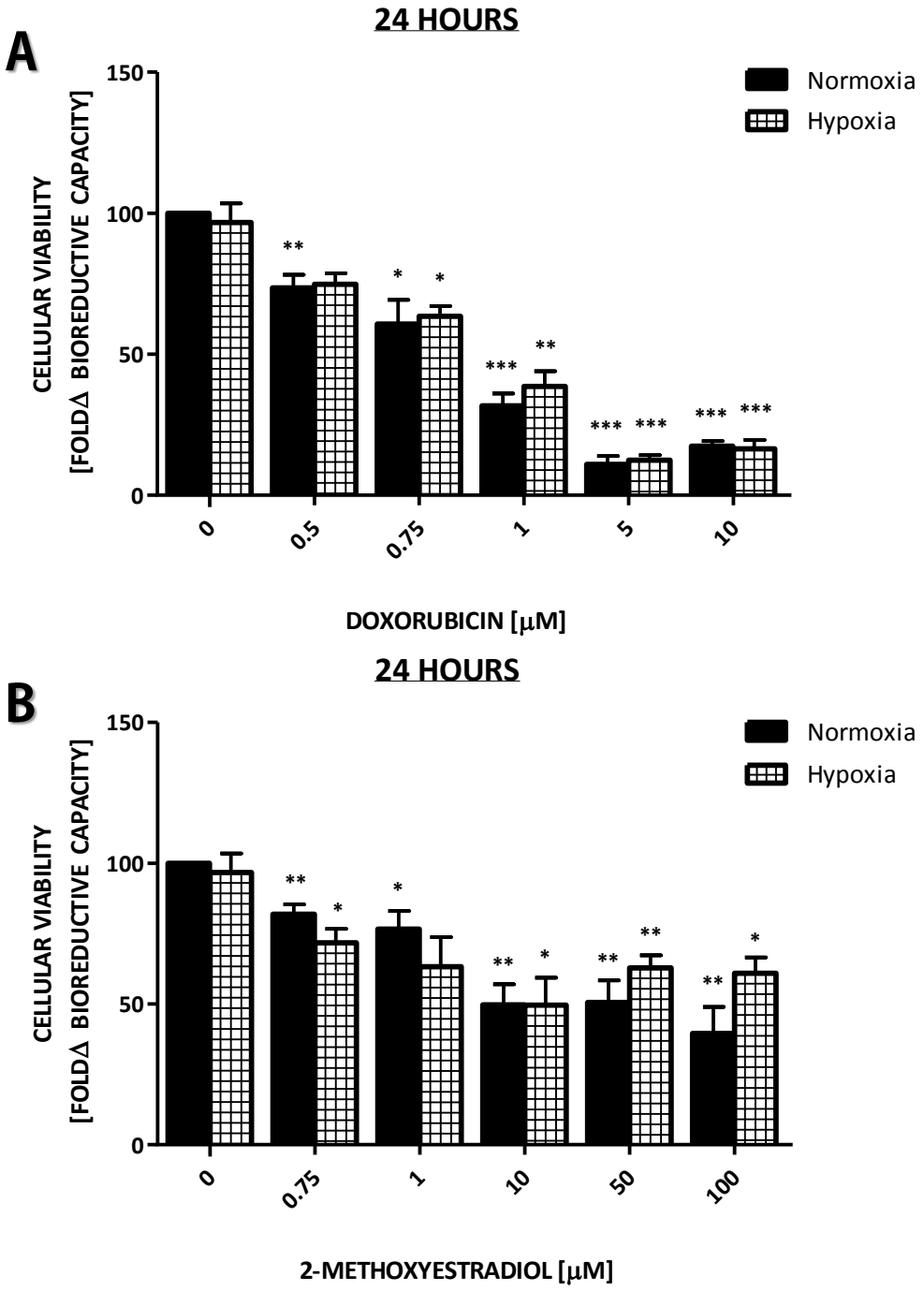


**Figure 3.1.1 The inhibitory effect on MCF-7 cells exposed to varying concentrations of doxorubicin and 2-methoxyestradiol under normoxic and hypoxic conditions for 12 hours.** The MTT assay was employed to measure bioreductive capacity which indirectly indicates cellular viability. The $IC_{50}$ values for (**A**) doxorubicin and (**B**) 2-methoxyestradiol were 1 µM and 10 µM, respectively. Values expressed as a percentage of the control (100%). *Columns*, mean survival fractions; *Bars*, ± SEM. The results are a representative of four independent experiments. * $p<0.05$ vs. normoxic control; ** $p<0.01$ vs. normoxic control; ***, $p<0.0001$ vs. normoxic control.

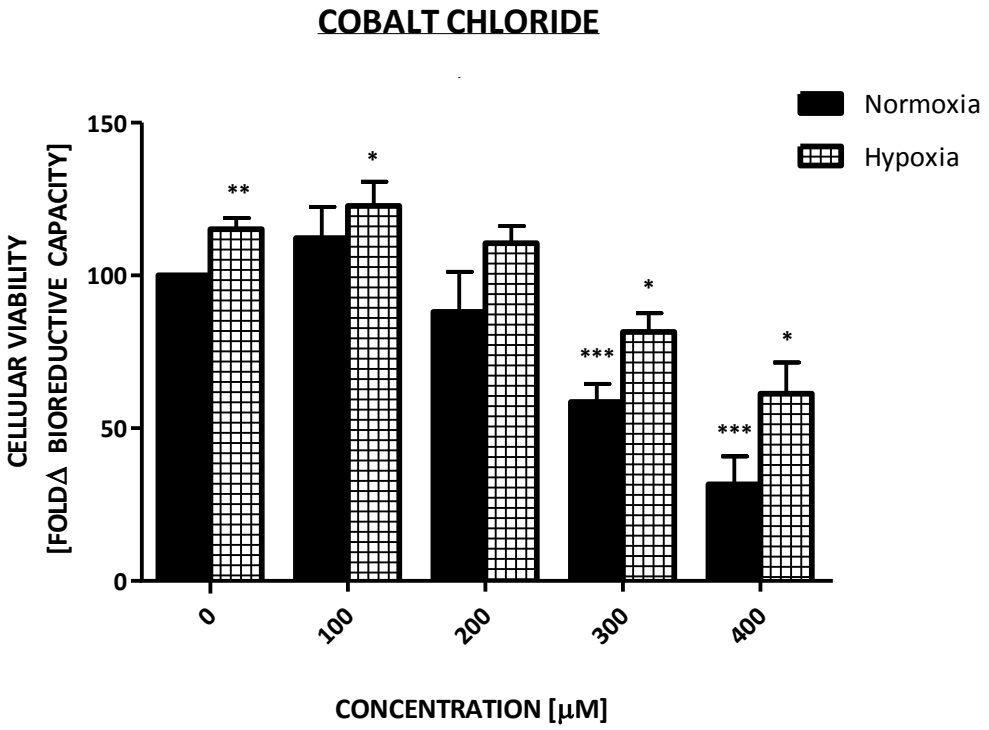


**Figure 3.1.2 The inhibitory effect on MCF-7 cells exposed to varying concentrations of cobalt chloride under normoxic and hypoxic conditions for 12 hours.** The MTT assay was employed to measure bioreductive capacity which indirectly indicates cellular viability. Values expressed as a percentage of the normoxic control (100%). *Columns*, mean survival fractions; *Bars*, ± SEM. The results are a representative of four independent experiments. * $p<0.05$ vs. normoxic control; ** $p<0.01$ vs. normoxic control; *** $p<0.0001$ vs. normoxic control.

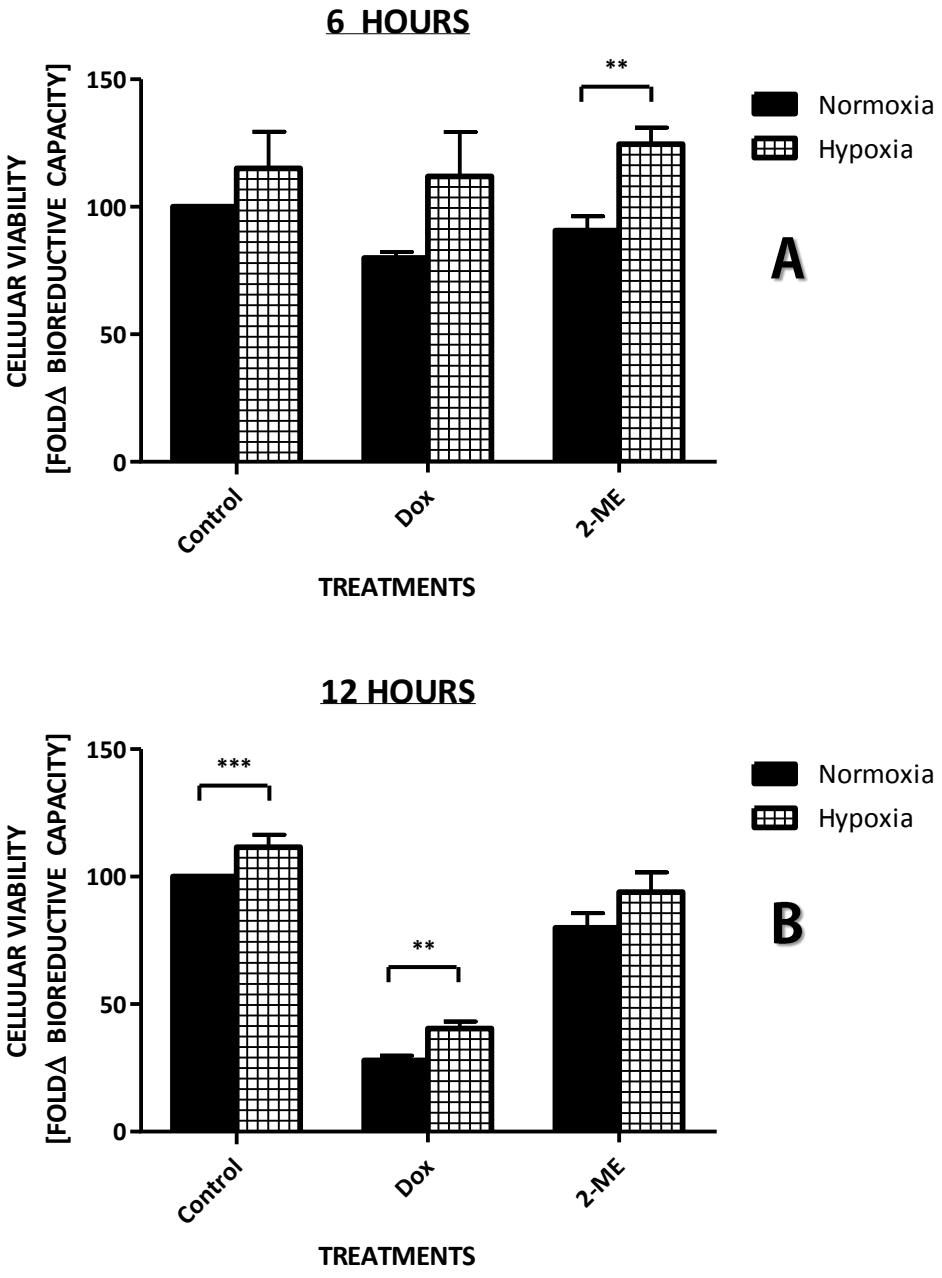


**Figure 3.2.1 The inhibitory effect on MCF-7 cells exposed to doxorubicin (1 μM) and 2-methoxyestradiol (10 μM) under normoxic and hypoxic conditions at different time points. (A) 6, and (B) 12 hours.** The MTT assay was employed to measure bioreductive capacity which indirectly indicates cellular viability. Values expressed as a percentage of the control (100%). *Columns*, mean survival fractions; *Bars*, ± SEM. The results are a representative of six independent experiments. ** $p<0.01$ vs. normoxic 2-ME (6 hours)/ normoxic doxorubicin (12 hours); *** $p<0.001$ vs. normoxic control.

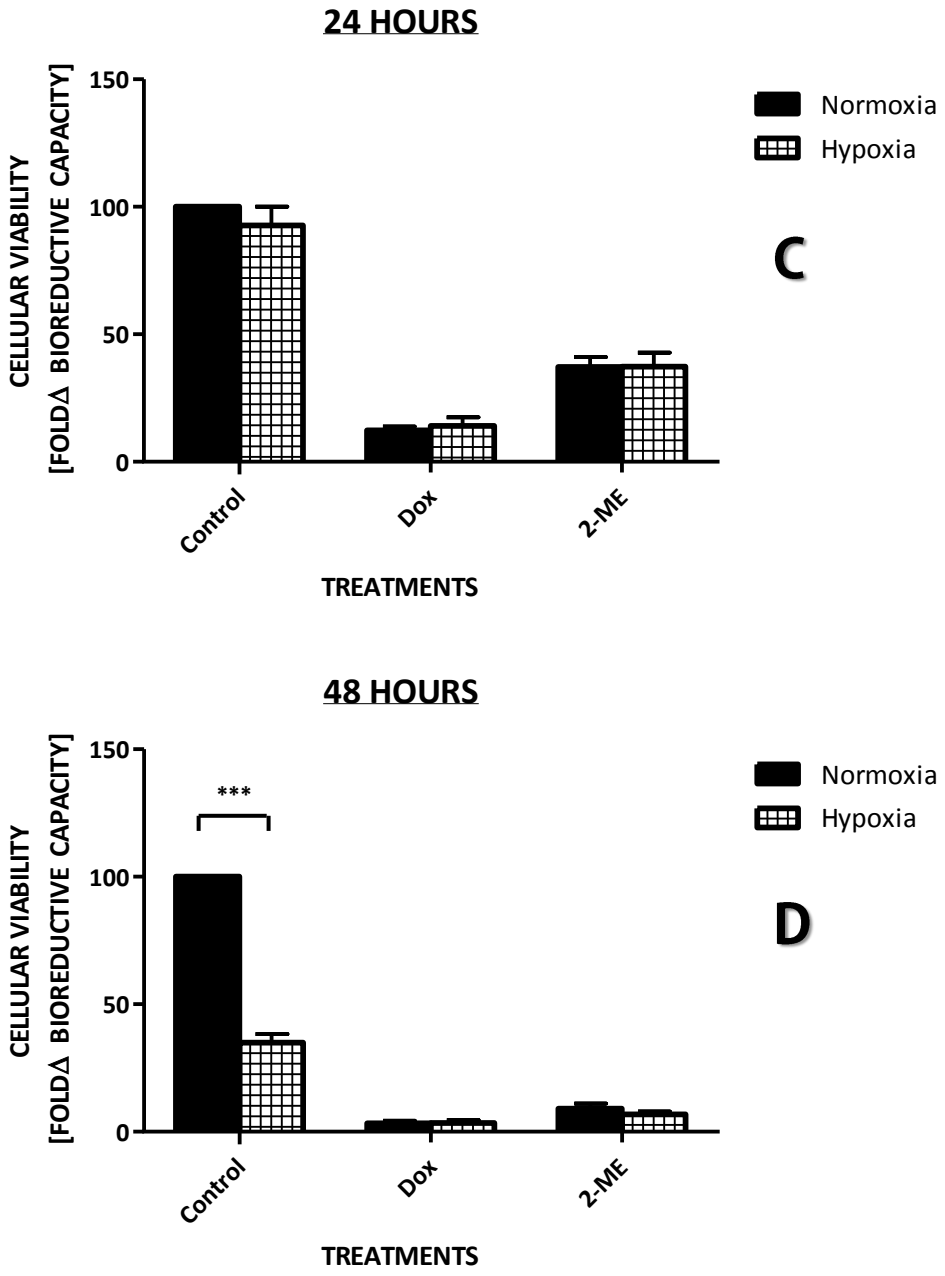


**Figure 3.2.2 The inhibitory effect on MCF-7 cells exposed to doxorubicin (1 μM) and 2-methoxyestradiol (10 μM) under normoxic and hypoxic conditions at different time points. (C) 24, and (D) 48 hours.** The MTT assay was employed to measure bioreductive capacity which indirectly indicates cellular viability. Values expressed as a percentage of the control (100%). *Columns*, mean survival fractions; *Bars*, ± SEM. The results are a representative of six independent experiments. *** $p<0.001$ vs. normoxic control.

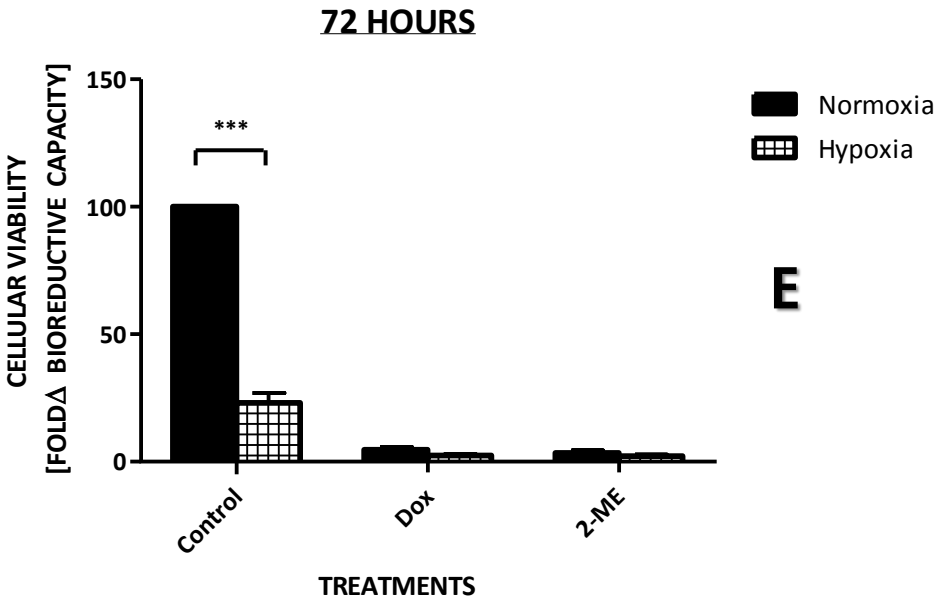


**Figure 3.2.3 The inhibitory effect on MCF-7 cells exposed to doxorubicin (1 μM) and 2-methoxyestradiol (10 μM) under normoxic and hypoxic conditions at different time points. (E) 72 hours.** The MTT assay was employed to measure bioreductive capacity which indirectly indicates cellular viability. Values expressed as a percentage of the control (100%). *Columns*, mean survival fractions; *Bars*, ± SEM. The results are a representative of six independent experiments. *** $p<0.001$ vs. normoxic control.

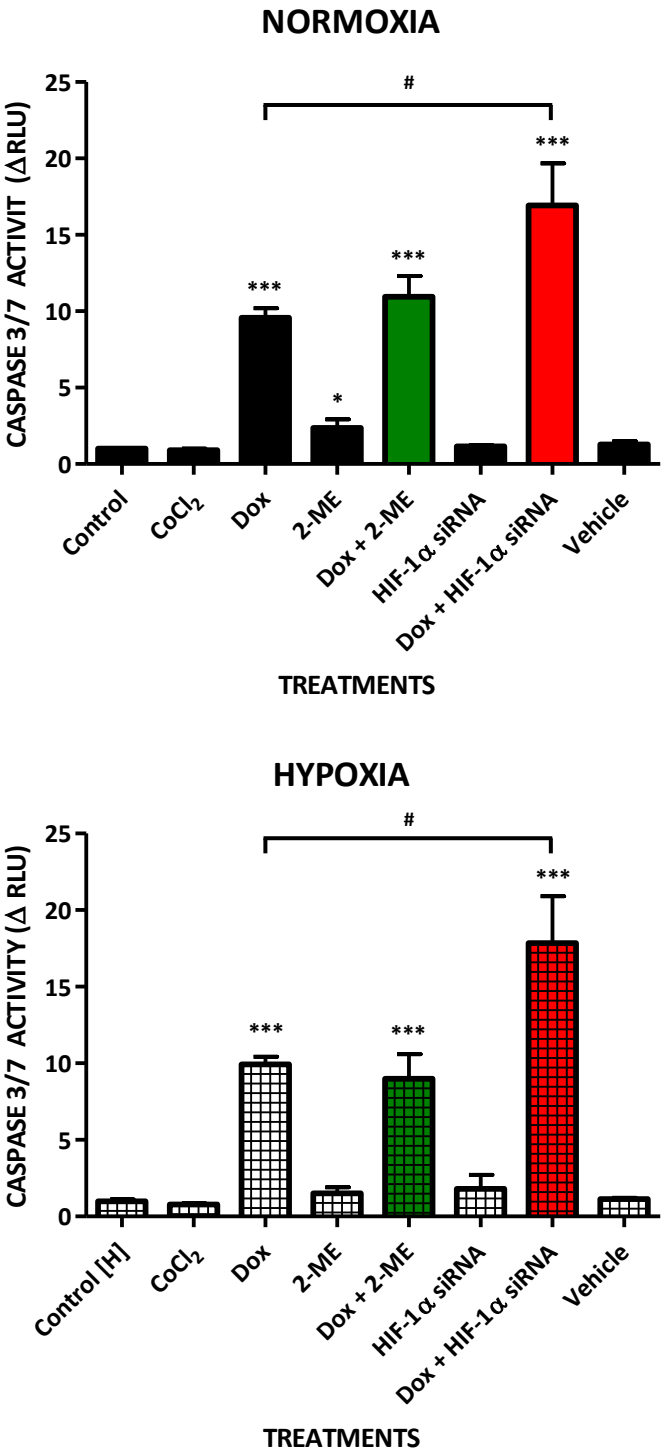


**Figure 3.3 The activity of caspase 3/7 in MCF-7 cells in response to the experimental regime.** Caspase 3/7 activity is directly proportional to the luminescent intensity produced. Values are expressed as a percentage of the normoxic control (100%). Columns, relative luminescence units (RLU); Bars, ± SEM. The results are a representative of six independent experiments. * $p<0.05$ vs. normoxic control; *** $p<0.001$ vs. normoxic control; # $p<0.05$ vs. normoxic doxorubicin.

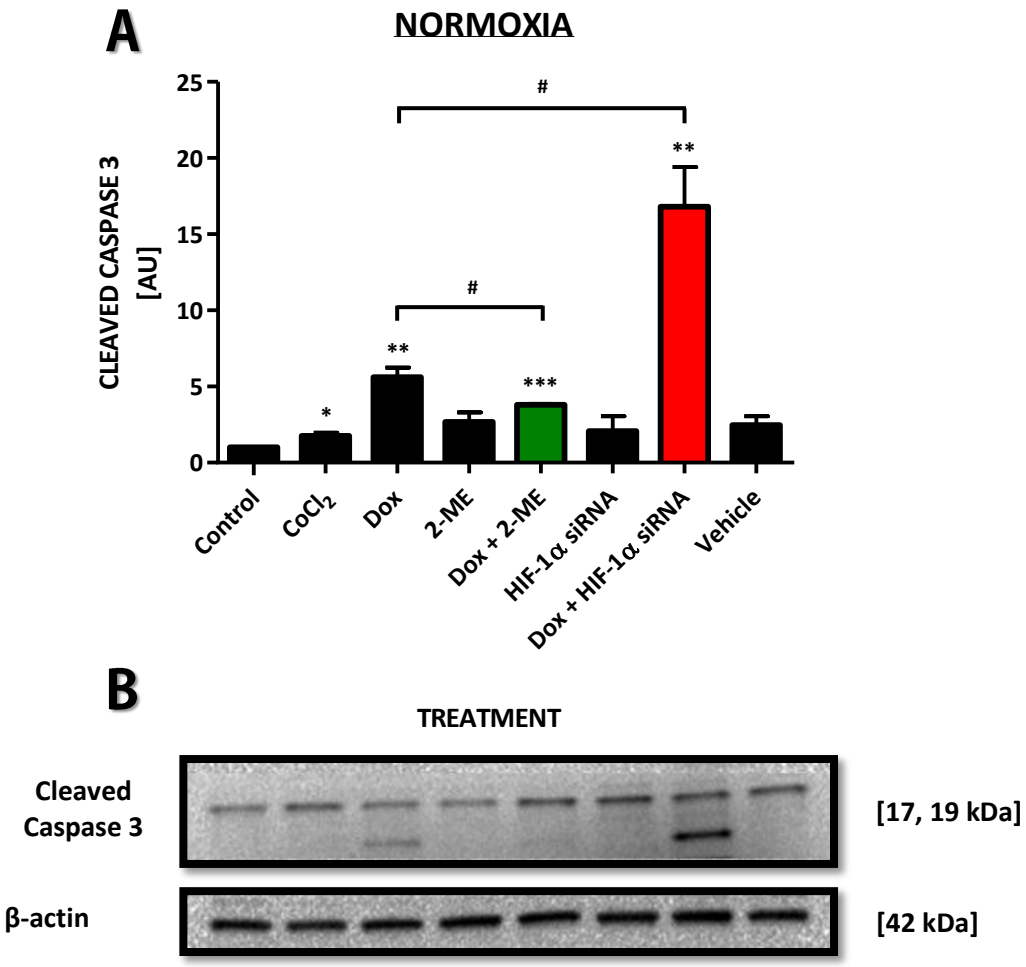


**Figure 3.4.1 The evaluation of the *in vitro* cleaved caspase 3 expression profile in response to the experimental regime under normoxic conditions.** The (**A**) densitometric analysis and (**B**) immunoblots are represented. A ratio was calculated relative to the control (set to 1). *Columns*, arbitrary units (AU); *Bars*, ± SEM. The results are a representative of three independent experiments. * $p<0.05$ vs. control; ** $p<0.01$ vs. control; *** $p<0.001$ vs. control; # $p<0.05$ vs. doxorubicin.

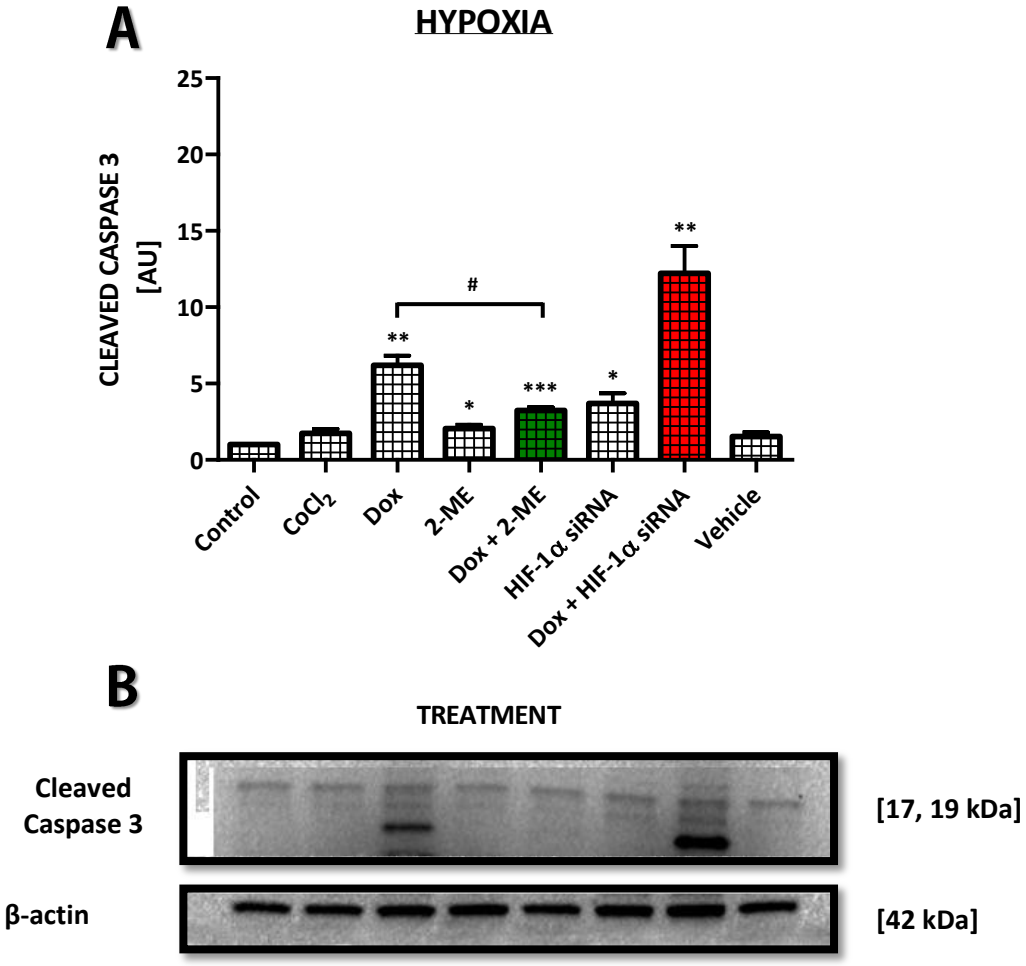


**Figure 3.4.2 The evaluation of the *in vitro* cleaved caspase 3 expression profile in response to the experimental regime under hypoxic conditions.** The (**A**) densitometric analysis and (**B**) immunoblots are represented. A ratio was calculated relative to the control (set to 1). Columns, arbitrary units (AU); Bars, ± SEM. The results are a representative of three independent experiments. * $p<0.05$ vs. control; ** $p<0.01$ vs. control; *** $p<0.001$ vs. control; # $p<0.05$ vs. doxorubicin.

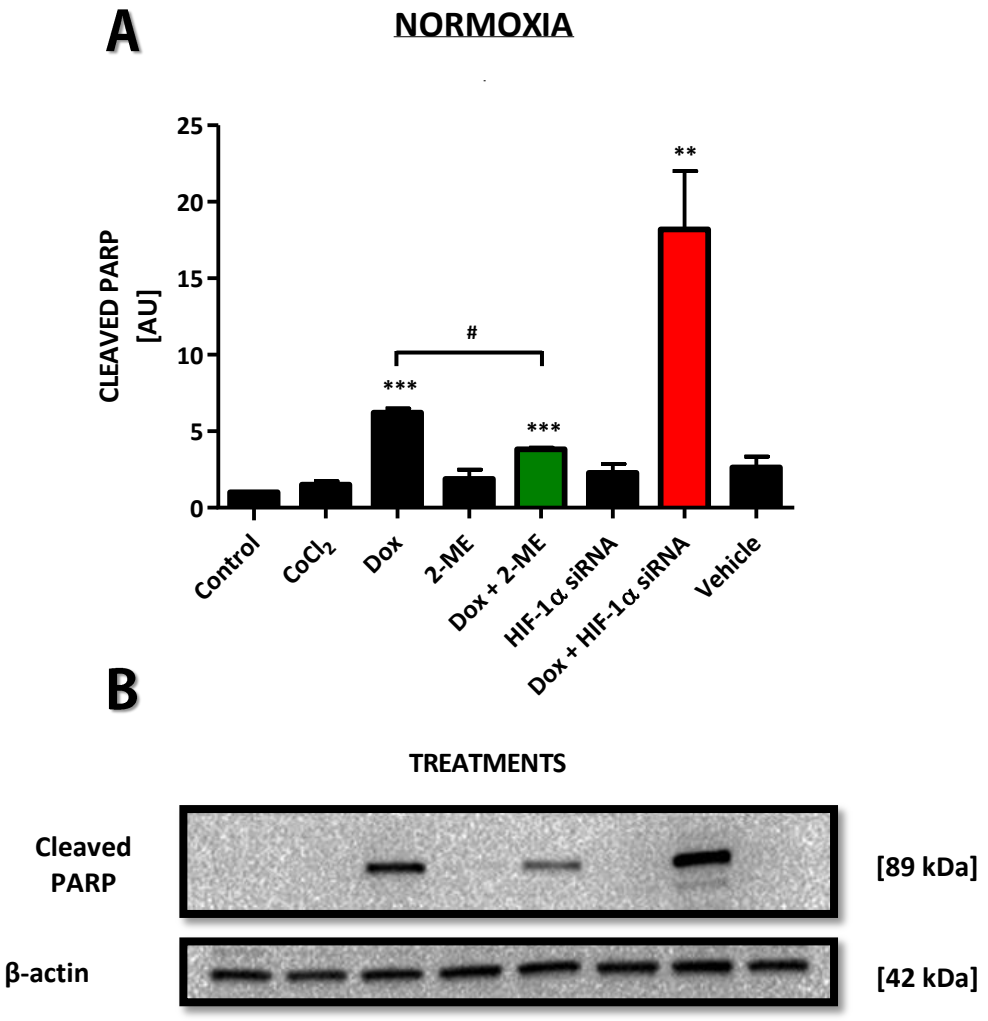


**Figure 3.5.1 The evaluation of the *in vitro* cleaved PARP expression profile in response to the experimental regime under normoxic conditions.** The (**A**) densitometric analysis and (**B**) immunoblots are represented. A ratio was calculated relative to the control (set to 1). Columns, arbitrary units (AU); Bars, ± SEM. The results are a representative of three independent experiments. ** p<0.01 vs. control; *** p<0.001 vs. control; # p<0.05 vs. doxorubicin.

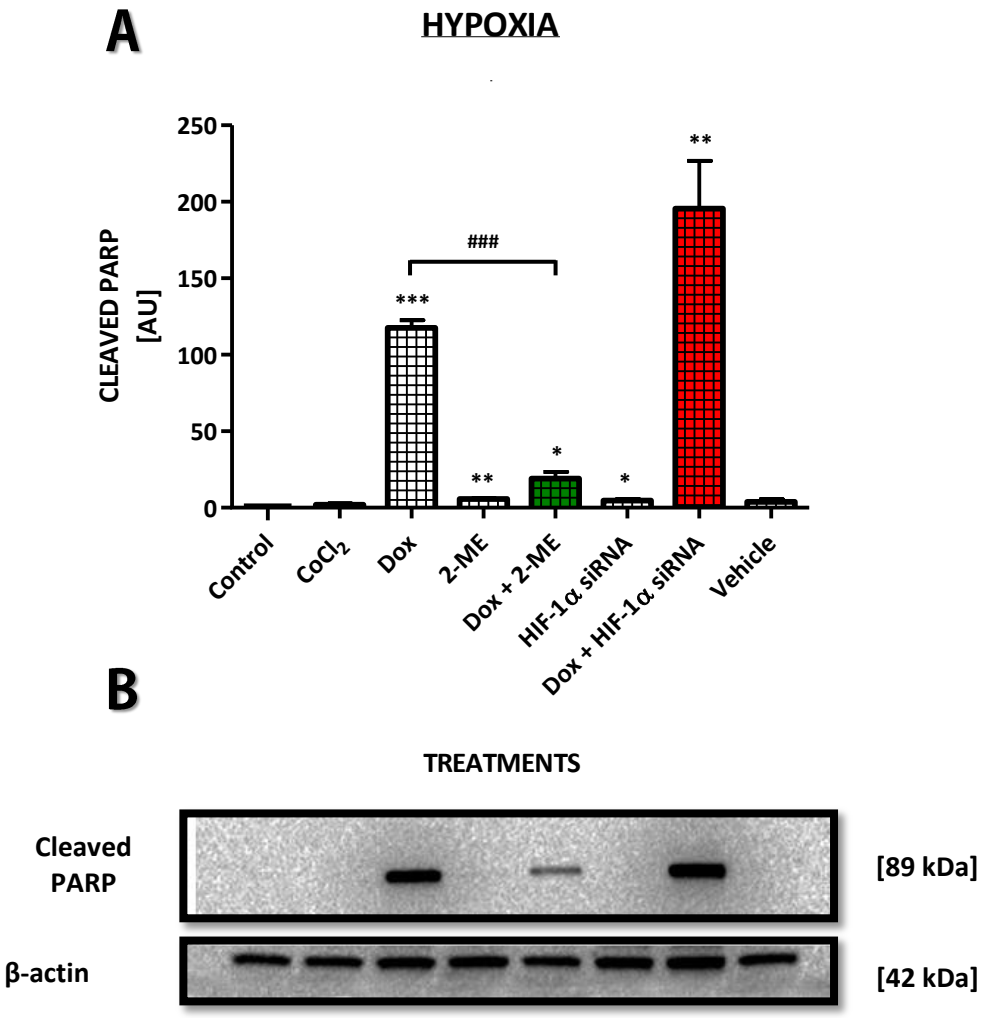


**Figure 3.5.2 The evaluation of the *in vitro* cleaved PARP expression profile in response to the experimental regime under hypoxic conditions.** The (**A**) densitometric analysis and (**B**) immunoblots are represented. A ratio was calculated relative to the control (set to 1). *Columns*, arbitrary units (AU); *Bars*, ± SEM. The results are a representative of three independent experiments. * $p<0.05$ vs. control; ** $p<0.01$ vs. control; *** $p<0.001$ vs. control; ### $p<0.001$ vs. doxorubicin.

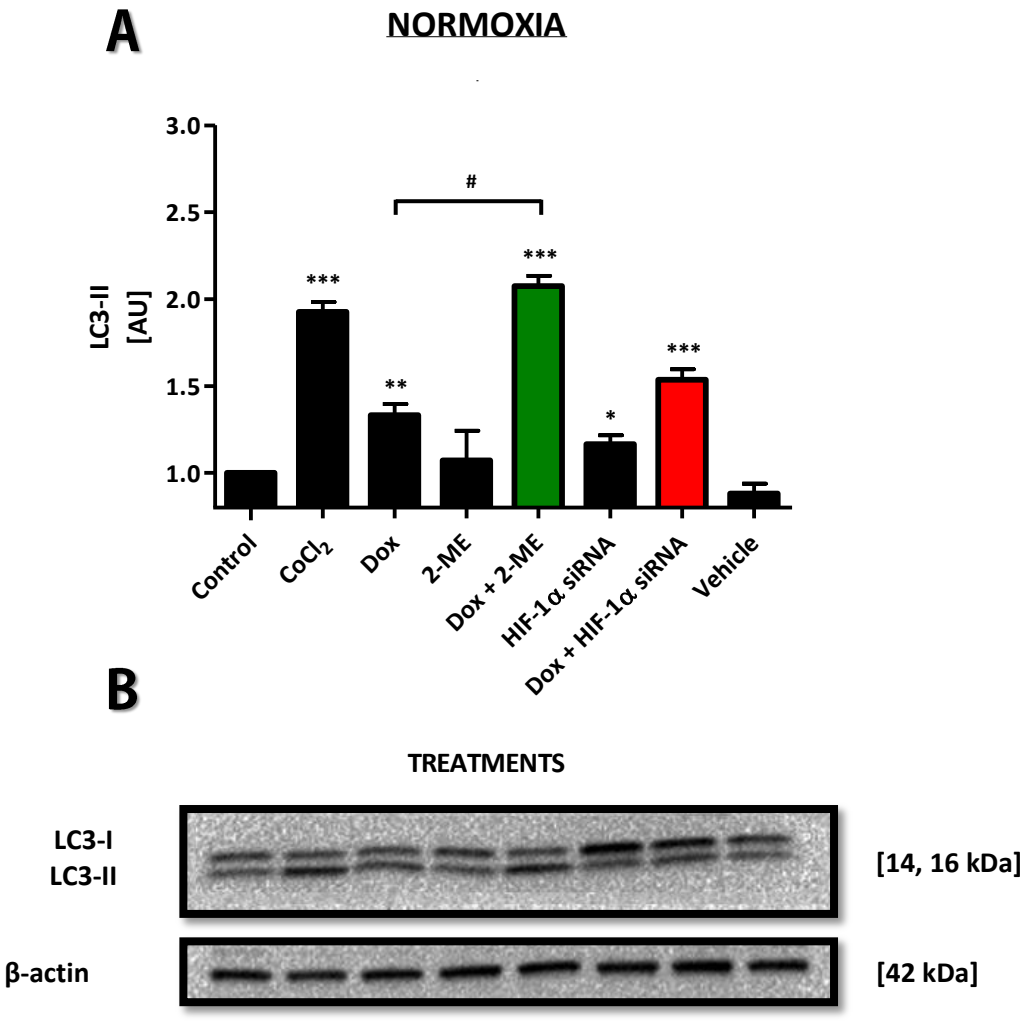


**Figure 3.6.1 The evaluation of the *in vitro* LC3-II expression profile in response to the experimental regime under normoxic conditions.** The (**A**) densitometric analysis and (**B**) immunoblots are represented. A ratio was calculated relative to the control (set to 1). Columns, arbitrary units (AU); Bars, ± SEM. The results are a representative of three independent experiments. * $p<0.05$ vs. control; ** $p<0.01$ vs. control; *** $p<0.001$ vs. control; # $p<0.05$ vs. doxorubicin.

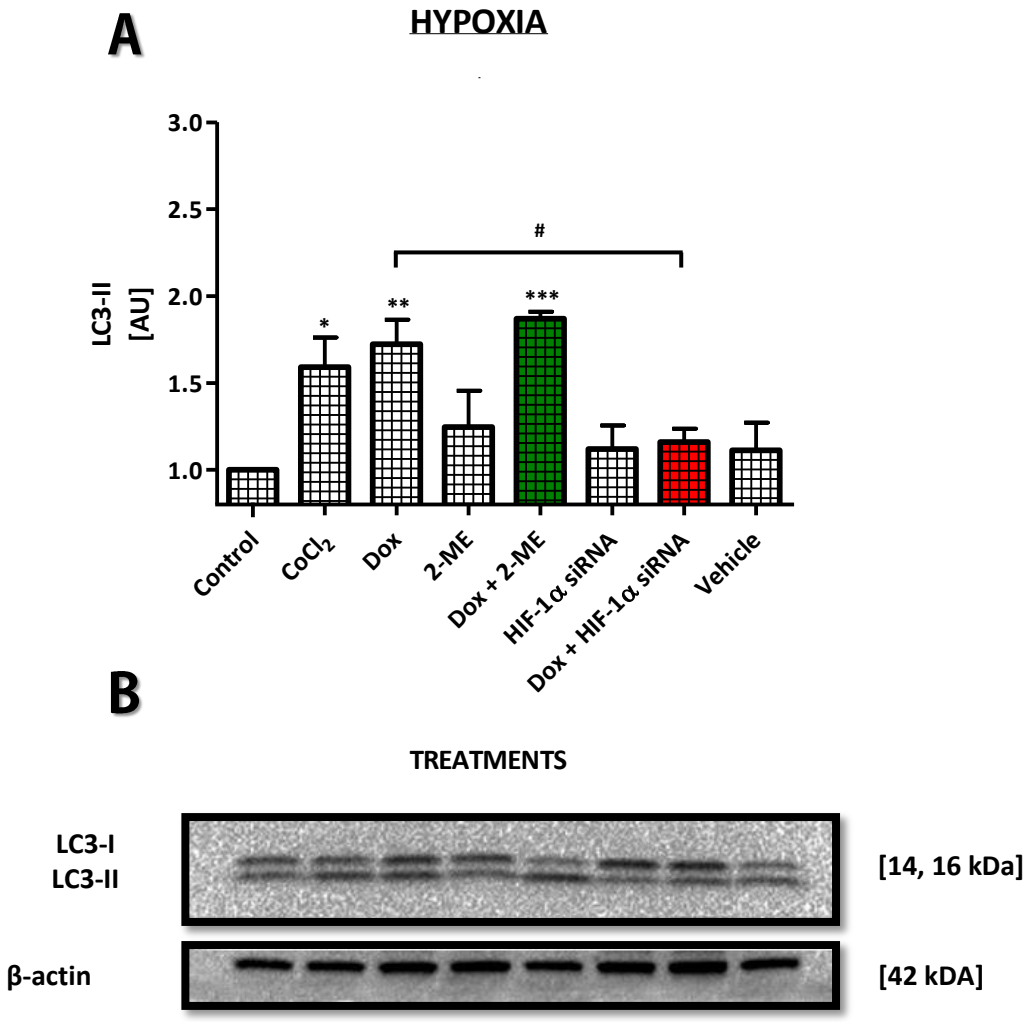


**Figure 3.6.2 The evaluation of the *in vitro* cleaved LC3-II expression profile in response to the experimental regime under hypoxic conditions.** The (**A**) densitometric analysis and (**B**) immunoblots are represented. A ratio was calculated relative to the control (set to 1). Columns, arbitrary units (AU); Bars, ± SEM. The results are a representative of three independent experiments. * $p<0.05$ vs. control; ** $p<0.01$ vs. control; *** $p<0.001$ vs. control; # $p<0.05$ vs. doxorubicin.

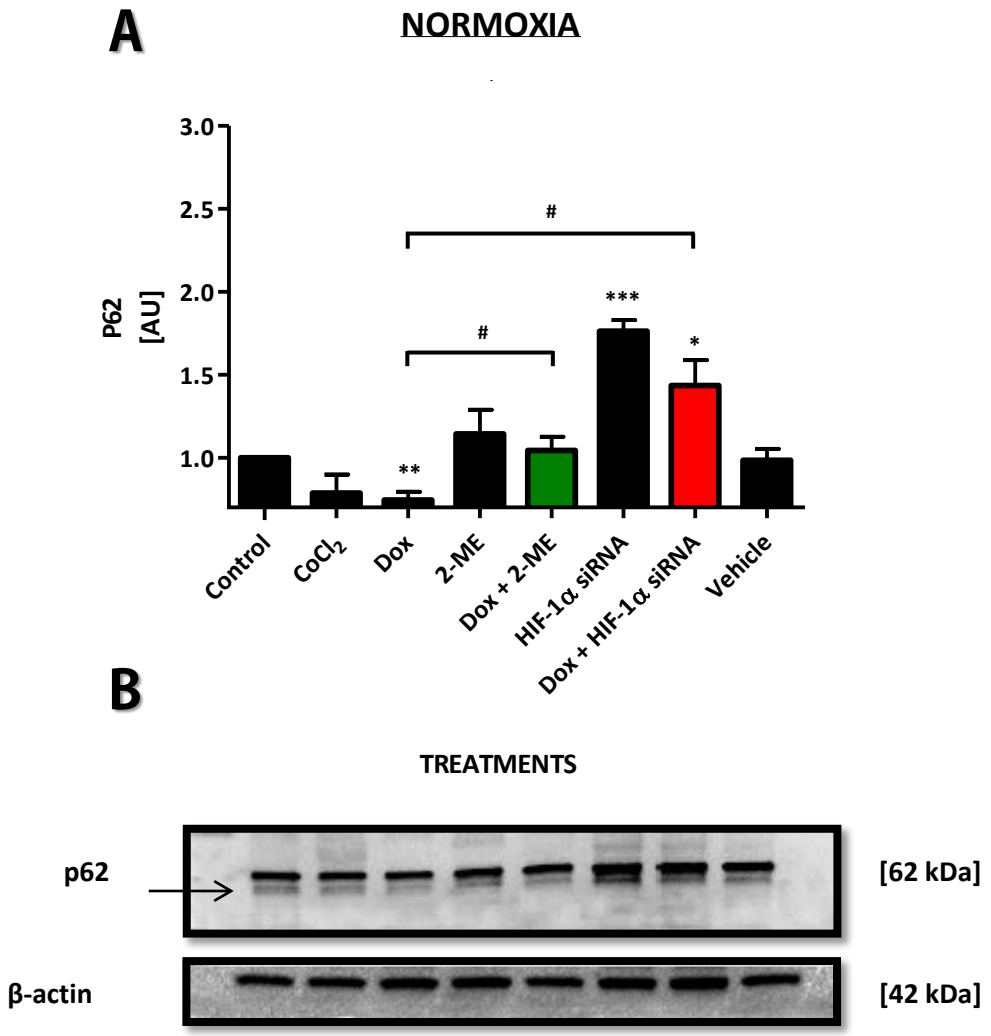


**Figure 3.7.1 The evaluation of the *in vitro* p62 expression profile in response to the experimental regime under normoxic conditions.** The (**A**) densitometric analysis and (**B**) immunoblots are represented. A ratio was calculated relative to the control (set to 1). Columns, arbitrary units (AU); Bars, ± SEM. The results are a representative of three independent experiments. * $p<0.05$ vs. control; ** $p<0.01$ vs. control; *** $p<0.001$ vs. control; # $p<0.05$ vs. doxorubicin.

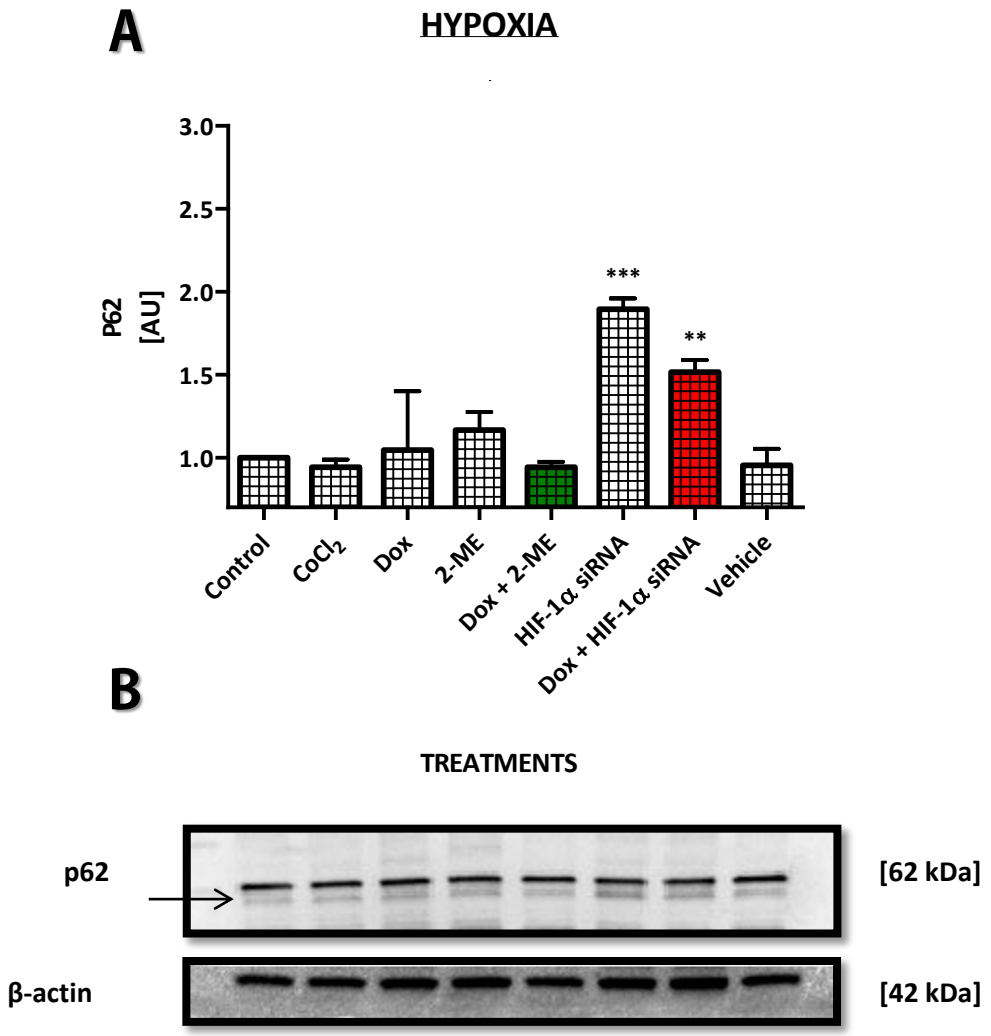


**Figure 3.7.2 The evaluation of the *in vitro* p62 expression profile in response to the experimental regime under hypoxic conditions.** The (**A**) densitometric analysis and (**B**) immunoblots are represented. A ratio was calculated relative to the control (set to 1). Columns, arbitrary units (AU); Bars, ± SEM. The results are a representative of three independent experiments. ** $p<0.01$ vs. control; *** $p<0.001$ vs. control.

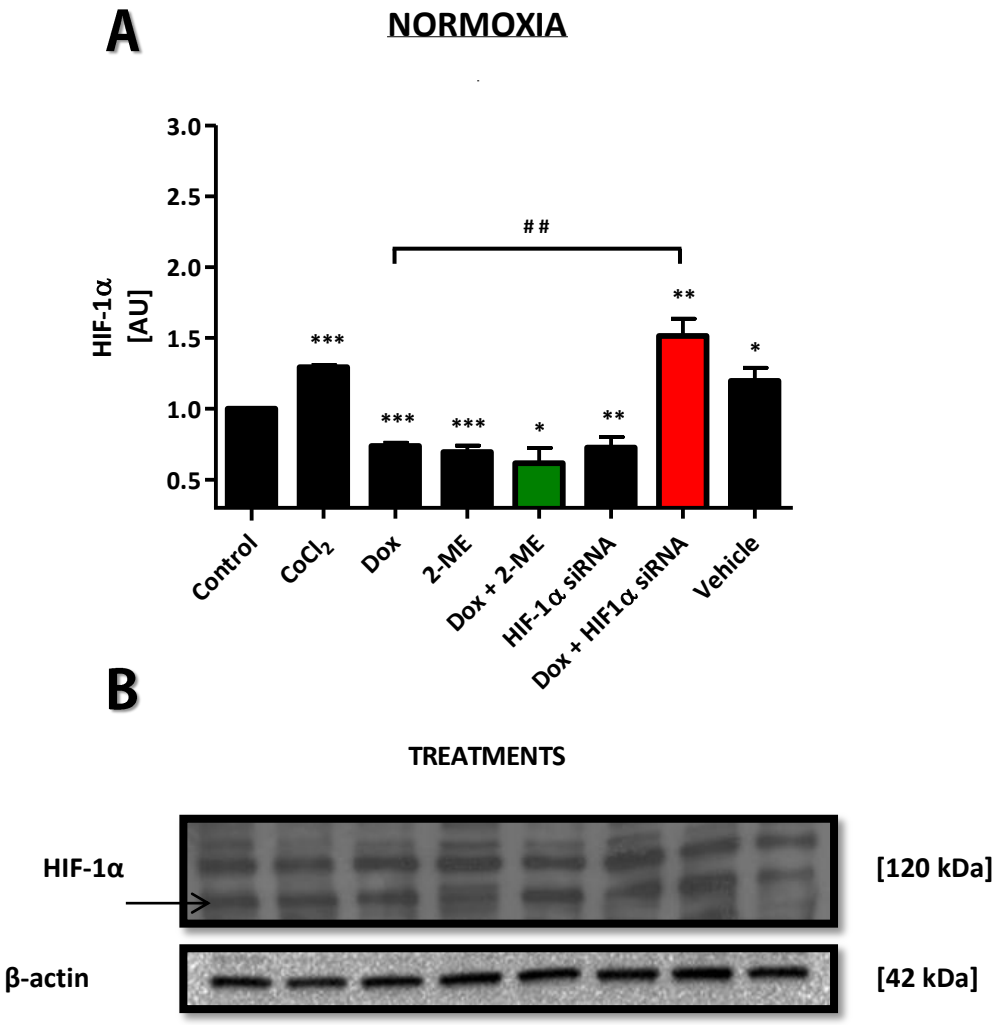


**Figure 3.8.1 The evaluation of the *in vitro* HIF-1α expression profile in response to the experimental regime under normoxic conditions.** The (**A**) densitometric analysis and (**B**) immunoblots are represented. A ratio was calculated relative to the control (set to 1). Columns, arbitrary units (AU); Bars, ± SEM. The results are a representative of three independent experiments. * $p<0.05$ vs. control; ** $p<0.01$ vs. control; *** $p<0.001$ vs. control; ## $p<0.01$ vs. doxorubicin.

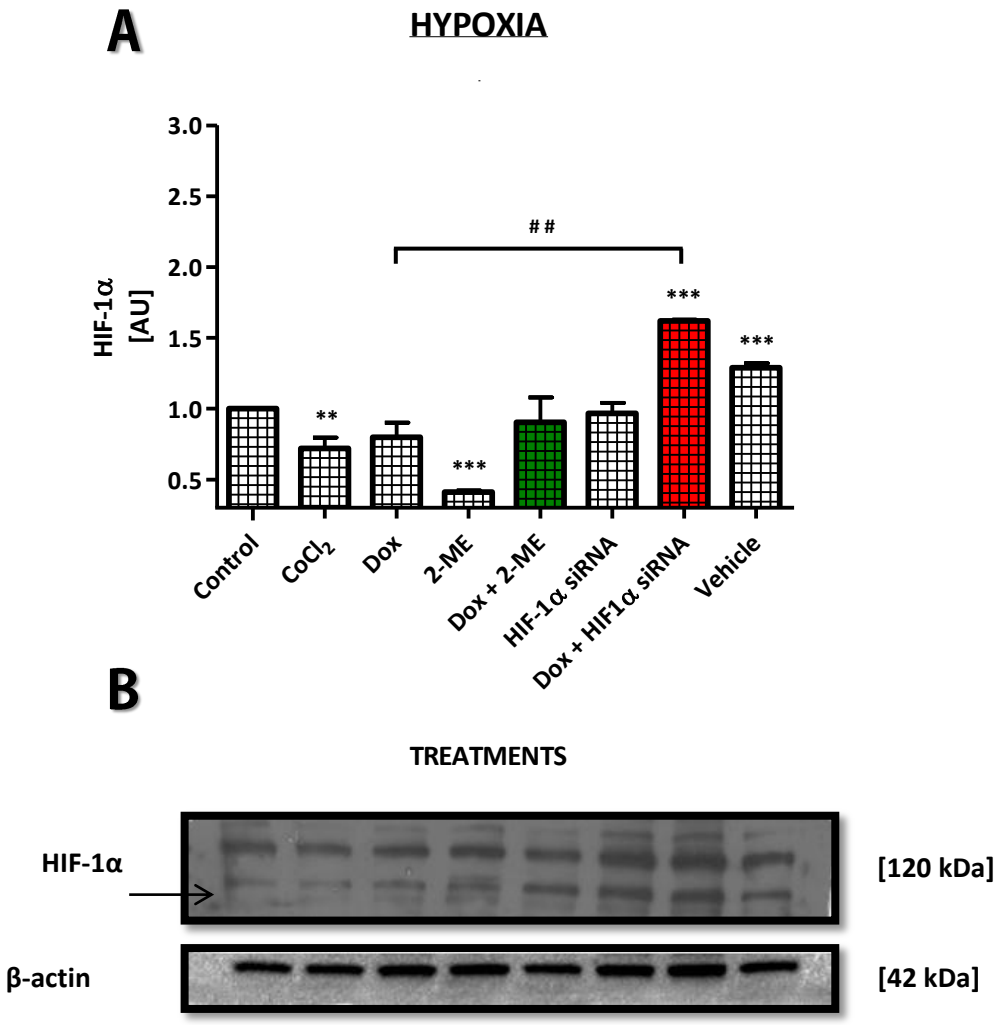


**Figure 3.8.2 The evaluation of the *in vitro* HIF-1α expression profile in response to the experimental regime under hypoxic conditions.** The (**A**) densitometric analysis and (**B**) immunoblots are represented. A ratio was calculated relative to the control (set to 1). Columns, arbitrary units (AU); Bars, ± SEM. The results are a representative of three independent experiments. ** p<0.01 vs. control; *** p<0.001 vs. control; ## p<0.01 vs. doxorubicin.

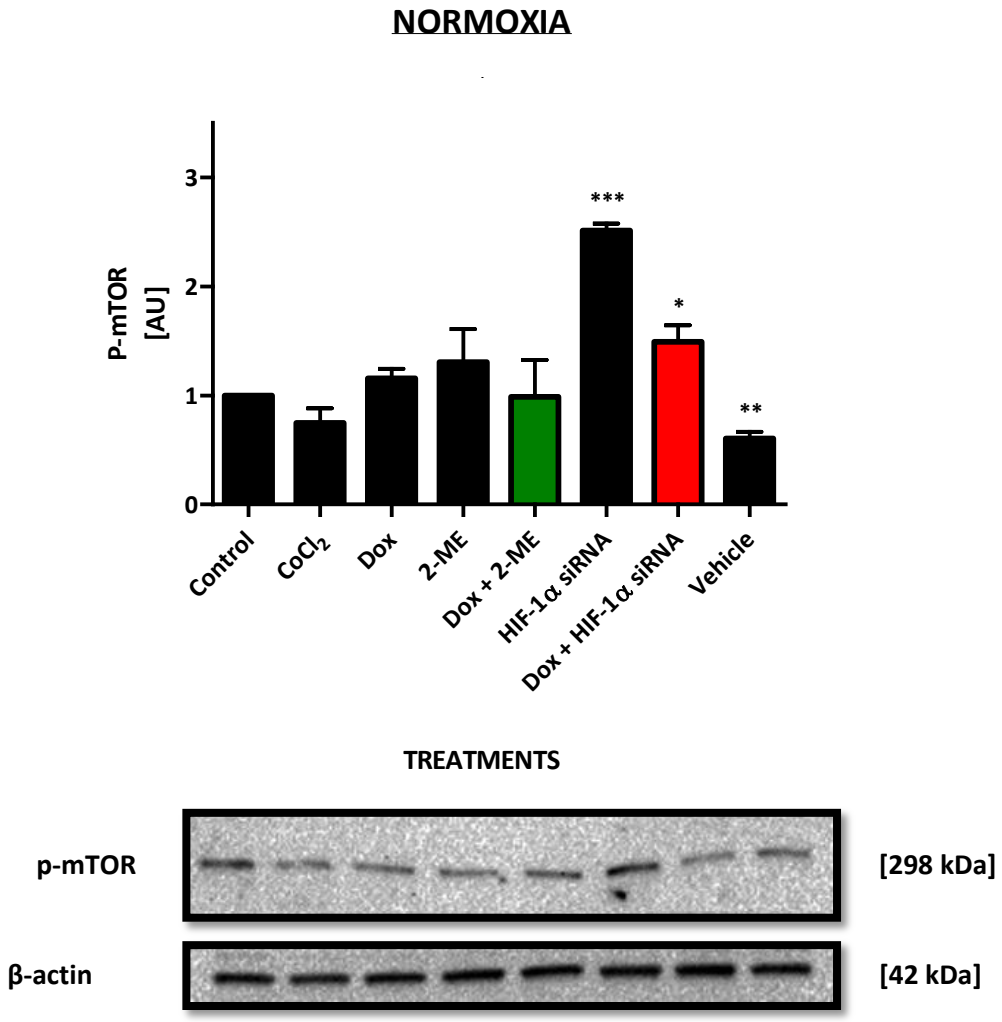


**Figure 3.9.1 The evaluation of the *in vitro* p-mTOR expression profile in response to the experimental regime under normoxic conditions.** The (**A**) densitometric analysis and (**B**) immunoblots are represented. A ratio was calculated relative to the control (set to 1). Columns, arbitrary units (AU); Bars, ± SEM. The results are a representative of three independent experiments. * $p<0.05$ vs. control; ** $p<0.01$ vs. control; *** $p<0.001$ vs. control.

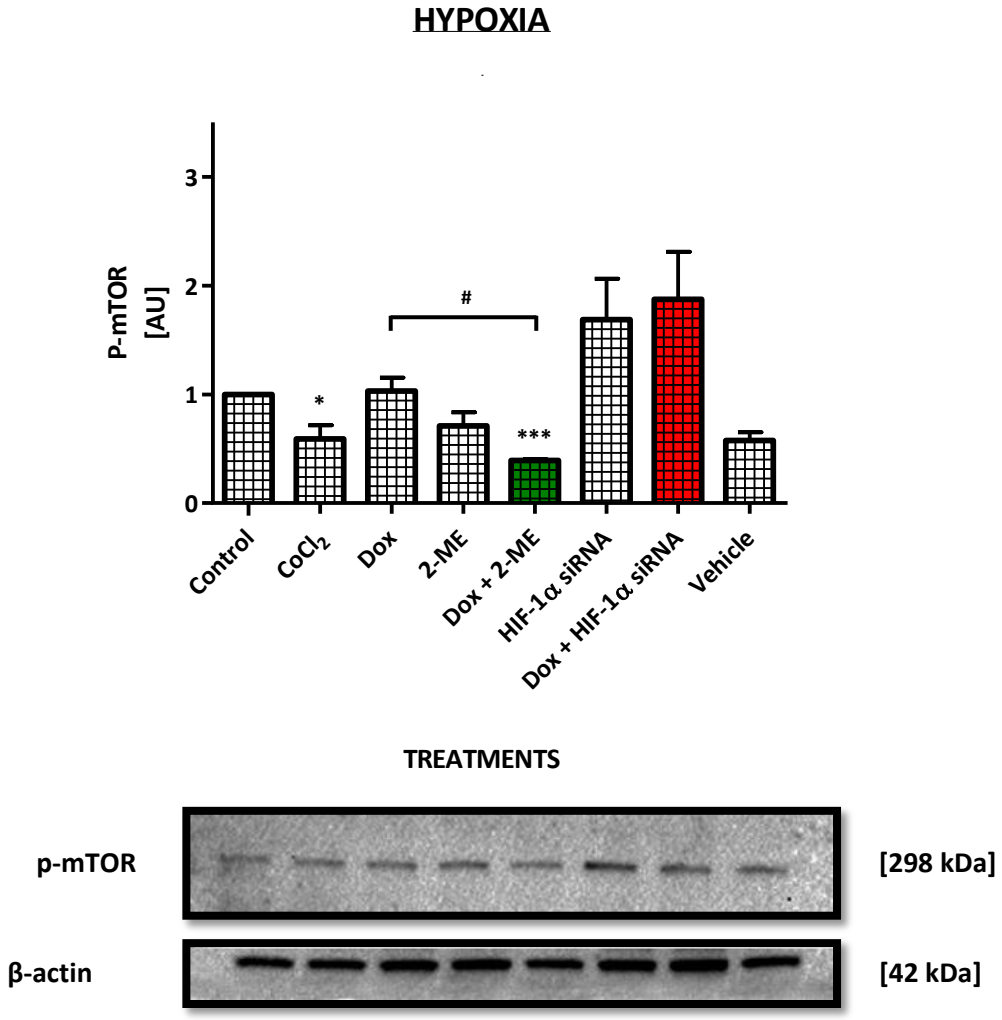


**Figure 3.9.2 The evaluation of the *in vitro* p-mTOR expression profile in response to the experimental regime under hypoxic conditions.** The (**A**) densitometric analysis and (**B**) immunoblots are represented. A ratio was calculated relative to the control (set to 1). Columns, arbitrary units (AU); Bars, ± SEM. The results are a representative of three independent experiments. * $p<0.05$ vs. control; *** $p<0.001$ vs. control; # $p<0.05$ vs. doxorubicin.

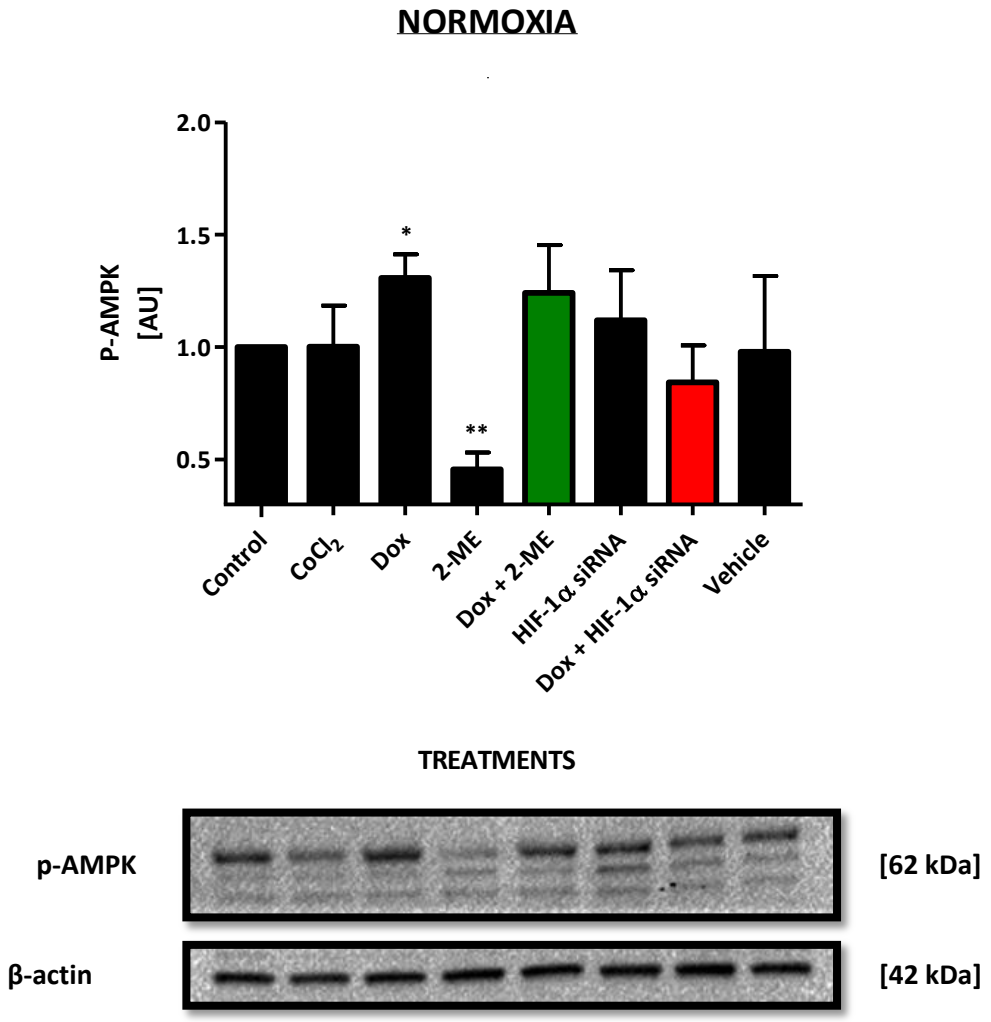


**Figure 3.10.1 The evaluation of the *in vitro* p-AMPK expression profile in response to the experimental regime under normoxia conditions.** The (**A**) densitometric analysis and (**B**) immunoblots are represented. A ratio was calculated relative to the control (set to 1). Columns, arbitrary units (AU); Bars, ± SEM. The results are a representative of three independent experiments. * p< 0.05 vs. control; ** p<0.01 vs. control.

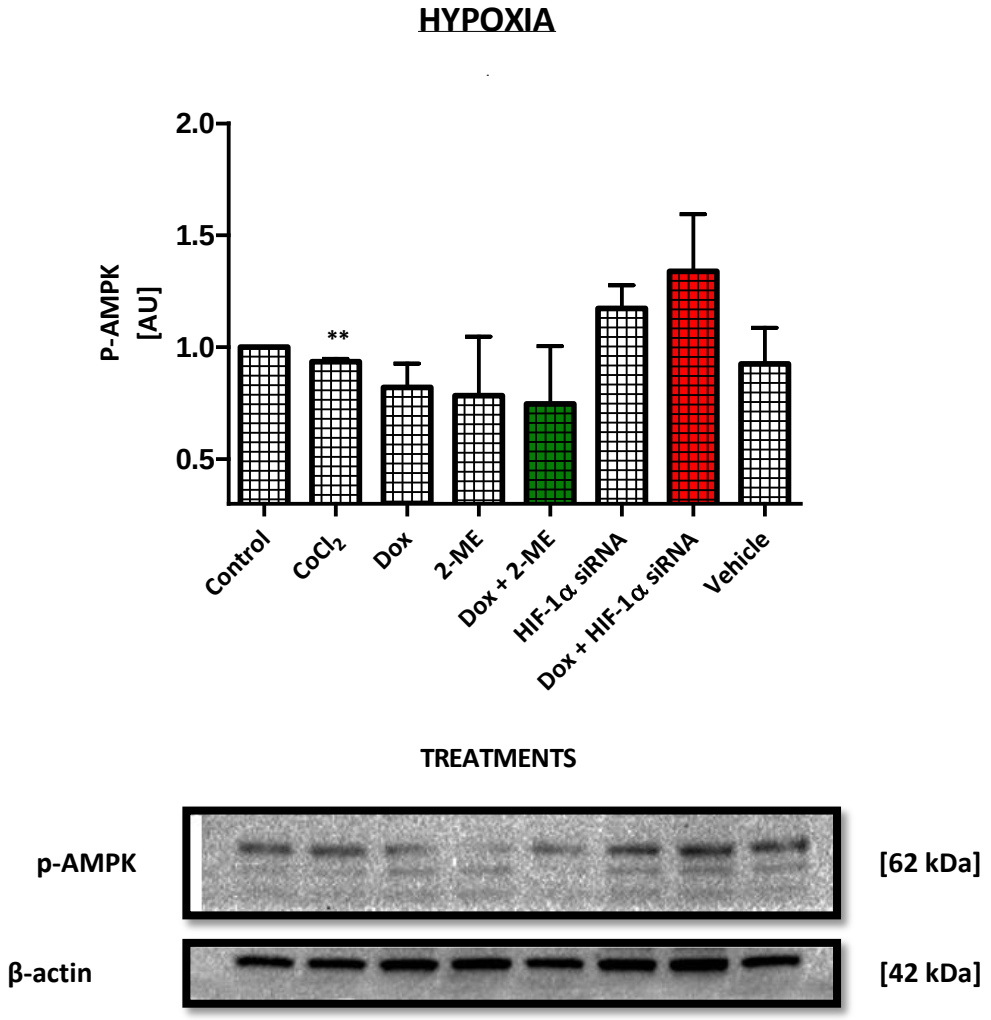


**Figure 3.10.2 The evaluation of the *in vitro* p-AMPK expression profile in response to the experimental regime under hypoxic conditions.** The (**A**) densitometric analysis and (**B**) immunoblots are represented. A ratio was calculated relative to the control (set to 1). Columns, arbitrary units (AU); Bars, ± SEM. The results are a representative of three independent experiments. ** $p<0.01$ vs. control.

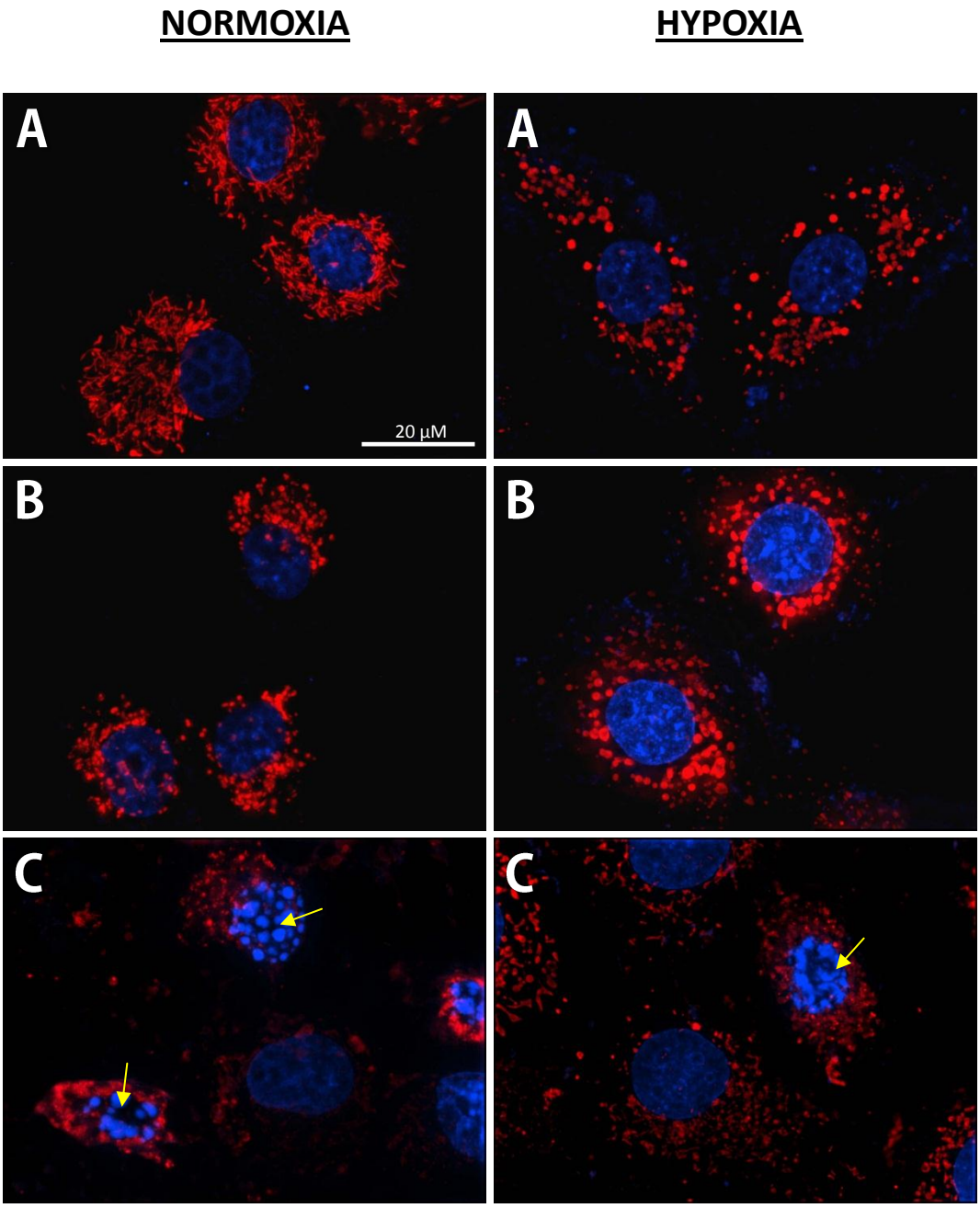


**Figure 3.11.1 Fluorescent imaging for the characterization of mitochondrial integrity of MCF-7 cells in response to the experimental regime.** Following the treatment regime, mitochondria were labelled with MitoTracker® Red CMXRos (1mM; displayed in red), while nuclei were counter-stained with Hoechst 33342 (1:200; dispayed in blue). Stained organelles within the MCF-7 cells were viewed with the Olympus IX81 inverted fluorescent microscope using a 100X objective and representative images captured with an F-view-II cooled CCD camera. The treatment groups were as follows: (**A**) control, (**B**) $CoCl_2$ (100 µM) (**C**) doxorubicin (1 µM). Condensed and fragmented nuclei are pointed by yellow arrows.

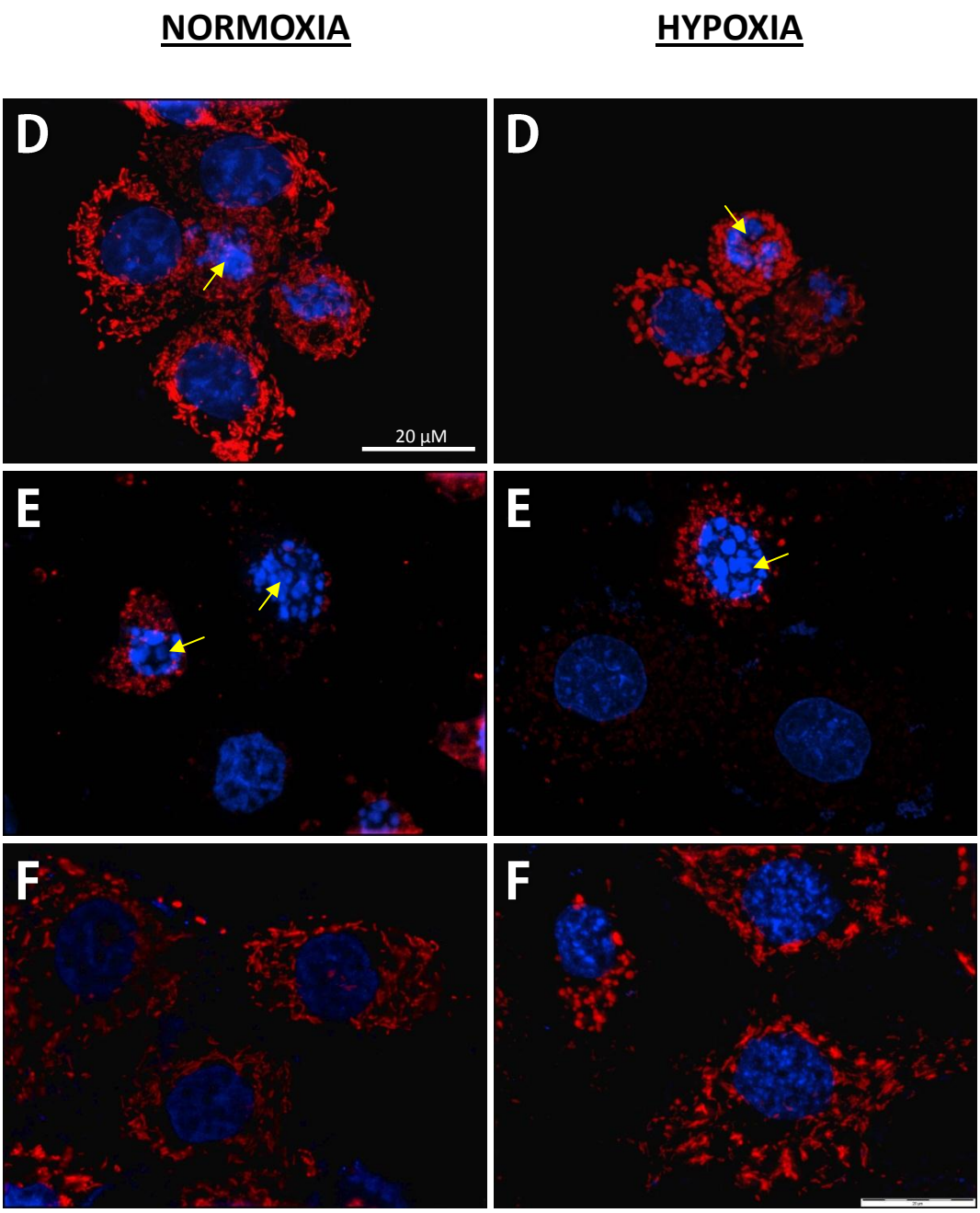


**Figure 3.11.2 Fluorescent imaging for the characterization of mitochondrial integrity of MCF-7 cells in response to the experimental regime.** Continued. (**D**) 2-methoxyestradiol (10 µM), (**E**) doxorubicin and 2-methoxyestradiol, (**F**) HIF-1α siRNA (400 nM). Condensed and fragmented nuclei are pointed by yellow arrows.

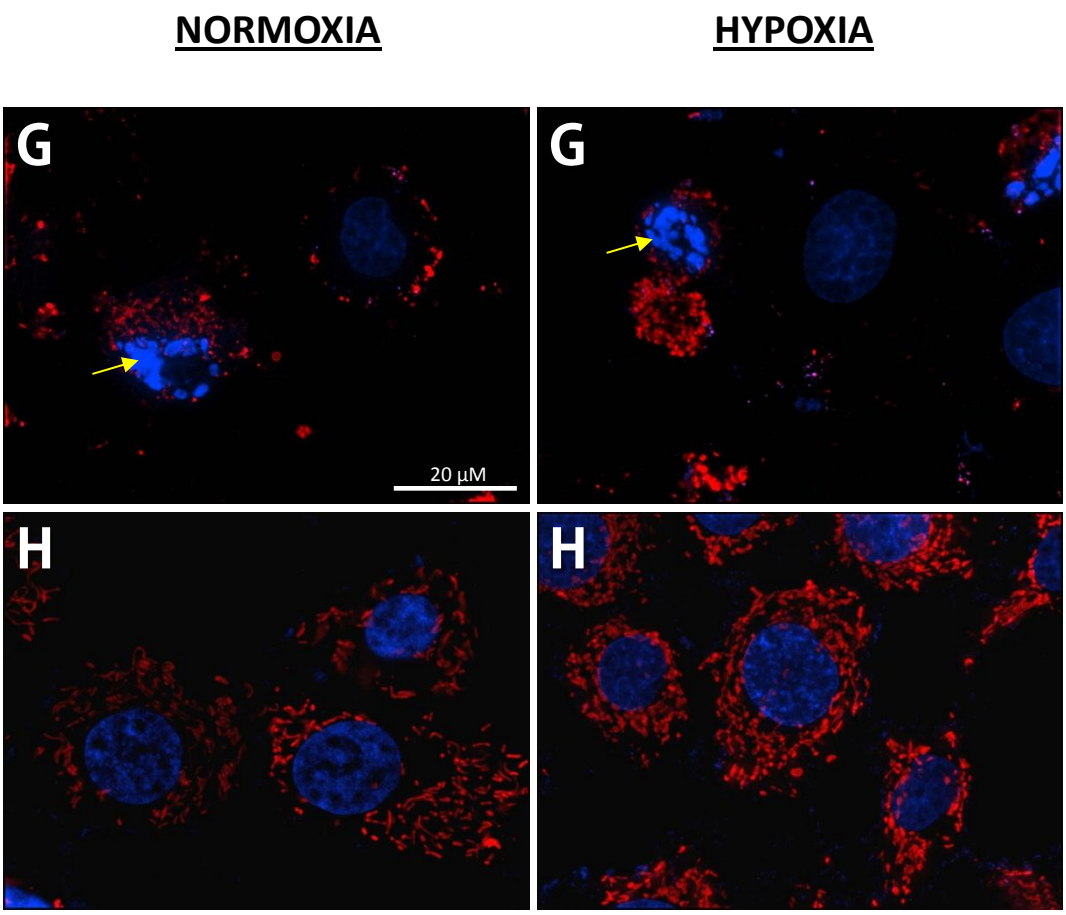


**Figure 3.11.3 Fluorescent imaging for the characterization of mitochondrial integrity of MCF-7 cells in response to the experimental regime.** Continued. (**G**) doxorubicin and HIF-1α siRNA, and (**H**) vehicle. Condensed and fragmented nuclei are pointed by yellow arrows.

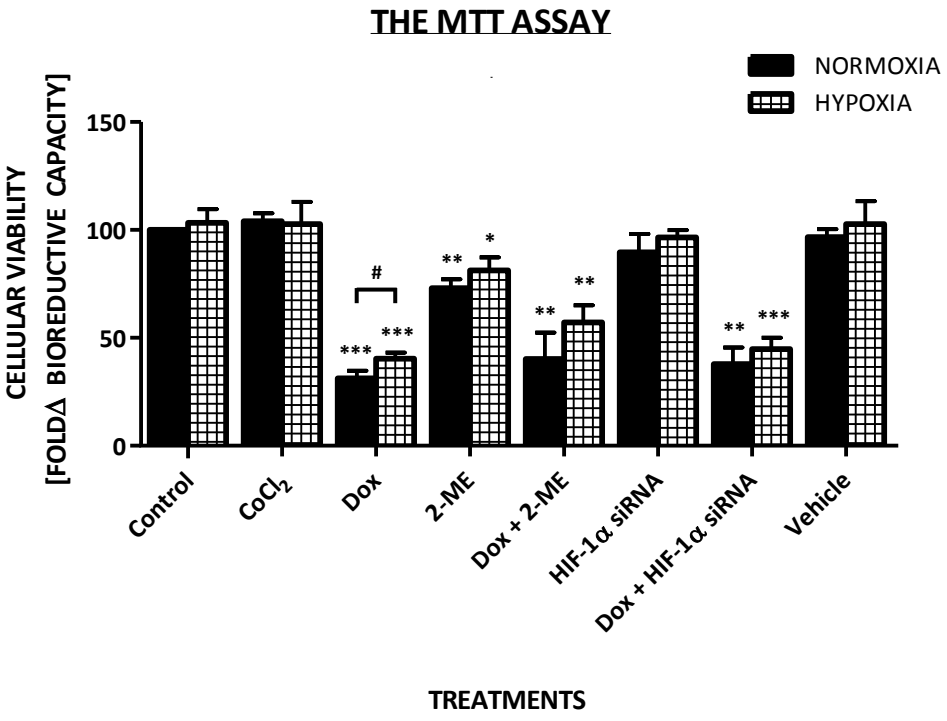


**Figure 3.12 The bioreductive capacity of MCF-7 cells in response to the experimental regime.** The MTT assay was employed to measure the capacity of MCF-7 cells to reduce the MTT salt to formazan crystals. Values expressed as a percentage of the control (100%). Columns, mean survival fractions; Bars, ± SEM. The results are a representative of four independent experiments. * $p<0.05$ vs. normoxic control; ** $p< 0.01$ vs. normoxic control; *** $p<0.001$ vs. normoxic control; # $p<0.05$ vs. normoxic doxorubicin.

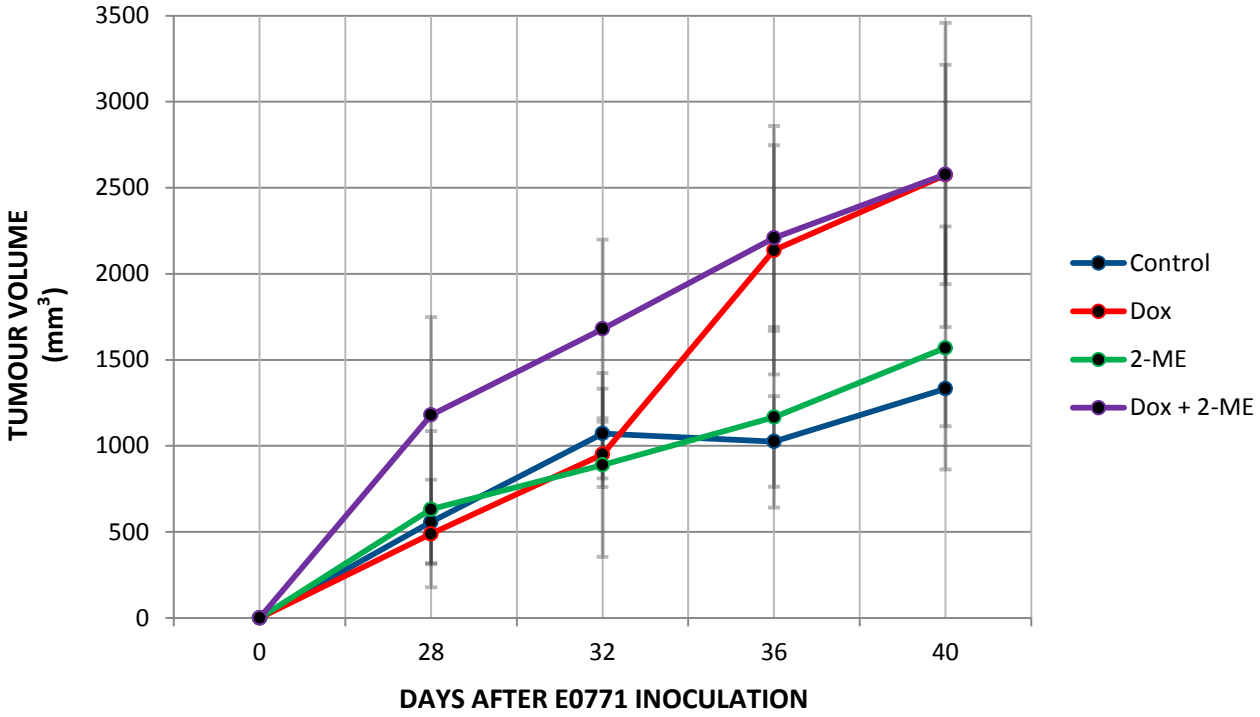


**Figure 3.13 The effect of the treatment regime on the rate of tumour growth for a duration of 14 days.** Day of E0771 inoculation was designated as 0. When tumours became palpable on day 28, mice were randomly sorted according to tumour size and grouped into: untreated control ( ), 5 mg/kg$^{-1}$ of doxorubicin ( ), 45 mg/kg$^{-1}$ of 2-methoxyestradiol ( ), and doxorubicin & 2-methoxyestradiol combined ( ). Treatment commenced from day 28 and was administered every four days, with each mouse receiving a total of four treatments.

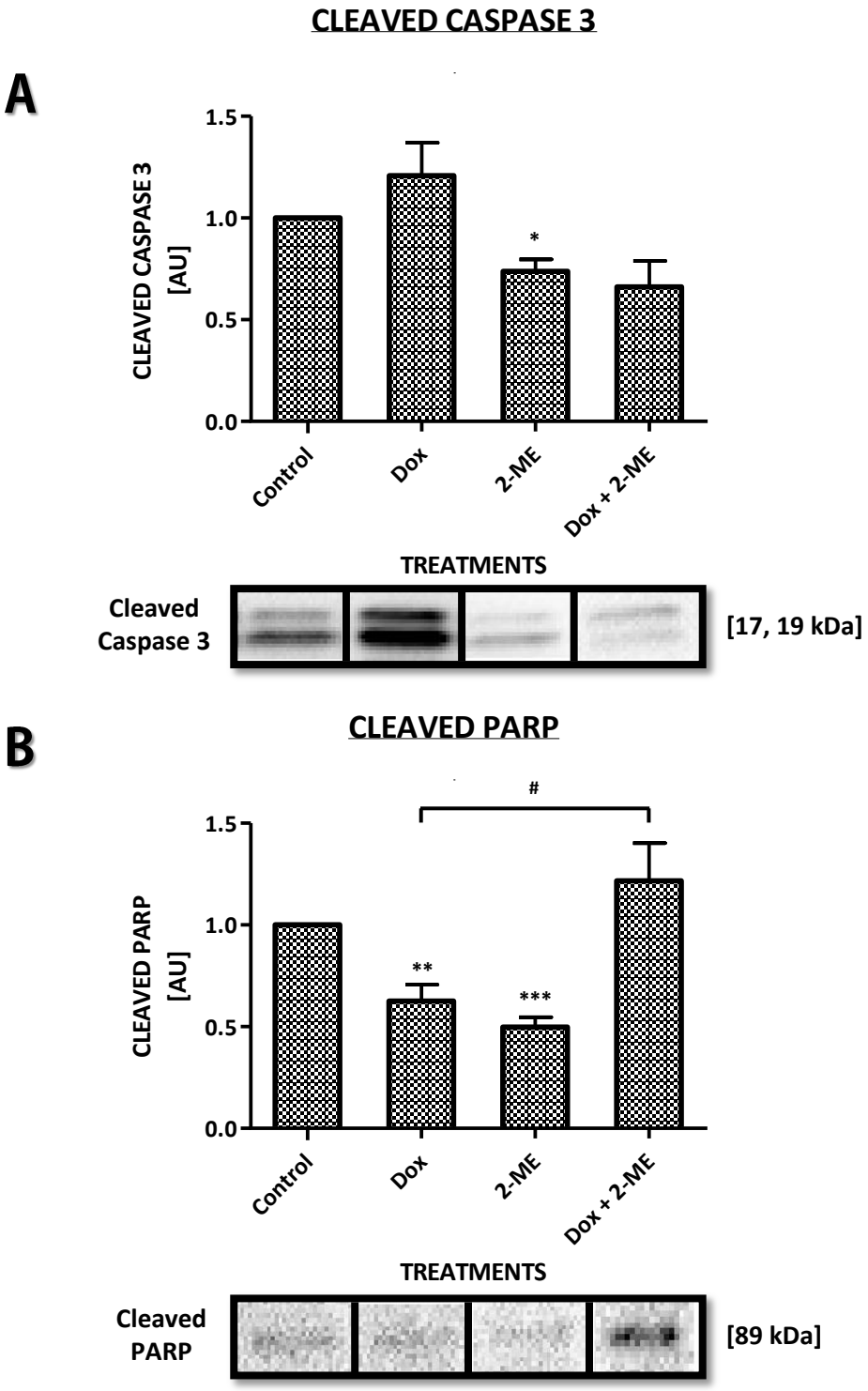


**Figure 3.14 The evaluation of the *in vivo* cleaved caspase 3 and cleaved PARP expression profiles present within tumours in response to the experimental regime.** The densitometric analysis and immunoblots are represented. (**A**) Cleaved caspase 3; (**B**) Cleaved PARP. A ratio was calculated relative to the control (set to 1). Columns, arbitrary units (AU); Bars, ± SEM. The results are a representative of three independent experiments. * $p<0.05$ vs. control; ** $p<0.01$ vs. control; # $p<0.05$ vs. doxorubicin.

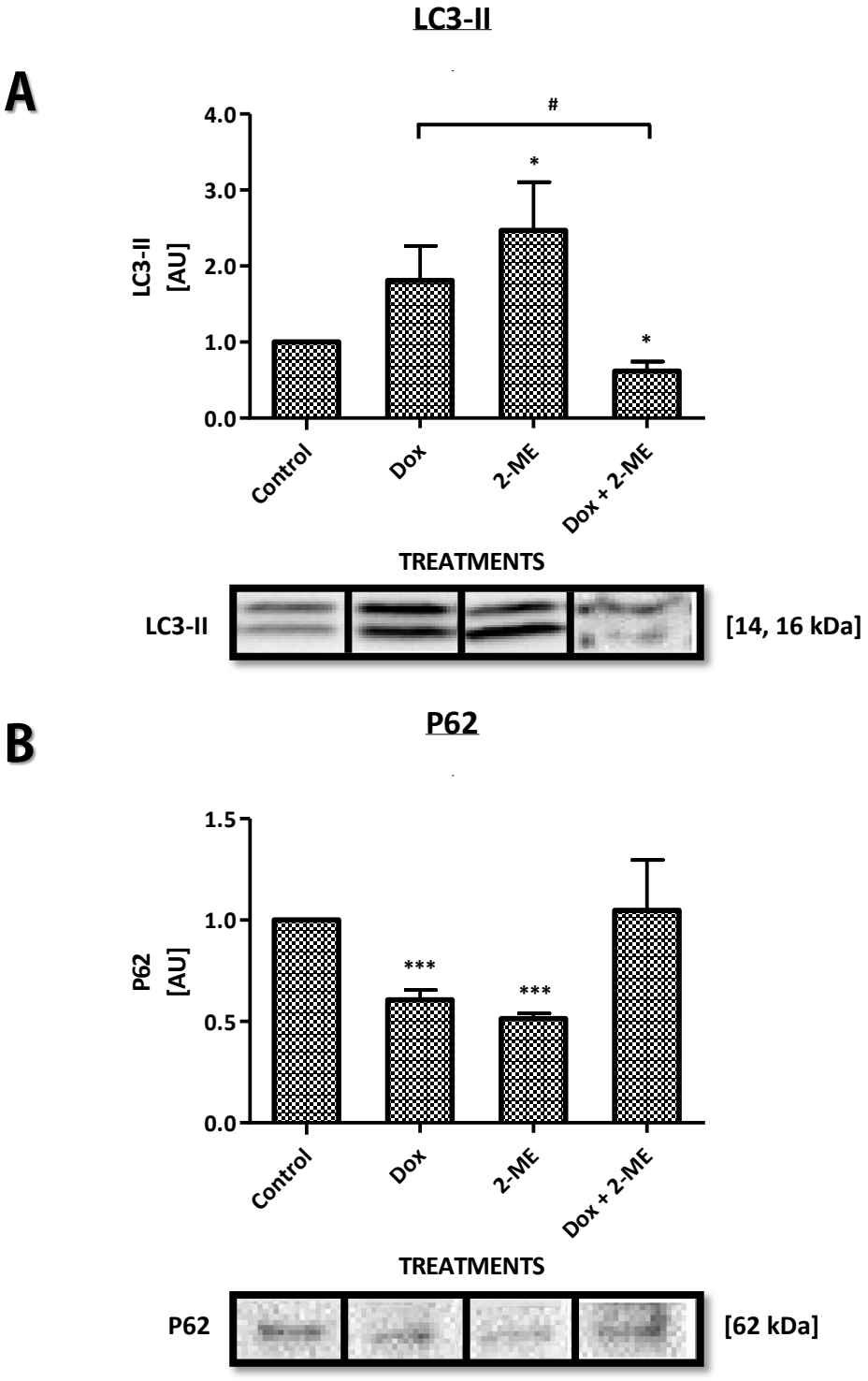


**Figure 3.15 The evaluation of the *in vivo* LC3-II and p62 expression profiles present within tumours in response to the experimental regime.** The densitometric analysis and immunoblots are represented. (**A**) LC3-II; (**B**) p62. A ratio was calculated relative to the control (set to 1). Columns, arbitrary units (AU); Bars, ± SEM. The results are a representative of three independent experiments. *** $p<0.001$ vs. control; # $p<0.05$ vs. doxorubicin.

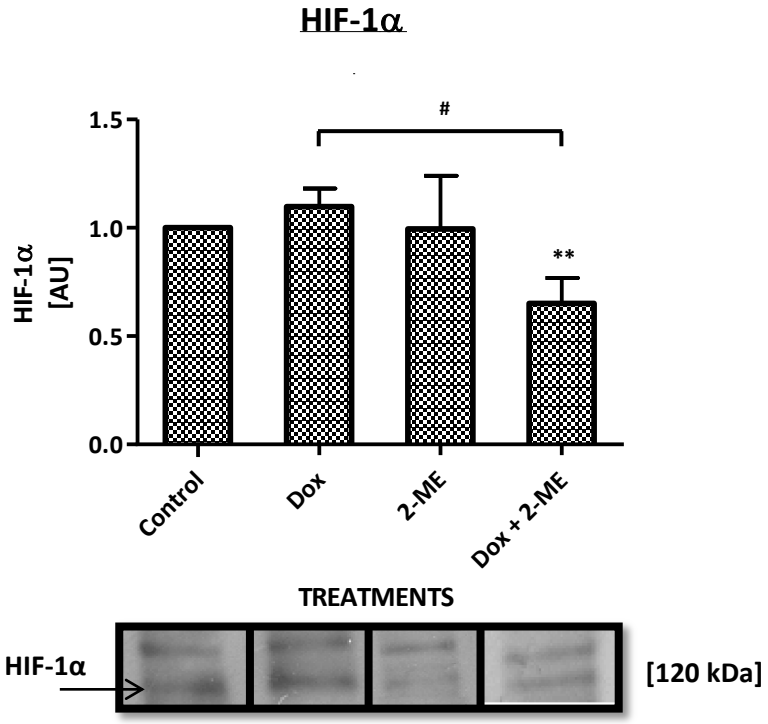


**Figure 3.16 The evaluation of the *in* vivo HIF-1α expression profile present within tumours in response to the experimental regime.** The densitometric analysis and immunoblots are represented. A ratio was calculated relative to the control (set to 1). Columns, arbitrary units (AU); Bars, ± SEM. The results are a representative of three independent experiments. ** $p<0.01$ vs. control; # $p< 0.05$ vs. doxorubicin

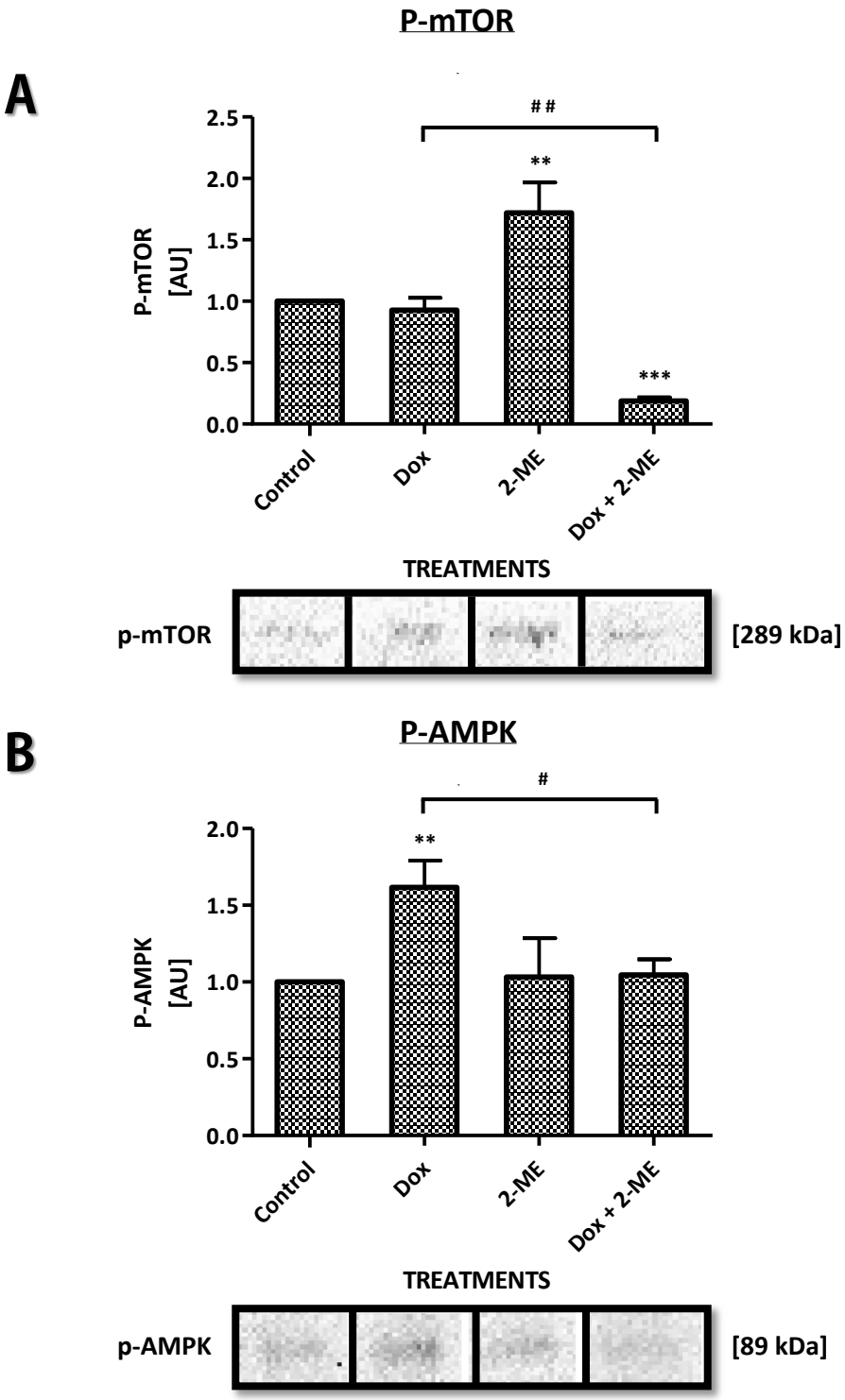


**Figure 3.17 The evaluation of the *in vivo* p-mTOR and p-AMPK expression profiles present within tumours in response to the experimental regime.** The densitometric analysis and immunoblots are represented. (**A**) p-mTOR; (**B**) p-AMPK. A ratio was calculated relative to the control (set to 1). Columns, arbitrary units (AU); Bars, ± SEM. The results are a representative of three independent experiments. **, P < 0.01 vs. control; *** p<0.001 vs. control; # p<0.05 vs. doxorubicin; ## p<0.01 vs. doxorubicin.

**Table 3.1 A summary of significant changes in markers of hypoxia, apoptosis, autophagy, and metabolism upon doxorubicin treatment (*in vitro*).** Hypoxia, HIF-α (hypoxia-inducible factor α); apoptosis, CC3 (cleaved caspase 3) and CP (cleaved PARP); autophagy, LC3-II (lipidated autophagosome-associated LC3) and p62 (sequestosome); metabolism, p-mTOR (phosphorylated-mammalian target of Rapamycin) and p-AMPK (phosphorylated-AMP-activated protein kinase); ↑, significant up-regulation of pathway; ↓, significant down-regulation of pathway

| VS. CONTROL | | NORMOXIA | HYPOXIA |
|---|---|---|---|
| | | Dox | Dox |
| HYPOXIA | HIF | ↓ | NS |
| | | | |
| APOPTOSIS | CC3 | ↑ | ↑ |
| | CP | ↑ | ↓ |
| | | | |
| AUTOPHAGY | LC3-II | ↑ | ↑ |
| | P62 | ↓ | NS |
| | | | |
| METABOLISM | P-MTOR | NS | NS |
| | P-AMPK | ↑ | NS |

**Table 3.2 A summary of significant changes in markers of hypoxia, apoptosis, autophagy, and metabolism upon induction and disruption of HIF-1α (*in vitro*).** Hypoxia, HIF-α (hypoxia-inducible factor α); apoptosis, CC3 (cleaved caspase 3) and CP (cleaved PARP); autophagy, LC3-II (lipidated autophagosome-associated LC3) and p62 (sequestosome); metabolism, p-mTOR (phosphorylated-mammalian target of Rapamycin) and p-AMPK (phosphorylated-AMP-activated protein kinase); ↑, significant up-regulation of pathway; ↓, significant down-regulation of pathway

| VS. CONTROL | | NORMOXIA | | | HYPOXIA | | |
|---|---|---|---|---|---|---|---|
| | | $CoCl_2$ | 2-ME | siRNA | $CoCl_2$ | 2-ME | siRNA |
| HYPOXIA | HIF | ↑ | ↓ | ↓ | ↓ | ↓ | NS |
| | | | | | | | |
| APOPTOSIS | CC3 | ↑ | NS | NS | NS | ↑ | ↑ |
| | CP | NS | NS | NS | NS | ↑ | ↑ |
| | | | | | | | |
| AUTOPHAGY | LC3-II | ↑ | NS | ↑ | ↑ | NS | NS |
| | P62 | NS | NS | ↑ | NS | NS | ↑ |
| | | | | | | | |
| METABOLISM | P-MTOR | NS | NS | ↑ | ↓ | NS | NS |
| | P-AMPK | NS | ↓ | NS | ↓ | NS | NS |

**Table 3.3 A summary of significant changes in markers of hypoxia, apoptosis, autophagy, and metabolism upon adjuvant treatment (*in vitro*).** Hypoxia, HIF-α (hypoxia-inducible factor α); apoptosis, CC3 (cleaved caspase 3) and CP (cleaved PARP); autophagy, LC3-II (lipidated autophagosome-associated LC3) and p62 (sequestosome); metabolism, p-mTOR (phosphorylated-mammalian target of Rapamycin) and p-AMPK (phosphorylated-AMP-activated protein kinase); ↑, significant up-regulation of pathway; ↓, significant down-regulation of pathway

| VS. DOX | | NORMOXIA | HYPOXIA |
|---|---|---|---|
| | | Dox + 2-ME | Dox + 2-ME |
| HYPOXIA | HIF | ↓ | NS |
| APOPTOSIS | CC3 | ↓ | ↓ |
| | CP | ↓ | ↓ |
| AUTOPHAGY | LC3-II | ↑ | NS |
| | P62 | ↑ | NS |
| METABOLISM | P-MTOR | NS | ↓ |
| | P-AMPK | NS | NS |

**Table 3.4 A summary of significant changes in markers of hypoxia, apoptosis, autophagy, and metabolism (*in vivo*).** Hypoxia, HIF-α (hypoxia-inducible factor α); apoptosis, CC3 (cleaved caspase 3) and CP (cleaved PARP); autophagy, LC3-II (lipidated autophagosome-associated LC3) and p62 (sequestosome); metabolism, p-mTOR (phosphorylated-mammalian target of Rapamycin) and p-AMPK (phosphorylated-AMP-activated protein kinase); ↑, significant up-regulation of pathway; ↓, significant down-regulation of pathway

| VS. CONTROL | | TUMOUR TISSUE | | | |
|---|---|---|---|---|---|
| | | Control | Dox | 2-ME | Dox + 2-ME |
| HYPOXIA | HIF | NS | NS | NS | ↓ |
| APOPTOSIS | CC3 | NS | NS | ↓ | NS |
| | CP | NS | ↓ | ↓ | NS |
| AUTOPHAGY | LC3-II | NS | NS | ↑ | ↓ |
| | P62 | NS | ↓ | ↓ | NS |
| METABOLISM | P-MTOR | NS | NS | ↑ | ↓ |
| | P-AMPK | NS | ↑ | NS | NS |

# CHAPTER 4 – DISCUSSION

## 4.1 INTRODUCTION

The deprivation of a sufficient oxygen supply is a hallmark of solid tumours that contributes to the pathophysiology of solid breast tumours (Lee, 2009). Within this oxygen-deprived environment, neoplastic cells respond by activating a variety of genes that promote their survival. These genes typically harbour a hypoxic-responsive element (HRE) and are regulated by the HIF-1 transcription factor. Upon binding to this core promoter, the activated HIF-1 heterodimeric complex mediates adaptive cellular responses which include anaerobic glycolysis, angiogenesis, apoptotic resistance and autophagy, all of which contribute to the malignancy of the cancer (Roudier & Perrin, 2009; Liu *et al.*, 2010). The over-expression of HIF-1 in malignant breast tissue has served as a negative prognostic indicator as survival of patients is dismal (Zhong *et al.,* 1999). As a result of an increased neoplastic viability induced by hypoxic conditions, the efficient treatment of solid tumours has become a challenging task. In addition to its prognostic value, the existence of HIF-1 has emerged as a relevant target for therapeutic intervention. By eradicating HIF-1, the hypoxia-related protective response which it confers upon tumour cells may potentially be eliminated and improve the efficacy of chemotherapeutic treatment.

Therefore this study was designed to provide insight into the molecular events that are responsible for the resistance of neoplastic cells to chemotherapeutic treatment under low oxygen tension, and to assess whether manipulation of these events can benefit treatment by sensitizing the neoplastic cells. The *in vitro* experimental model employed doxorubicin, an anthracycline antibiotic that is extensively utilized in clinical settings to treat patients diagnosed with breast cancer. This study was performed on the MCF-7 cell line, a breast adenocarcinoma which is an estrogen-receptor positive cell model. Prior to execution of the *in vitro* experimental model, a suitable concentration and time regiment of the chemotherapeutic drug was selected based on the MTT viability data. Specifically, the capacity of doxorubicin to elicit a differential viability effect on tumorigenic MCF-7 cells after normoxic and hypoxic exposure, and in favour of the latter, was selected as an end point. The concentrations of the HIF-1α inducer ($CoCl_2$) and inhibitors (2-methoxyestradiol; siRNA duplex) chosen for this study were based on the successful induction and inhibition of this protein in previously reported studies. Using molecular (Caspase-Glo® 3/7 Assay; Western Blotting; MTT) and visual techniques (Live Cell Imaging/Fluorescent Microscopy), the study proceeded to investigate the putative link between cell death, oxygen availability and metabolic sensors, bioreductive capacity, mitochondrial morphology and hypoxia. The following aims were formulated:

1. To determine whether hypoxic conditions confer a survival advantage to the MCF-7 tumorigenic cells in response to doxorubicin treatment.
2. To characterize the molecular events responsible for the selective resistance under hypoxia.
3. To link these molecular events to the expression levels of the HIF-1 master regulator.
4. To assess whether the abrogation of the hypoxic response by HIF-1α inhibition can sensitize the tumorigenic cell line to doxorubicin treatment, therefore producing a synergistic effect.

The impact of treatments on the viability of cells was monitored at all times. The experiment was repeated in an *in vivo* model to assess the level of reproducibility of the *in vitro* experiment model and efficacy of treatments in animal tissue.

The western blotting technique monitored specific biomarkers based on their electrophoretic mobility. With respect to apoptosis, two proteins specific to the apoptotic cellular pathway were chosen: (1) the cysteine protease, caspase 3, which becomes activated upon cleavage and is the main instigator of apoptosis execution, and (2) PARP, a substrate which is subsequently proteolysed by caspase 3 activity.

Autophagy is generally monitored by western blotting to assess the conversion of the microtubule-associated light chain 3 (LC3) from LC3-I to LC3-II. During the initiation stage of the autophagic process, the formation of autophagosomes requires the lipidation of the cytosolic form LC3-I, followed by the incorporation of the product LC3-II into the outer and inner membranes of the early autophagic vesicles. It is known that the maturation of autophagosomes entails their fusion with acidic lysosomes to degrade the encapsulated cargo. Since LC3-II molecules are present on both outer and the inner membranes of the autophagosomes, the degradation of the cargo along with the inner membrane will also digest the LC3-II.

The accumulation of LC3-II generally indicates one of two situations and may therefore potentially suffer misinterpretation (Mizushima & T Yoshimori, 2007). The detection of LC3-II by western blotting may indicate the beginning stages of the autophagic process. Less LC3-II is detected in the later stages of autophagy upon fusion with, and digestion by, the lysosomes. Both signify that autophagy is occurring. However, many inhibitors of the autophagic process block the fusion of autophagosomes with lysosomes. This prevents the turn-over of LC3-II, allowing it to be visualised by immuno-detection. Therefore, in order to elucidate whether LC3-II detection represents early autophagosome genesis of an uninterrupted autophagic flow or the amassing of these vesicles due to a dysfunction in their degradation requiring the coupling to p62, an alternative marker of autophagy, the levels of p62 were evaluated in addition to the LC3 conversion.

The metabolic state of a cell determines its ability to grow and proliferate. The MTT colorimetric assay (Mosmann, 1983) was developed to measure the viability of a cellular population. The reduction of the yellow tetrazolium dye to a purple formazan salt, which when solubilized can be quantified spectrophotometrically, is mainly attributed to the mitochondrial dehydrogenase enzymes. This technique has been used to evaluate the cytotoxicity of drugs (Di *et al.*, 2009; Vengellur & LaPres, 2004; Van Zijl & Lottering, 2008).

However, a variety of cancer cell lines have been identified to display the ‘Warburg phenomenon’, a pattern of metabolism where cells preferentially utilize glycolysis in spite of a sufficient supply of oxygen (Ferreira, 2010). Furthermore, hypoxia has been shown to stimulate the metabolic switch from oxidative phosphorylation to anaerobic glycolysis (Kroemer & Pouyssegur, 2008). These alterations

have been shown to be beneficial to the growth of the tumour. In these scenarios, the cells remain viable regardless of the reduced mitochondrial activity. Therefore, the results from the MTT assay do not necessarily indicate viability, but rather the bioreductive potential, or mitochondrial function, of a cellular population at that time. A more direct method of measuring the viability of the cellular population would be through the vital dye Trypan Blue, where retention of the dye is indicative of a damaged plasma membrane. Alternatively, the staining of DNA by intercalation with the red-fluorescent vital dye Propidium Iodide may also be used to differentiate between living and dead cells and is typically analysed via flow cytometry.

## *4.2 IN VITRO*

### 4.2.1 Evaluation of the inducers and inhibitors of HIF-1α expression

This section aimed to address the potential of $CoCl_2$ to stabilize HIF-1α, and 2-methoxyestadiol and siRNA transfection to inhibit its expression.

Results revealed that the exposure of the MCF-7 cell line to 100 µM of $CoCl_2$ for a duration of 12 hours adequately stabilized HIF-1α under normoxic conditions compared to the baseline levels present under normoxia (**Fig. 3.8.1**). Stabilization of HIF-1α occurred without significantly affecting the viability of cells (**Fig. 3.1.2**). $CoCl_2$ was therefore employed as a positive control for the *in vitro* study. To simulate the reduced oxygen environment that is characteristically witnessed within the microenvironment of solid tumours, MCF-7 cells were experimentally rendered hypoxic by subjecting them to a hypoxic environment of ~0.1% oxygen ($PO_2$ = 0.8 mm Hg). $CoCl_2$ treatment under hypoxic conditions caused a slightly reduced expression of HIF-1α compared to the baseline levels established within the hypoxic control group (**Fig. 3.8.2**). To establish a HIF-1α-knockdown phenotype in the *in vitro* experiment, HIF-1α siRNA transfection was employed at a concentration of 400 nM/1 L. This concentration adequately abolished the expression of HIF-1α which is usually present at normoxic baseline levels (**Fig. 3.8.1**). In contrast, the levels of HIF-1α under hypoxia seemed to be unaffected (**Fig. 3.8.2**). This study employed 2-methoxyestradiol at 10 µM for a duration of 12 hours. This concentration was capable of significantly attenuating the expression of HIF-1α by 31% and 59% in normoxia (**Fig. 3.8.1**) and hypoxia (**Fig. 3.8.2**), respectively. 2-Methoxyestradiol treatment caused a significant decrease in viability of the MCF-7 cells (**Fig. 3.12**), although this cytotoxicity was mild compared to that inflicted by doxorubicin.

Cobalt chloride interferes with the activity of prolyl hydroxylases and has previously been used to mimic the conditions of hypoxia and stabilize HIF-1α both *in vitro* (Chan & Sutphin, 2005; Nardinocchi *et al.*, 2009) and *in vivo* (Razeghi *et al.*, 2001). The non-cytotoxic stabilization of HIF-1α under normoxic conditions after the addition of 100 µM $CoCl_2$ is supported by a study carried out on the human glioblastoma U251 cell line, where concentrations of $CoCl_2$ between 50 µM and 200 µM enabled the expression of a 118 kDa-sized HIF-1α protein without adversely affecting cellular viability (Al-Okail, 2010). The higher levels of HIF-1α after $CoCl_2$ treatment indicate that the functional prolyl

hydroxylases present within the normoxia control group (21% oxygen; $PO_2$ = 160 mm Hg) subject the HIF-1α to ubiquitination and proteasomal degradation. In spite of this negative oxygen-dependent, post-translational regulation, there is a constitutive expression of HIF-1α under normoxia at low levels. This most likely demonstrates an oxygen-independent stabilization of HIF-1α that could result from the deregulation of gain-of-function oncogenes or loss-of-function tumour suppressor genes. The human epidermal growth factor receptor 2 (HER2), for example, is a proto-oncogene over-expressed in ~15% of advanced breast tumours (Dean-Colomb & Esteva, 2008). It is a transmembrane receptor possessing tyrosine kinase activity which is capable of stimulating the phosphatidylinositol 3-kinase (PI3K-Akt) and mitogen-activated protein kinase (MAPK) signal transducing cascades, both of which have been shown to upregulate HIF-1α (Dean-Colomb & Esteva, 2008; Laughner & Taghavi, 2001). Moreover, mutations in tumour suppressors that lead to stabilization of HIF-1α include the von Hippel-Lindau (VHL) protein, such as that in renal cell carcinoma (Razorenova *et al.*, 2011), and phosphatase and tensing homolog (PTEN) protein, as seen in glioblastoma (Zundel & Schindler, 2000).

Oxygen has been shown to be one of the rate-limiting factors for the function of prolyl hydroxylases, in addition to the α-ketoglutarate co-substrate and $Fe^{2+}$ co-factor (Hansen *et al.*, 2011; Bruick & McKnight, 2001). The oxygen concentration at which HIF-1α becomes expressed is dependent on cell type (Bracken *et al.*, 2006). Experiments carried out by Robey *et al*. (2005) on the MCF-7 cell line showed elevated levels of HIF-1α increased the expression of its associated transcriptional targets, including GLUT-3 and VEGF, when exposed to oxygen concentrations below ≤2% compared to normoxia (Robey *et al.*, 2005). Therefore it is presumed that the 12 hour exposure at ~0.1% $O_2$ utilized in this study is sufficient to prevent proline hydroxylation, and therefore stabilize HIF-1α at higher levels under hypoxia (**Fig. 3.8.2**).

The weaker HIF-1α expression level observed under hypoxia after $CoCl_2$ treatment was also noticed in a 2010 study by Zhang *et al*. where HeLa cells were treated with 200 µM of $CoCl_2$ which served as a positive control (Zhang *et al.*, 2010). It could be speculated that the capacity of $CoCl_2$ to stabilize HIF-1α is limited and overrides any further expression.

The depletion of HIF-1α during normoxia after siRNA transfection is supported by Doublier *et al.* (2012) who demonstrated that at 400 nM/1 L of the siRNA duplex, the expression of the multi-drug resistance protein termed P-glycoprotein, which has previously been shown to be upregulated by HIF-1α under hypoxic conditions (Comerford *et al.*, 2002), was decreased in MCF-7 cells suggesting an effective concentration (Doublier *et al.*, 2012).

Concerning the unaffected HIF-1α protein levels witnessed after siRNA intervention during hypoxia, a possible reason could be that the siRNA duplex deactivated the irrelevant isoform of the alpha subunit that was upregulated under hypoxia. Various researchers have discovered the presence of both isoforms of the alpha subunit, namely HIF-1α and HIF-2α, in MCF-7 cells (Mole *et al.*, 2009; Larsen *et al.*, 2008). It has been shown that stability of these isoforms may be regulated differentially (Keith *et al.*, 2011). Uchida *et al*. demonstrated that the duration of exposure of the human lung

adenocarcinoma cell line, A549, to hypoxia caused a distinct expression in the HIF-α subunits (Uchida *et al.*, 2004). Exposing A549 cells to hypoxia (0.5%) allowed both isoforms to be detected at a 4 hour time point, while at 12 hours the HIF-1α expression was diminished with HIF-2α levels remaining elevated.

Since this study employed a siRNA duplex specifically targeting HIF-1α, and a primary antibody of polyclonal origin, the detection of the protein in the "HIF-1α siRNA" group could possibly represent unaffected HIF-2α.

Results obtained from a study conducted by Mabjeesh *et al.* (2003) mirror those acquired in this study with respect to the treatment of MCF-7 cells with 2-methoxyestradiol (Mabjeesh *et al.*, 2003). They revealed that the exposure of the human breast cancer cell line, MDA-MB-231, and the human prostate cancer cell line, PC-3, to 2-methoxyestradiol under both normoxic and hypoxic conditions had an inhibitory effect on HIF-1α expression that was dependent on the concentration of the drug. Similarly, this inhibitory effect was observed with HIF-2α. In the study, 10 µM of 2-methoxyestradiol was sufficient to eradicate the expression of HIF-1α and HIF-2α, albeit for a duration of 16 hours, supporting the findings in this study.

Of the two strategies employed, 2-methoxyestradiol was more effective in reducing normoxic and hypoxic HIF-1α protein levels in MCF-7 cells compared to siRNA transfection. Therefore the experiment proceeded by assessing the modulation effect of 2-methoxyestradiol alone.

### 4.2.2 The role of HIF-1α expression on apoptosis and autophagy

This section explored whether a relationship exists between apoptotic or autophagic induction, and the stabilized subunit of the hypoxic responsive transcription factor, HIF-1α.

While the reduced expression of HIF-1α by 2-methoxyestradiol and siRNA transfection did not affect apoptosis in the presence of 21% oxygen (**Fig. 3.4.1**; **Fig. 3.5.1**), the activation of caspase 3 followed by the cleavage of PARP was significantly induced in the 2-methoxyestradiol group when oxygen dropped to 0.1% (**Fig. 3.4.2**; **Fig. 3.5.2**). The stabilized HIF-1α after $CoCl_2$ treatment at the low oxygen tension did not exhibit signs of apoptosis. These results indicate that under hypoxic conditions, an inverse relationship exists between HIF-1α and apoptotic induction. Therefore, the stabilization of HIF-1α serves as a negative regulator of apoptosis and could potentially contribute to the resistance against the doxorubicin-induced apoptosis. A link between HIF-1α and autophagy was suggested based on the results obtained under normoxic conditions where the knock-down of HIF-1α expression was effective (**Fig. 3.8.1**). Transfection with siRNA appeared to disrupt autophagy after the formation of autophagosomes, as marked by the higher levels of the autophagic-vesicle associated LC3-II (**Fig. 3.6.1**) accompanied by the concomitant aggregation of p62 (**Fig. 3.7.1**). In contrast, the adequate stabilization of HIF-1α under normoxia by $CoCl_2$ caused an increase in autophagy (**Fig. 3.6.1**). This suggests that autophagy upregulation is dependent on the expression of

HIF-1α. The stabilization of HIF-1α by $CoCl_2$ under hypoxia caused a significant increase in cellular viability, as evident from the concentration-response curve (**Fig. 3.1.2**), suggesting that the upregulation of autophagy in this group could be responsible for the protective effect. With regards to the dissimilar outcomes on the autophagic process by the HIF-1α inhibitors used in this study (**Table 3.1**), it is likely that the direct inhibition of HIF-1α seen with siRNA transfection is not imitated by 2-methoxyestradiol, which may have an alternative target and rather an indirect mode of deactivating HIF-1α.

The ability of 2-methoxyestradiol to induce apoptosis in the MCF-7 cell line has been reported by various researchers (Stander *et al.*, 2010; Van Zijl & Lottering, 2008). A study carried out in 2004 by Erler *et al.* on three colon carcinoma cell lines demonstrated that the post-transcriptional suppression of HIF-1α with small interfering RNA induced the expression of the pro-apoptotic protein, Bid, under hypoxic conditions (Erler *et al.*, 2004). This further supports the relationship between HIF-1α and apoptosis that was recognized in this study.

The suggested relationship between autophagy and HIF-1α is supported by Liu *et al.* (2010) whose research reported a reduced conversion of LC3-I to LC3-II when the cervical HeLa cancer cell line was transfected with a plasmid encoding HIF-1α siRNA (Liu *et al.*, 2010).

According to Mabjeesh *et al.* (2003), the inhibition of HIF-1α was a consequence of microtubule disruption within the human ovarian carcinoma cell line, 1A9 (Mabjeesh *et al.*, 2003). This supports the different downstream effects observed when 2-methoxyestadiol and the siRNA duplex were utilized to ablate HIF-1α expression. Based on this deviation, it would be possible for the microtubule disruptor to cause off-target effects.

### 4.2.3 Characterization of cellular death pathways and the oxygen sensor, AMPK, upon doxorubicin treatment

This section aimed to assess the molecular changes that the anthracycline anti-tumour agent, doxorubicin, confers upon the cellular death pathways, apoptosis and autophagy, and the AMPK energy sensor.

A prominent cleavage of PARP and caspase 3 was revealed after the treatment with doxorubicin. This effect is indicative of apoptosis and was seen under both normoxic and hypoxic conditions (**Fig. 3.4.1**; **Fig. 3.4.2**; **Fig. 3.5.1**; **Fig. 3.5.2**). The data obtained from western blotting were strengthened by the Caspase-Glo® 3/7 Assay, where the elevated luminescent signal produced by MCF-7 cancer cells in response to doxorubicin designated an elevated amount of activity of the two executioner caspases, 3 and 7 (**Fig. 3.3**). Under normoxic conditions, the magnitude of autophagy increased as evident from a decrease in the levels of p62 (**Fig 3.7.1**) and a concomitant increase in LC3-II (**Fig. 3.6.1**), the latter possibly representing early autophagosomes. This increased autophagic response is most likely a HIF-1α-independent process, as the decline in HIF-1α (**Fig. 3.8.1**) was not followed by a decline in

autophagic activity, an event which was expected based on the link established above (section **4.2.2**). As doxorubicin increased the activation of the energy sensor, AMPK, under normoxic conditions (**Fig. 3.10.1**), this would rather suggest that the autophagic machinery upregulated in this normoxic setting to be an AMPK-dependent process. Although LC3-II was present at a greater intensity within doxorubicin-treated MCF-7 cells that were exposed to a hypoxic environment, the turnover of p62 remained constant (**Fig. 3.6.2**; **Fig. 3.7.2**). This does not necessarily suggest that the flux of p62 remained unchanged, but rather that the formation of p62 is balanced out by its removal, whether flux is increased or decreased. In this scenario, the increased LC3-II could represent either increased or decreased autophagy. Regardless, autophagy is still functional as p62 did not accumulate compared to the control. Although a baseline expression of P-AMPK was stimulated in the untreated hypoxic MCF-7 cells (**Fig. 3.10.2**), the addition of 1 µM doxorubicin for 12 hours did not significantly affect P-AMPK expression. Despite the attenuation in the bioreductive capacity of MCF-7 cells, a significant differential effect between normoxic and hypoxic exposure was witnessed in the MTT assay when cells were exposed to doxorubicin for the duration of 12 hours (**Fig. 3.12**). This data it is indicative that hypoxic conditions conferred resistance to cytotoxic effects of doxorubicin. This prominent differential influence by hypoxia served as the basis for the time point selection of this study. In contrast to normoxia, the HIF-1α levels remain elevated (**Fig. 3.8.2**) and therefore the appearance of autophagosomes present at ~0.1% $O_2$ may represent a HIF-1 dependent cytoprotective response, promoting the survival of cells in spite of the damaging effects of chemotherapy.

Along with doxorubicin's reputation of being a topoisomerase-II poison, it also leads to DNA damage via the production of reactive oxygen species, and/or the formation of doxorubicin-DNA adducts (Minotti *et al.*, 2004). A general response to the DNA damage is via the type I cellular death pathway, apoptosis. The apoptotic effects of doxorubicin witnessed in this study are in agreement with Brantley-Finley *et al*. (2003) whose 1 µM drug treatment caused apoptotic cell death in the KB-3 human carcinoma cell line, which displayed a molecular profile of significant PARP proteolysis and caspase 3 activation (Brantley-Finley *et al.*, 2003). Furthermore, the recent research carried out by Chen *et al*. demonstrated a similar activation of the AMPK sensor upon doxorubicin treatment (Chen *et al.*, 2011). They verified that AMPK contributed to doxorubicin-induced apoptotic cell death based on the increased cellular viability and decreased caspase 3 cleavage when AMPK was deactivated by siRNA or compound C. They concluded that ROS generated by mitochondria after doxorubicin treatment was the stimulus for AMPK expression.

While autophagy has been shown to be responsible for the cytotoxic effects of some anticancer agents (Kanzawa *et al.*, 2003; Gozuacik & Kimchi, 2004), in other scenarios, the autophagic process upregulated by neoplastic cells may contribute to the survival of that population in response to adverse treatments (Katayama *et al.*, 2007). In this *in vitro* experimental model, the autophagic process that is stimulated by doxorubicin under normoxic conditions could signify an alternative mode of cell death, namely type II, which is activated to augment the killing of MCF-7 cells by this antineoplastic drug. The possibility that AMPK, which becomes increasingly activated under normoxia, may be responsible for the autophagic boost (**Table 3.2**) is supported by Egan *et al*. who

showed that the nutrient sensor was capable of phosphorylating ULK1, a kinase required for the induction of autophagy (Egan *et al.*, 2011). The baseline expression of AMPK in the hypoxic control group (**Fig. 3.10.2**) is supported by a study conducted by Mungai *et al*. (2011) which revealed that the augmented ROS produced by mitochondria under hypoxic conditions (1.5% $O_2$) caused an increased activation of AMPK, independent of the AMP/ATP ratio (Mungai *et al.*, 2011). As the elevated levels of both AMPK and HIF-1α protein were unaffected after doxorubicin treatment, it is challenging to clarify whether the autophagy upregulated in this group under hypoxia is dependent on AMPK or HIF-1α (**Table 3.2**). Although hypoxia is capable of upregulating AMPK and HIF-1α, the severity and duration of low oxygen tension will most likely determine which protein is preferentially activated (Solaini *et al.*, 2010).

The finding that the bioreductive capacity was significantly decreased after 12 hours of doxorubicin exposure is indirectly strengthened by a study conducted by Kuznetsov et al. who, with the aid of confocal microscopy, measured the mitochondrial oxidative state of MCF-7 cells using the native autofluorescence of NADH (Kuznetsov *et al.*, 2011). After the addition of doxorubicin, the mitochondrial NADH autofluorescence declined indicating the mitochondrial reduction was decreased. The conclusion is in agreement with the results obtained in this study through the MTT assay. The suggestion that autophagy may be responsible for this decreased cell death rate under hypoxia is supported by Song *et al*. (2009) whose research revealed that the sensitivity of hepatocellular carcinoma cells to the chemotherapeutic agent, cisplatin, under hypoxic conditions became restored when autophagy was inhibited by siRNA-mediated knockdown of Beclin 1 (Song *et al.*, 2009). This implicates that autophagy activation mediated the resistance under hypoxia in this scenario.

### 4.2.4 Characterization of cellular death pathways and the oxygen sensor (AMPK) upon adjuvant therapy

The clinical combination of anticancer drugs that possess different molecular targets and/or mechanism of action have had a profound impact on the treatment of chemo-resistant tumours. The aim of this component of the study was therefore to investigate whether the simultaneous inclusion of the HIF-1α inhibitor, 2-methoxyestradiol, could modulate the cytotoxic effects of the antineoplastic agent, doxorubicin.

In the current study, the simultaneous treatment of MCF-7 cells with doxorubicin and 2-methoxyestradiol, when incubated under normoxia, displayed a significant decrease in the autophagic pathway (**Fig. 3.6.1**; **Fig. 3.7.1**; **Table 3.3**) compared to the levels induced by doxorubicin alone. While this occurred concurrently with a decrease in the levels of HIF-1α, the depletion of the master regulator failed to induce apoptotic cell death. This was unexpected based on the link establish above (section **4.2.2**). Instead, the amount of caspase 3 activation and PARP proteolysis became significantly reduced, indicating less apoptotic cell death (**Fig. 3.4.1**; **Fig. 3.5.1**). Whereas a similar effect on the cleavage of caspase 3 and its substrate PARP was witnessed under hypoxia (**Fig. 3.4.2**;

**Fig. 3.5.2**), indicating an inhibitory effect on doxorubicin-induced apoptosis, the combined treatment did not influence autophagy as evident from non-significant changes in LC3-II and p62 protein expression (**Fig. 3.6.2**; **Fig. 3.7.2**; **Table 3.3**). The HIF-1α and p-AMPK levels present in this condition remained elevated similar to those observed under the hypoxia control conditions (**Fig. 3.8.2**; **Fig. 3.10.2**). This may indicate that 2-methoxyestradiol was incapable of disrupting the HIF-1α. Autophagy remained elevated and may therefore have sustained the growth of MCF-7 cells, being stimulated by either HIF-1α or p-AMPK. According to the MTT assay, when HIF-1α was silenced by pharmacological (2-methoxyestradiol) therapy, the treatment of MCF-7 cells with doxorubicin abolished the significant differential bioreductive capacity that was produced when wild-type MCF-7 cells were treated with doxorubicin alone (**Fig. 3.12**). However, this was not due to an increase in cell death in the hypoxic group as expected. As noticeable from the MTT data, the bioreductive capacity of adjuvant doxorubicin-2-methoxyestradiol treatment group (normoxia, 40% viable; hypoxia, 57% viable) was less affected than when the neoplastic cells were treated with doxorubicin alone (normoxia, 31% viable; hypoxia, 40% viable). This suggests that an antagonistic effect was at play. The data indicates that the combined treatment sustained the survival of the neoplastic cells.

A 2009 study conducted by Di *et al*. investigated the alternative modes of cell death in the MCF-7 tumorigenic breast cell line, MCF-7, upon Adriamycin exposure and concluded that, in addition to the rise in apoptosis and autophagy, this antineoplastic agent may stimulate an irreversible state of growth arrest termed senescence (Di *et al.*, 2009). Similarly, cell-cycle analysis showed that 2-methoxyestadiol treatment caused growth arrest of human aortic smooth muscle cells in the $G_0/G_1$ and $G_2$/M-phases (Barchiesi *et al.*, 2006). Since there was no significant change in cellular viability in this group compared when doxorubicin was used alone (**Fig 3.12**), it is likely that the combination of doxorubicin and 2-methoxyestradiol under normoxic conditions could promote the progression of MCF-7 cells to a state of senescence. This form of growth arrest could potentially allow for tumour recurrence, as Elmore *et al*. (2005) showed that following an early senescent arrest, breast cancer cells were capable of recovering (Elmore *et al.*, 2005).

A possible reason for the non-significant change in the elevated hypoxic HIF-1α levels could be attributed to the changing cellular metabolism under hypoxia. The likelihood that reactive oxygen species (ROS) can act as signalling molecules implicated in the stabilization of HIF-1α has been challenged by several researchers [reviewed in (Gogvadze *et al.*, 2010)]. The prime site of ROS generation is the mitochondrial electron transport chain (complex I and III) (Solaini *et al.*, 2010). However, hypoxic conditions have been shown to amplify the amount of ROS produced, specifically at complex III (Chandel *et al.*, 2000). This is supported by findings from Chandel *et al*. (1998) who quantified the intracellular ROS intensity of human hepatoma cell line, Hep3B, by fluorescence microscopy where the oxidation of the non-fluorescent dichlorofluorescin (DCFH) diacetate by ROS generated a dichlorofluorescin (DCF) fluorescent signal (Chandel, 1998). There it was shown that the amount of fluorescence, signifying ROS, increased as experimental oxygen concentrations decreased below 8%. Furthermore, this upregulation was supported with the increased expression of VEGF and glycolytic enzymes, which are downstream products of HIF-1α transcriptional activity. The ROS was

shown to be dependent on the mitochondria as subjection of a respiration-deficient Hep3B cell line to the same experimental conditions failed to reproduce these effects. The relationship between mitochondrial ROS and HIF-1α was confirmed by follow-up studies (Jung *et al.*, 2008; Chandel *et al.*, 2000). The generation of ROS by doxorubicin (Lüpertz *et al.*, 2010; Du & Lou, 2008) and 2-methoxyestradiol (Salama *et al.*, 2011; Stander *et al.*, 2010) has been validated by several studies. Therefore, it is possible that the ineffective disruption of HIF-1α by 2-methoxyestradiol could be a result of the combined effects of hypoxia, doxorubicin and 2-methoxyestradiol which may lead to the augmented stabilization of HIF-1α by ROS production observed in cells exposed to hypoxia.

The decrease in the tricarboxylic acid cycle rate as a consequence of lower oxygen availability and leading to the build-up of intermediates is another metabolic transformation occurring under hypoxia (Solaini *et al.*, 2010). These TCA intermediates, specifically succinate and fumarate, were shown by means of Electrospray Ionization-Mass Spectrometry (ESI-MS) and co-crystallization experiments to compete with the 2-oxoglutarate-biniding site on the prolyl hydroxylases enzymes (Hewitson *et al.*, 2007). As 2-oxoglutarate, or α-ketoglutarate, is an essential co-substrate required for the hydroxylation activity of these enzymes, this competitive binding of TCA intermediates in conjunction with oxygen deprivation could intensify the stabilization and transcriptional activity of HIF-1α. Research carried out by Koivunen *et al*. (2007) in an attempt to assess the effect of TCA intermediates on HIF-1α disclosed that the interference of two TCA cycle enzymes, fumurate hydratase and succinate dehydrogenase, by the inclusion of the dual inhibitor 3-nitropropionic acid, stabilized the expression of HIF-1α which was shown to be transcriptionally active as evident from the upregulation of VEGF, one of its downstream targets (Koivunen *et al.*, 2007). Therefore, combining doxorubicin and 2-methoxyestradiol under hypoxia may potentiate the accumulation of TCA intermediates and a concomitant expression of HIF-1α.

Experiments measuring the production of ROS and concentration of TCA intermediates, along with the expression of HIF-1α are suggested for future studies in order to clarify whether they influence the stability of the master regulator.

In an attempt to expose a possible synergistic cytotoxic effect, Han *et al*. (2005) combined the two anti-cancer drugs, doxorubicin and 2-methoxyestradiol, at similar doses (Han *et al.*, 2005). To their surprise, the combination treatment displayed antagonism to the expected anti-proliferative effect on the growth of breast cancer cell lines. This could possibly be attributed to the residual estrogenic activity of 2-methoxyestradiol.

17β-estradiol is initially oxidized to estrone, which may then be converted to the catechol estrogens, 4-hydroxyestradiol and 2-hydroxyestradiol, by a cytochrome-P450-catalyzed reaction (Mueck & Seeger, 2010). 2-Hydroxyestradiol is subsequently methylated by catechol-ortho-methyltransferase (COMT) to produce 2-methoxyestradiol. While this latter metabolite was shown to possess mild estrogenic activity, the molecules it is derived from display greater estrogenic activity (Sutherland *et al.*, 2007). In addition to enzymatically oxidizing 17β-estradiol to the catechol estrogens, cytochrome P450 1A1 (CYP1A1) and cytochrome P450 1B1 (CYP1B1) were revealed to catalyse the

demethylation of 2-methyoxyestradiol to 2-hydroxyestradiol in experiments carried out by Dawling *et al*. (Dawling *et al.*, 2003). Normal and tumorigenic breast cancer tissue has revealed the expression of the cytochrome P450 enzymes by reverse-transcriptase-PCR (Iscan *et al.*, 2001). By the inclusion of gangalin, a flavonoid known to inhibit the CY-P450-enzyme, LaVallee *et al*. indicated that the mitogenic effect on MCF-7 cells after 2-methoxyestradiol became attenuated, and thus proposed that the CY-P450-catalyzed conversion of 2-methoxyestradiol to 2-hydroxyestradiol was responsible for the stimulation of growth (LaVallee *et al.*, 2002). Moreover, this mitogenic effect was shown to disappear when the estrogen receptors were antagonized (Liu & Zhu, 2004).

Since our study employed the tumorigenic MCF-7 breast cell line which is estrogen-receptor positive (American Type Culture Collection, 2009), this metabolic conversion to the active estrogenic compounds may be possible. It can therefore be postulated that the doxorubicin component of the adjuvant therapy might be capable of reverting 2-methoxyestradiol back to its chemically reactive estrogenic derivate, 2-hydroxyestradiol, enabling it to engage with the ER-receptor and induce a mitogenic effect.

### 4.2.5 The effect on mitochondrial integrity upon induction and inhibition of HIF-1α

The mitochondria are ATP-producing organelles whose existence is crucial to satisfy the bioenergetic requirements of eukaryotic cells (Galluzzi *et al.*, 2010). Beyond their role in bioenergetic production via aerobic respiration, these 'power-houses' are also implicated in buffering intracellular calcium levels, and in the apoptotic cellular death pathway. A dynamic relationship between the fission and fusion of mitochondria exists (Twig *et al.*, 2008). This constant cycle determines both the functional and structural (morphology and spatial distribution) characteristics of these organelles within the cell (Chen & Chan, 2005).

In this study, the treatment of the MCF-7 cell line with $CoCl_2$ stabilized HIF-1α in the normoxic setting (**Fig. 3.8.1**). As seen in the fluorescence micrographs, $CoCl_2$ also stimulated the morphological transformation of mitochondria from an elongated network to enlarged disc-like pattern (**Fig. 3.11.1B**), an effect that was noticeable under hypoxia (**Fig 3.11.1A**). Since $CoCl_2$ is known to mimic hypoxia by stabilizing HIF-1α, the data in this experimental setting are suggestive that HIF-1α is responsible for this morphological effect.

It was therefore investigated whether the inhibition of HIF-1α should revert the morphology back to that present under normoxia. This was vaguely evident in the fluorescent micrographs of the 2-methoxyestradiol-treated group (**Fig. 3.11.2D**). However, morphological features of apoptotic cellular death were noticeable by the condensed chromatin suggesting the sensitivity to apoptosis was increased. This correlates with immunoblotting data where biomarkers for type I cell death (cleaved caspase 3 & cleaved PARP) were increased upon 2-methoxyestradiol treatment (**Fig. 3.4.2**; **Fig. 3.5.2**).

Hypoxia has been shown to confer heterogeneity to the structural and functional characteristics of mitochondria. The appearance of the enlarged disc-like mitochondria in the hypoxic setting of this study mirror the observations made by Chiche *et al*. whose examination of electron micrographs identified the mitochondria of the colon carcinoma cell line, LS174, to assume an enlarged, circular morphology upon exposure to hypoxia. When standard atmospheric oxygen was re-established, the tubular network that is typically present within these cells became restored (Chiche *et al.*, 2010). They attributed this transformation to the hypoxic upregulation of Mfn1, a GTPase that has previously been shown to promote the fusion of mitochondria (Koshiba *et al.*, 2004; Chen *et al.*, 2005). These enlarged mitochondria were also shown to be less sensitive to apoptotic inducers (Chiche *et al.*, 2010). Earlier it was suggested that HIF-1α negatively regulates apoptosis based on our immunoblotting results (**Table 3.1**). Furthermore, while HIF-1α stabilization ($CoCl_2$ treatment) promoted the formation of these enlarged mitochondria, the ablation of HIF-1α with 2-methoxyestradiol increased the amount of apoptotic cell death, further implicating the master regulator to play a role in this morphological 'protective' adaptation.

### 4.2.7 The effect on mitochondrial integrity upon doxorubicin treatment

Examination of the fluorescent images revealed that the mitochondria were adversely affected when MCF-7 cells were subjected to doxorubicin treatment (**Fig. 3.11.1C**). In addition to exhibiting the distinguishing apoptotic features including cellular shrinkage and detachment (shift in focal plane), membrane blebbing and nuclear pyknosis and karyorrhexis, the mitochondria to became fragmented and formed dot-like irregular structures.

Our imaging data is supported by a 2001 study where Frank *et al*. treated HeLa cervical cancer cells with etoposide, a DNA-damaging anticancer agent known to induce apoptosis, and this caused a phenotypic change in the mitochondria, from elongated to punctiform (Frank *et al.*, 2001).

However, the MCF-7 cells appeared to possess a greater mitochondrial functionality under 0.1% oxygen after doxorubicin treatment compared to normoxic conditions (**Fig. 3.12**). In addition to the change in mitochondrial redox state, Kuznetsov *et al*. also demonstrated that doxorubicin treatment dissipated the mitochondrial membrane potential (Kuznetsov *et al.*, 2011). The fusion of mitochondria has been shown to maintain the membrane potential ($\Delta\Psi$), allowing the cells to evade potential cellular dysfunction (Chen *et al.*, 2005). Although it is only mildly noticeable from our micrographs that some hypoxic cells retained enlarged mitochondria, the greater mitochondria functionality based on our MTT results could be attributed to the fused disc-like mitochondria which manifest under hypoxia, an effect which could protect the cells from depolarization induced by doxorubicin. The HIF-1-inducible autophagic proteins, BNIP3 and BNIP3L, were also linked to a similar protective enlargement of the mitochondria (Chiche *et al.*, 2010). Therefore the enlarged disc-like structures that manifest after 12 hours of hypoxic treatment could also indicate a survival pathway through the autophagic degradation of potentially damaged mitochondria by doxorubicin (**Fig. 3.11.1C**). This process is termed mitophagy. A beneficial role of BNIP3-regulated mitophagy in mouse embryonic

fibroblasts was described in 2008 by Zhang *et al*. where the knock-down of BNIP3 caused an increase in mitochondrial mass and hypoxia-induced cellular demise. This effect was reversed when BNIP3 expression was forced (Zhang *et al.*, 2008). Therefore, in the scenario of this study, HIF-1 induced mitophagy may reduce the oxidative damage conferred by doxorubicin. Further studies are required to assess the extent of mitophagy and the oxidative phosphorylation status.

Upon the ablation of HIF-1, this defensive process of mitochondrial fusion or mitophagy should be mitigated, and thus augment the fragmentation of mitochondria while decreasing its functionality in the presence of the antineoplastic drug, doxorubicin.

## 4.3 *IN VIVO*

The efficacy of the adjuvant treatment was investigated in an *in vivo* setting in order to determine whether the effects observed within the *in vitro* component of this study would be translated into an animal model. By exploiting the hypoxic response that would otherwise fuel the growth of a solid tumour, the sensitivity to chemotherapeutic intervention could be improved. For the treatment of mice bearing an E0771 xenograft (~4 week growth), the dosages of the drugs employed were based on those previously reported in the literature that combined effectiveness while simultaneously limiting harmful side effects. The aims of the *in vivo* component of the study were as follows:

1. To evaluate to effect of doxorubicin treatment, either alone or in combination with 2-methoxyestradiol, on the rate of tumour growth.
2. To assess the degree of systemic toxicity conferred upon mice after treatment with doxorubicin, either alone or combination with 2-methoxyestradiol.
3. To characterize the molecular events within the tumour tissue in response to doxorubicin treatment, either alone or in combination with 2-methoxyestradiol.

### 4.3.1 The effect of treatment on the tumour growth rate and systemic toxicity

While a non-significant change in body weight of all animals during the two week treatment period provided an indication of low systemic toxicity, mice treated with doxorubicin, in absence and presence of 2-methoxyestradiol, exhibited slight tissue blistering at the infusion site.

The intraperitoneal administration of doxorubicin (5 $mg.kg^{-1}$) and 2-methoxyestradiol (45 $mg.kg^{-1}$), separately and in combination, had no significant effect on the rate of tumour growth after the two week treatment regime (**Fig. 3.13**). Despite the lack of changes in the size of the tumour, the treatment did cause variations on the molecular level.

### 4.3.2 The effect of treatment on cellular death pathways, the oxygen sensor (AMPK) and hypoxia

In relation to the E0771 tumour xenografts of mice that did not receive any treatment, doxorubicin caused a significant decrease in the amount of apoptosis as evident from the reduced cleavage of PARP (**Fig. 3.14**), while the diminishing levels of p62 signified an elevation in autophagy in this group (**Fig. 3.15**). The metabolic sensor, AMPK, became increasingly activated by a significant degree (**Fig. 3.17**) in response to chemotherapeutic treatment while the expression of HIF-1α remained unaffected (**Fig. 3.16**).

2-methoxyestradiol treatment caused a response in tumour-bearing mice that was analogous to the doxorubicin treated group in terms of the cellular death pathways (**Fig. 3.14**; **Fig. 3.15**). In contrast to the *in vitro* results, rather than increasing the amount of apoptotic cell death, 2-methoxyestradiol

induced the opposite effect instead. Likewise, HIF-1α expression was not disrupted after the administration of 45 $mg.kg^{-1}$ of this compound (**Fig. 3.16**).

The ability of the adjuvant therapy to induce the apoptotic cellular death pathway while simultaneously inhibiting the autophagic pathway was unexpected. A primary reason for this dismal expectation was firstly due to the fact that 2-methoxyestradiol was incapable of inhibiting the expression of HIF-1α in the *in vivo* setting, an occurrence which would concomitantly induce apoptosis according to the *in vitro* results. Secondly, there was no change in the growth rate of the tumour in this group. Adjuvant therapy, however, reduced HIF-1α expression (**Fig. 3.16**) along with autophagy (**Fig. 3.15**), while yielding a greater amount of type I cell death (**Fig 3.14**).

The non-significant change in the growth of the doxorubicin-treated tumours could represent a putatively 'protective' mechanism instigated by AMPK, allowing the neoplasm to continue proliferating regardless of antineoplastic drug administration. This suggestion can be supported by the finding of the AMPK-dependent upregulation of autophagy and diminished apoptotic potential in this group. These processes were HIF-1α-independent (**Fig. 3.16**) and incapable of manipulating the growth of the tumour.

Similar to the unaffected rate of tumour growth witnessed in the 2-methoxestradiol treated animals, Ireson *et al*. demonstrated the failure of this metabolite to manipulate the growth of an MDA-MB-435 xenograft that had been transplanted into mice (Ireson *et al.*, 2004). They attributed this result to the half-life of the estrogenic derivate which was estimated to be approximately 14 minutes when administered intravenously. There is a possibility that during the *in vivo* experiment, intraperitoneal administration of the drug could accidentally have penetrated other non-specific tissues. The ineffective drug administration may be supported by the appearance of the slight tissue loss/blistering at the injection site after doxorubicin treatment. If a major blood vessel had been penetrated, the direct delivery of 2-methoxyestradiol to the bloodstream would lead to a decreased bioavailability as a result of rapid clearance, preventing this compound from exerting its anti-proliferative and anti-angiogenic functions proficiently.

The non-significant change in tumour growth rate witnessed upon adjuvant therapeutic administration is in disagreement with the outcome of the study carried out by Azab *et al*. (2008). Their combined administration of 5 $mg.kg^{-1}$ doxorubicin and 30 $mg.kg^{-1}$ 2-methoxyestadiol produced a synergistic effect by significantly reducing the growth of doxorubicin-resistant MCF-7 tumour xenografts compared to the untreated tumour-bearing mice (Azab *et al.*, 2008).

There are many additional reasons that could explain the unexpected differences between groups within the animal study.

Firstly, tumours were allowed to reach a measureable volume before the treatment regime commenced. After inoculation of the mice with E0771 cancer the tumours grew at different rates and, by the end of the fourth week (day 28), the mice displayed different-sized tumours. In an attempt to achieve a representative sample of the entire population, mice were allocated to groups so that each

would have a similar-sized tumour. Moreover, the pathophysiological oxygenation status of a tumour is dependent both 'chronic' and 'acute' hypoxia which could lead to an intermittent supply of oxygen to the cancerous cells. The outcome of both factors would be a heterogeneous phenotype manifested within tumours, both in location and intensity (Magagnin *et al.*, 2006). Therefore, while tumours may display a similar size, the oxygenation pattern within is bound to vary between them. It can therefore be surmised that, although the mice were allocated to incorporate a representative degree of tumour sizes, the unexpected variations may be due to the unique hypoxic phenotype of the individual tumours of mice within each group, prior to treatment.

Secondly, an ineffective concentration for doxorubicin and 2-methoxyestradiol and/or the timing of treatment initiation might be responsible for a lack in the expected differences. Furthermore, the two week treatment period could have been insufficient to allow these molecular variations to manifest in a physical change of the rapidly growing tumour. If this was the case, then the effects in the doxorubicin- and/or 2-methoxyestradiol-treated groups would represent the average basal levels of the tumours within that group. Judging from the HIF-1α protein levels which become significantly reduced during adjuvant therapy (**Fig. 3.16**), this would ultimately suggest the existence of another HIF-1α disrupting mechanism that is independent of 2-methoxyestradiol action.

## 4.4 DIFFERENCES BETWEEN *IN VITRO* AND *IN VIVO* EXPERIMENTAL RESULTS

The differences in our results between the *in vitro* and *in vivo* aspect of our study may be attributed to the parameters controlled.

Although the *in vitro* normoxic and hypoxic experimental conditions required cells to be subjected to controlled conditions of 21% ($PO_2$ = 160 mm Hg) and ~0.1% ($PO_2$ = 0.8 mm Hg), respectively, the tissue oxygenation levels within *in vivo* models are rather different. Physiologically, the concentration of oxygen that is normally delivered to tissue is ~5% ($PO_2$ = 40 mm Hg) (Becker & Casabianca, 2009). The pathology of solid tumours, as mentioned above, experiences oxygen levels that are constantly fluctuating resulting in oxygen gradients.

Furthermore, the tumour forms a dynamic relationship with its microenvironment, influenced by several factors including heterogeneous patterns of oxygenation, nutrient and growth factor availability, and neoplastic cellular growth rates. Although these factors may exist simultaneously, it is possible that they may occur exclusively of one another.

While the *in vitro* study focused on the contribution of oxygenation to the status of chemotherapeutic resistance in isolation, it is challenging to control other associated parameters when attempting the same experiment in an *in vivo* setting. The fewer the parameters that are controlled for, the more complex it becomes to extrapolate relationships due to potential irrelevant variation.

Therefore, the extent to which *in vitro* monolayer experiments can be reproduced in an *in vivo* model is limited. The *in vitro* experimental models which elucidate relationships may preclude fundamental aspects of tumour biology.

# CHAPTER 5: CONCLUSION

To overcome the major obstacle of chemotherapeutic resistance that is frequently manifested by breast cancer patients bearing solid tumours, the key mechanisms responsible for the reduced sensitivity of tumours to anticancer treatment needs to be identified before they may be exploited for therapeutic benefit. Furthermore, the conventional use of doxorubicin, an anti-carcinogenic used to treat the pathological state of breast cancer, may potentially cause cardio-toxic effects that could be implicated directly after administration, or manifest months or years later due to excessive build-up of the drug (Minotti *et al.*, 2004).

An extensively studied characteristic present within the microenvironment of solid tumours are the hypoxic regions. The transcription factor HIF-1α elicits a multi-target response from hypoxia-inducible genes that mediate adaptation to this physiologically destructive environment. HIF-1α expression is elevated in tumorigenic breast tissue compared to their non-tumorigenic counterparts, with the level of this expression increasing as the degree of malignancy advances (Zhong *et al.*, 1999; Bos & Zhong, 2001; Schindl & Schoppmann, 2002).

In the pathophysiological context of neoplastic disease, the presence of the autophagic pathway has been considered to act as a survival mechanism. Its activity has been recognized to increase under hypoxia, nutrient deprivation and/or upon chemotherapeutic administration (Chen *et al.*, 2010). It promotes the growth and proliferation of neoplastic cells through the recycling of damaged organelles and proteins, while simultaneously providing the required bioenergetic fuel. In the context of hypoxia, autophagy upregulation is mediated through the expression of the HIF-1α-inducible protein, BNIP3 (Sowter *et al.*, 2001; Zhang *et al.*, 2008). Therefore HIF-1α has become recognized as one of the main instigators in cancer progression under hypoxic conditions.

This study was formulated to uncover the extent to which oxygen deprivation, or hypoxia, contributes to the development of chemotherapeutic resistance. This study aimed to circumvent the hypoxic response by attenuating the HIF-1α master regulator using pharmacological (2-methoxyestradiol) and genetic (siRNA transfection) approaches. In this scenario, the resistance of hypoxic neoplastic cells to doxorubicin is proposed to become abolished. Moreover, the combination of therapies exhibiting different modes of action may allow for the maximum mitigation of tumorigenic cells, while simultaneously being used at sub-toxic doses that would otherwise target and potentially destroy non-malignant cells. While both strategies were capable of mitigating the resistant effect conferred by hypoxia upon doxorubicin-treated MCF-7 cells, the mechanism of action differed between the two. Although the suppression of the HIF-1α mRNA transcript by transcriptional intervention with siRNA was unsuccessful under hypoxic conditions, an alternative approach using the novel HIF-1α-inhibiting drug, 2-methoxyestradiol, effectively abrogated the protein expression and was therefore utilized throughout the study. Furthermore, $CoCl_2$ was able to stabilize the expression of HIF-1α and served as a positive control.

To exploit the autophagic machinery for therapeutic benefit, an understanding of its role in the context of the tumour microenvironment is necessary. With the aid of an inducer and inhibitor of HIF-1α, this aim was satisfied when it was established that the autophagy in the *in vitro* experimental settings was dependent on HIF-1α. This study provided evidence that MCF-7 cells were resistant to doxorubicin treatment under hypoxic conditions (~0.1%; 12 hours), displaying an upregulation of the autophagic pathway. While the upregulation of autophagy under normoxia was attributed to the induced activation of the AMPK energy sensor, we were unable to distinguish the regulator of the lysosomal survival pathway under hypoxia as both AMPK and HIF-1α remained active. The qualitative fluorescent data suggested that the HIF-1α-induced fusion of mitochondria may aid in the hypoxic defence mechanism and protect these organelles from the cytotoxicity of doxorubicin treatment. This hypoxic fusion has also been linked to BNIP3/BNIP3L-dependent autophagy (Chiche *et al.*, 2010).

Rather than eliciting a synergistic cytotoxic effect on the neoplastic MCF-7 growth, the *in vitro* combination of 2-methoxyetradiol with doxorubicin produced an antagonistic effect on cellular viability instead. We suspected this phenomenon to be ascribed to different reasons, depending on the oxygenation status of the environment. Since the combined treatment under normoxia caused a HIF-1-dependent attenuation of autophagy, yet no adverse toxicity on the cellular viability, we propose that the MCF-7 cells under the experimental conditions of the study would possibly enter a state of growth arrest. Senescence may provide a mechanism to avoid anti-proliferative signalling, and allow for tumour recurrence (Hanahan & Weinberg, 2011; Elmore *et al.*, 2005). In contrast, when the neoplastic cells received adjuvant therapy while being exposed to a ~0.1% oxygen environment, HIF-1α remained stabilized. We propose this unaffected protein expression to be the result of a potentiated stabilization of HIF-1α caused by mitochondrial dysfunction upon adjuvant therapy under hypoxic conditions. This mitochondrial dysfunction would lead to the build-up of ROS and TCA cycle intermediates, both of which have been shown to stabilize HIF-1α (Jung *et al.*, 2008; Koivunen *et al.*, 2007). Furthermore, the slight mitogenic effect observed with the MTT assay in this treatment group may be caused by the residual estrogenic activity of 2-methoxyestradiol. We speculate the activity of doxorubicin might induce the demethylation of 2-methoxyestradiol to a more active estrogenic metabolite that can stimulate the ER-receptors of MCF-7 cells.

In the context of the *in vivo* animal model, although the normoxic AMPK-upregulated autophagic process was mimicked in response to doxorubicin administration, its effect on tumour growth was negligible. Similarly, 2-Methoxyestradiol unexpectedly decreased the amount of type I cell death while simultaneously augmenting autophagy, both of which had no prominent consequence on tumour growth rate. To the contrary, a synergistic molecular profile after adjuvant therapeutic administration decreased the autophagy that was upregulated within the tumours. Despite these findings, the adjuvant therapy failed to repress the rate of tumour growth. We conclude that the *in vivo model* requires the treatment regime to be reconsidered in terms of the dosage, the time of initiation, period of treatment, and/or the mode of administration. If administration had been successful, our results would imply the dynamics of the tumour microenvironment to be multi-faceted and demand future *in vivo* studies to control for more parameters.

We therefore reject our hypothesis on the basis that an antagonistic effect, rather than a synergistic effect, was witnessed when the neoplastic breast cell line was treated with the adjuvant therapy. Furthermore, the significant synergistic effect that becomes noticeable *in vivo* at a molecular level failed to manifest significant changes in tumour growth.

The results obtained clearly warrant the need for a more practical, yet extensive testing of 2-methoxyestradiol to reveal its precise pharmacokinetics. Only then can it be optimally employed in adjuvant therapy with doxorubicin and possibly identify a possible hypoxia-targeting therapy.

# CHAPTER 6: LIMITATIONS & FUTURE STUDIES

## 6.1 *IN VITRO*

Although we assessed the expression of HIF-1α, it does not necessarily imply that the stabilized form is transcriptionally active. The synthetic YC-1 compound (Chun *et al.*, 2001) and antibiotic derivate geldanamycin (Mabjeesh *et al.*, 2002) are examples of HIF-1α inhibitors which mediate their effects post-translationally (O'Donnell *et al.*, 2006). The detection of HIF-1α levels may represent expressed HIF-1α prior to protein degradation and may therefore be inaccurate. An evaluation of its transcriptional activity would therefore provide additional validation. This could be achieved by using a HIF-1α responsive reporter assay where the firefly luciferase gene contains an HRE promoter, entailing its transcriptional activation by HIF-1α to be captured as bioluminescent light. Alternatively, immuno-detection of downstream proteins that are known to be HIF-1α-inducible would not only indicate transcriptional activity, but also the specific profile of upregulated proteins.

Since this study focused primarily on cellular death pathways, the metabolic profile of the cancer cell line in the absence or presence of treatments could further be evaluated to compliment the study. The functionality or preference of a pathway may be revealed by inhibiting specific steps in metabolism, such as glycolysis (2-deoxy-D-glucose) and oxidative phosphorylation (oligomycin), and monitoring the changes in ATP availability and the mitochondrial membrane potential. This would enable one to delineate the role of aerobic respiration not only under hypoxic exposure, but within the cancer cells themselves. A technique used to quantify ATP includes a luciferin-luciferase based ATP bioluminescence Assay (Katayama *et al.*, 2007), while mitochondrial membrane potential may be measured by fluorescent microscopy using the potentiometric-sensitive dye tetramethylrhodamine ethyl ester (TMRE) (Kuznetsov *et al.*, 2011). The rate of respiration/$O_2$ consumption before and after anticancer drug-afflicted damage, as well as the possibility of recovery after the damage, may also be monitored with the aid of clark-type electrode (e.g. Hansatech Instrument Oxygraph). With regard to our study, implicating ROS in the hypoxic stabilization of HIF-1α in MCF-7 cells responding to the combined treatment of doxorubicin and 2-methoxyestradiol would entail the measurement of oxygen radicals. ROS measurement has been achieved by fluorescent microscopy using the probes, 2,7'-dichlorofluorescein diacetate (DCFH-DA) (Salama *et al.*, 2011), and MitoSOX™ Red (Kuznetsov *et al.*, 2011).

Aside from the metabolic profile functionally validating our qualitative fluorescent imaging data, the role of mitochondria dynamics can further be unravelled by evaluating the mitochondrial fusion (Mfn1, Mfn2, and OPA1) and fission (DRP1) proteins (Chiche *et al.*, 2010; Frank *et al.*, 2001).

To elucidate whether the mitogenic effect identified in this study was due to the 2-methoxyestradiol's residual estrogenic activity, the experiment should be repeated on ER-negative breast cancer cells (e.g. MDA-MB-231). As 2-methoxyestradiol has a low affinity for estrogen receptors, its potential biotransformation to more reactive estrogen metabolites can mitigated by including inhibitors of cytochrome P450 enzymes. The identification of the precise receptors with which 2-methoxyestradiol

engages to mediate its anti-proliferative and anti-angiogenic effects would enable researchers to successfully exploit its antitumor properties.

To more accurately simulate the native microenvironment of a tumour, the growth of 3-dimensional *in vitro* spheroids rather than a monolayer culture could provide a more relevant representation of tumour structural and functional dynamics. Furthermore, characterisation of the molecular profile using the 3-D *in vitro* analogy testing could then be easily translated into a preclinical *in vivo* model (Doublier *et al.*, 2012).

Lastly, reproducing the experiment in a non-tumorigenic epithelial cell line (e.g. MCF-12A) would allow us to delineate a concentration and time protocol that is selectively cytotoxic to the cancerous MCF-7 cell line, while exert a minimal effect on the normal cell line.

## 6.2 *IN VIVO*

The *in vivo* animal model may be improved by assessing the hypoxic fraction of tumours prior to allocation of the mice, therefore enabling a more accurate representative sample of the population to be identified. One solution would be to use the *in vivo* Imaging System (IVIS), a non-invasive technique that enables the spatial and temporal distribution of fluorescent or bioluminescent markers to be visualized within living animals. By exploiting a reporter gene system where the HIF-1α gene was fused to the firefly luciferase gene, Viola *et al*. (2008) were able to quantify the expression of HIF-1α by measurement of the luciferase signal (Viola *et al.*, 2008). This imaging system also facilitated the changes in the response of HIF-1α to chemotherapy to be monitored. It is therefore an attractive technique that may aid future studies that aim to assess the role of HIF-1α as a potential regulator of drug resistance in cancer treatment.

With regards to the results on tumour growth in the *in vivo* animal model, we suggest this could be attributed to either an unsuccessful intraperitoneal administration of the drugs, or the short-half-life of 2-methoxyestradiol should it have entered the bloodstream of the animal. A solution to this issue would be employing a 2-methoxyestradiol analogue with a slower clearance rate so as to enable the drug to exert its anti-proliferative and anti-angiogenic functions on the tumour growths in our in vivo model. This increased efficacy was noticed by Ireson *et al.* when they compared the pharmacokinetics of 2-methoxyestradiol and its sulphamoylated analogue, 2-methoxyestradiol-bis-sulphamate (2-MeOE2bisMATE) (Ireson *et al.*, 2004). Compared to the low bioavailability of its derivate molecule, oral administration of 2-MeOE2bisMATE (10 $mg.kg^{-1}$) presented a bioavailability of ~85% in *Wistar* rats which peaked after 3 hours and remained detectable in plasma after 24 hours. An oral dosage of 20 $mg.kg^{-1}$ of the analogue was capable of significantly reducing the growth of MDA-MB-435 xenografts after 2 weeks, while the same treatment regime with 2-methoxyestradiol had no effect.

Finally, we recommend that dose- and time-response curves of each individual drug used in the *in vivo* model be implemented prior to confirm effective dosages and time points reported in literature.

Evaluating the precise role of HIF-1α within breast cancer malignancies as well as an efficient means of inhibiting the concomitant hypoxic response may entail the full potential of the antineoplastic drug to be exploited while simultaneously minimizing the adverse toxic side effects associated with its administration.

## REFERENCES


Airley, R., 2009a. Classical anticancer agents. In *Cancer Chemotherapy: Basic Science to the Clinic.* pp. 67 – 116.

Airley, R., 2009b. Histopathology of cancer. In *Cancer Chemotherapy: Basic Science to the Clinic.* pp. 13 – 18.

Airley, R., 2009c. Oncogenesis. In *Cancer Chemotherapy: Basic Science to the Clinic.* pp. 23 – 35.

Airley, R., 2009d. Tumour hypoxia. In *Cancer Chemotherapy: Basic Science to the Clinic.* pp. 177 – 198.

Al-Okail, M.S., 2010. Cobalt chloride, a chemical inducer of hypoxia-inducible factor-1α in U251 human glioblastoma cell line. *Journal of Saudi Chemical Society*, 14(2), pp.197–201.

Alvarez-Gonzalez, R. et al., 1999. Selective loss of poly(ADP-ribose) and the 85-kDa fragment of poly(ADP-ribose) polymerase in nucleoli during alkylation-induced apoptosis of HeLa cells. *The Journal of Biological Chemistry*, 274(45), pp.32122–6.

American Type Culture Collection, 2009. Product information sheet for HTB-22 ™ cell line designation : MCF-7. *ATCC*, (Dm), pp.1 – 4. Available at: http://www.atcc.org/attachments/17392.pdf [Accessed November 26, 2012].

Anlar, B. et al., 2003. Apoptosis in the developing human brain: a preliminary study of the frontal region. *Early Human Development*, 71(1), pp.53–60.

Azab, S.S. et al., 2008. 2-Methoxyestradiol reverses doxorubicin resistance in human breast tumor xenograft. *Cancer Chemotherapy and Pharmacology*, 62(5), pp.893–902.

Barchiesi, F. et al., 2006. 2-Methoxyestradiol, an estradiol metabolite, inhibits neointima formation and smooth muscle cell growth via double blockade of the cell cycle. *Circulation Research*, 99(3), pp.266–74.

Becker, D.E. & Casabianca, A.B., 2009. Respiratory monitoring: physiological and technical considerations. *Anesthesia Progress*, 56(1), pp.14–20; quiz 21–2.

Bos, R. & Zhong, H., 2001. Levels of hypoxia-inducible factor-1α during breast carcinogenesis. *Journal of the National Cancer Institute*, 93(4), pp.309–314. Available at: http://jnci.oxfordjournals.org/content/93/4/309.short [Accessed December 9, 2012].

Botto, M., 2004. Phosphatidylserine receptor and apoptosis : consequences of a non-ingested meal. *Arthritis Research & Therapy*, 6(4), pp.147–150.

Bracken, C.P. et al., 2006. Cell-specific regulation of hypoxia-inducible factor (HIF)-1alpha and HIF-2alpha stabilization and transactivation in a graded oxygen environment. *The Journal of Biological Chemistry*, 281(32), pp.22575–85.

Bradford, M.M., 1976. A rapid and sensitive method for the quantitation of microgram quantities of protein utilizing the principle of protein-dye binding. *Analytical Biochemistry*, 72, pp.248–54.

Brantley-Finley, C. et al., 2003. The JNK, ERK and p53 pathways play distinct roles in apoptosis mediated by the antitumor agents vinblastine, doxorubicin, and etoposide. *Biochemical Pharmacology*, 66(3), pp.459–469.

Brizel, D.M. et al., 2001. Elevated tumor lactate concentrations predict for an increased risk of metastases in head-and-neck cancer. *International Journal of Radiation Oncology*, 51(2), pp.349 – 353.

Bruick, R.K. & McKnight, S.L., 2001. A conserved family of prolyl-4-hydroxylases that modify HIF. *Science*, 294(5545), pp.1337–40.

Bu, S. et al., 2002. Mechanisms for 2-methoxyestradiol-induced apoptosis of prostate cancer cells. *FEBS Letters*, 531(2), pp.141–51.

Cancer Research UK, 2012. World Cancer Fact Sheet, 2008. *International Agency for Research on Cancer*, 2008(2008), pp.1 – 4. Available at: http://gicr.iarc.fr/files/resources/20120906-WorldCancerFactSheet.pdf [Accessed November 26, 2012].

Carew, J. & Medina, E., 2010. Autophagy inhibition enhances vorinostat-• induced apoptosis via ubiquitinated protein accumulation. *Journal of Cellular and Molecular Medicine*, 14(10), pp.2448–2459.

Chan, D. & Sutphin, P., 2005. Coordinate regulation of the oxygen-dependent degradation domains of hypoxia-inducible factor 1α. *Molecular and Cellular Biology*, 25(15), pp.6415 – 6426.

Chandel, N., 1998. Mitochondrial reactive oxygen species trigger hypoxia-induced transcription. *Proceedings of the National Academy of Sciences*, 95, pp.11715–11720.

Chandel, N.S. et al., 2000. Reactive oxygen species generated at mitochondrial complex III stabilize hypoxia-inducible factor-1alpha during hypoxia: a mechanism of O2 sensing. *The Journal of Biological Chemistry*, 275(33), pp.25130–8.

Chen, H. & Chan, D.C., 2005. Emerging functions of mammalian mitochondrial fusion and fission. *Human Molecular Genetics*, 14(2), pp.283–9.

Chen, H., Chomyn, A. & Chan, D.C., 2005. Disruption of fusion results in mitochondrial heterogeneity and dysfunction. *The Journal of Biological Chemistry*, 280(28), pp.26185–92.

Chen, M. et al., 2011. Activation of AMP-activated protein kinase contributes to doxorubicin-induced cell death and apoptosis in cultured myocardial H9c2 cells. *Cell Biochemistry and Biophysics*, 60(3), pp.311–22.

Chen, Nan & Debnath, J., 2010. Autophagy and tumorigenesis. *FEBS Letters*, 584(7), pp.1427–35.

Chen, Ning & Karantza-Wadsworth, V., 2009. Role and regulation of autophagy in cancer. *Biochimica et Biophysica Acta*, 1793(9), pp.1516–23.

Chen, S. et al., 2010. Autophagy is a therapeutic target in anticancer drug resistance. *Biochimica et Biophysica Acta*, 1806(2), pp.220–9.

Cheung, N.K. et al., 2001. N7: a novel multi-modality therapy of high risk neuroblastoma (NB) in children diagnosed over 1 year of age. *Medical and Pediatric Oncology*, 36(1), pp.227 – 230.

Chiche, J. et al., 2010. Hypoxic enlarged mitochondria protect cancer cells from apoptotic stimuli. *Journal of Cellular Physiology*, 222(3), pp.648–57.

Chun, Y.S. et al., 2001. Inhibitory effect of YC-1 on the hypoxic induction of erythropoietin and vascular endothelial growth factor in Hep3B cells. *Biochemical Pharmacology*, 61(8), pp.947–54.

Clayton, J.R. & Hardwick, J.M., 2008. Apoptosis and Virus Infection. In *Encyclopedia of Virology (Third Edition)*. pp. 154–162.

Comerford, K., Wallace, T. & Karhausen, J., 2002. Hypoxia-inducible factor-1-dependent regulation of the multidrug resistance (MDR1) gene. *Cancer Research*, 62, pp.3387–3394.

Cutts, S., Rephaeli, A. & Nudelman, A., 2001. Molecular basis for the synergistic interaction of adriamycin with the formaldehyde-releasing prodrug pivaloyloxymethyl butyrate (AN-9). *Cancer Research*, 61, pp.8194–8202.

Dahut, W. & Lakhani, N., 2006. Phase I clinical trial of oral 2-methoxyestradiol, an antiangiogenic and apoptotic agent, in patients with solid tumors. *Cancer Biology & Therapy*, 5(1), pp.22–27.

Dai, Y., Bae, K. & Siemann, D.W., 2011. Impact of hypoxia on the metastatic potential of human prostate cancer cells. *International Journal of Radiation Oncology, Biology, Physics*, 81(2), pp.521–8.

Dawling, S., Roodi, N. & Parl, F.F., 2003. Methoxyestrogens Exert Feedback Inhibition on Cytochrome P450 1A1 and 1B1. *Cancer Research*, 63, pp.3127–3132.

Dean-Colomb, W. & Esteva, F.J., 2008. Her2-positive breast cancer: herceptin and beyond. *European Journal of Cancer*, 44(18), pp.2806–12.

Degenhardt, K. et al., 2010. Autophagy promotes tumor cell survival and restricts necrosis, inflammation, and tumorigensis. *Cancer Cell*, 10(1), pp.51–64.

Degterev, A., Boyce, M. & Yuan, J., 2003. A decade of caspases. *Oncogene*, 22(53), pp.8543–67.

Di, X. et al., 2009. Apoptosis, autophagy, accelerated senescence and reactive oxygen in the response of human breast tumor cells to adriamycin. *Biochemical Pharmacology*, 77(7), pp.1139–50.

Dome, B. et al., 2009. Circulating endothelial cells, bone marrow-derived endothelial progenitor cells and proangiogenic hematopoietic cells in cancer: From biology to therapy. *Critical Reviews in Oncology/Hematology*, 69(2), pp.108–24.

Doublier, S. et al., 2012. HIF-1 activation induces doxorubicin resistance in MCF7 3-D spheroids via P-glycoprotein expression: a potential model of the chemo-resistance of invasive micropapillary carcinoma of the breast. *BMC Cancer*, 12, p.4.

Du, Y. & Lou, H., 2008. Catechin and proanthocyanidin B4 from grape seeds prevent doxorubicin-induced toxicity in cardiomyocytes. *European Journal of Pharmacology*, 591(1-3), pp.96–101.

Dubey, R.K. & Jackson, E.K., 2009. Potential vascular actions of 2-methoxyestradiol. *Trends in Endocrinology and Metabolism*, 20(8), pp.374–9.

Edinger, A.L. & Thompson, Craig B, 2004. Death by design: apoptosis, necrosis and autophagy. *Current Opinion in Cell Biology*, 16(6), pp.663–9.

Egan, D.F. et al., 2011. Phosphorylation of ULK1 (hATG1) by AMP-activated protein kinase connects energy sensing to mitophagy. *Science*, 331(6016), pp.456 – 461.

Elmore, L.W. et al., 2005. Evasion of a single-step, chemotherapy-induced senescence in breast cancer cells: implications for treatment response. *Clinical Cancer Research*, 11(7), pp.2637–43.

Epstein, A., Gleadle, J. & McNeill, L., 2001. C. elegans EGL-9 and Mammalian Homologs Define a Family of Dioxygenases that Regulate HIF by Prolyl Hydroxylation. *Cell*, 107, pp.43–54.

Erler, J.T. et al., 2004. Hypoxia-mediated down-regulation of Bid and Bax in tumors occurs via hypoxia-inducible factor 1-dependent and -independent mechanisms and contributes to drug resistance. *Molecular and Cellular Biology*, 24(7), pp.2875–2889.

Erlich, S., Mizrachy, L. & Segev, O., 2007. Differential interactions between Beclin 1 and Bcl-2 family members. *Autophagy*, 3(6), pp.561–568.

Eskelinen, E. & Saftig, P., 2009. Autophagy: a lysosomal degradation pathway with a central role in health and disease. *Biochimica et Biophysica Acta*, 1793(4), pp.664–73.

Ferreira, L.M.R., 2010. Cancer metabolism: The Warburg effect today. *Experimental and Molecular Pathology*, 89(3), pp.372–380.

Frank, S. et al., 2001. The role of dynamin-related protein 1, a mediator of mitochondrial fission, in apoptosis. *Developmental Cell*, 1(4), pp.515–25.

Fujita, M. et al., 2002. Blockade of angiotensin AT1a receptor signaling reduces tumor growth, angiogenesis, and metastasis. *Biochemical and Biophysical Research Communications*, 294(2), pp.441 – 447.

Fujita, N. et al., 2008. The Atg16L complex specifies the site of LC3 lipidation for membrane biogenesis in autophagy. *Molecular Biology of the Cell*, 19(5), pp.2092 – 2100.

Fukumura, D. & Jain, R.K., 2007. Tumor microvasculature and microenvironment: targets for anti-angiogenesis and normalization. *Microvascular Research*, 74(2-3), pp.72–84.

Galluzzi, L. et al., 2010. Mitochondrial gateways to cancer. *Molecular Aspects of Medicine*, 31(1), pp.1–20.

Gewirtz, D., 1999. A critical evaluation of the mechanisms of action proposed for the antitumor effects of the anthracycline antibiotics adriamycin and daunorubicin. *Biochemical Pharmacology*, 57(98), pp.727–741.

Globocan, 2010. World Cancer Fact Sheet, 2008. *International Agency for Research on Cancer*, pp.1–7. Available at: http://globocan.iarc.fr/factsheet.asp [Accessed November 26, 2012].

Gogvadze, V., Zhivotovsky, B. & Orrenius, S., 2010. The Warburg effect and mitochondrial stability in cancer cells. *Molecular Aspects of Medicine*, 31(1), pp.60–74.

González-Polo, R. et al., 2005. The apoptosis/autophagy paradox: autophagic vacuolization before apoptotic death. *Journal of Cell Science*, 118(14), pp.3091–102.

Gozuacik, D. & Kimchi, Adi, 2004. Autophagy as a cell death and tumor suppressor mechanism. *Oncogene*, 23(16), pp.2891–906.

Graeber, T.G. et al., 1996. Hypoxia-mediated selection of cells with diminished apoptotic potential in solid tumours. *Nature*, 4(379), pp.88 – 91.

Han, G. et al., 2005. Synergism between the anticancer actions of 2-methoxyestradiol and microtubule-disrupting agents in human breast cancer. *Cancer Research*, 65, pp.387–393.

Hanahan, D. & Weinberg, R.A., 2011. Hallmarks of cancer: the next generation. *Cell*, 144(5), pp.646–74.

Hansen, A.E. et al., 2011. Hypoxia-inducible factors--regulation, role and comparative aspects in tumourigenesis. *Veterinary and Comparative Oncology*, 9(1), pp.16–37.

Hardie, D.G., 2004. The AMP-activated protein kinase pathway - new players upstream and downstream. *Journal of Cell Science*, 117(23), pp.5479–87.

Harrison, M.R. et al., 2011. A Phase II study of 2-methoxyestradiol (2ME2) NanoCrystal®Dispersion (NCD) in patients with taxane-refractory, metastatic castrate-resistant prostate cancer (CRPC). *Invest New Drugs*, 29(6), pp.1465–1474.

Hatam, N. et al., 2011. Quality of life and toxicity in breast cancer patients using adjuvant TAC (docetaxel, doxorubicin, cyclophosphamide), in comparison with FAC (doxorubicin, cyclophosphamide, 5-fluorouracil). *Archives of Gynecology and Obstetrics*, 284(1), pp.215–20.

Hewitson, K.S. et al., 2007. Structural and mechanistic studies on the inhibition of the hypoxia-inducible transcription factor hydroxylases by tricarboxylic acid cycle intermediates. *The Journal of Biological Chemistry*, 282(5), pp.3293–301.

Hoffmann, P.R. & Ogden, C.A., 2001. Phosphatidylserine (PS) induces PS receptor–mediated macropinocytosis and promotes clearance of apoptotic cells. *The Journal of Cellular Biology*, 155(4), pp.649–659. Available at: http://jcb.rupress.org/content/155/4/649.abstract [Accessed December 9, 2012].

Huang, P. et al., 2000. Superoxide dismutase as a target for the selective killing of cancer cells. *Letters to Nature*, 407(September), pp.390 – 395.

Ireson, C.R. et al., 2004. Pharmacokinetics and efficacy of 2-methoxyoestradiol and 2-methoxyoestradiol-bis-sulphamate in vivo in rodents. *British Journal of Cancer*, 90(4), pp.932–7.

Iscan, M. et al., 2001. The expression of cytochrome P450 enzymes in human breast tumours and normal breast tissue. *Breast Cancer Research & Treatment*, 70.(1), pp.47 – 54.

James, J. et al., 2006. Phase I safety , pharmacokinetic and pharmacodynamic studies of 2-methoxyestradiol alone or in combination with docetaxel in patients with locally recurrent or metastatic breast cancer. *Invest New Drugs*, 25, pp.41–48.

Jiang, X. & Wang, X., 2004. Cytochrome C-mediated apoptosis. *Annual Review of Biochemistry*, 73, pp.87–106.

Jung, C.H. et al., 2010. mTOR regulation of autophagy. *FEBS Letters*, 584(7), pp.1287–95.

Jung, S. et al., 2008. Reactive oxygen species stabilize hypoxia-inducible factor-1 alpha protein and stimulate transcriptional activity via AMP-activated protein kinase in DU145 human prostate cancer cells. *Carcinogenesis*, 29(4), pp.713–21.

Kanzawa, T. et al., 2003. Induction of autophagic cell death in malignant glioma cells by arsenic trioxide. *Cancer Research*, 63, pp.2103–2108.

Katayama, M. et al., 2007. DNA damaging agent-induced autophagy produces a cytoprotective adenosine triphosphate surge in malignant glioma cells. *Cell Death and Differentiation*, 14(3), pp.548–58.

Kato, S. et al., 2008. 2-Methoxyestradiol mediates apoptosis through cancer cells but not in normal counterparts. *Reproductive Sciences*, 15(9), pp.878 – 894.

Keith, B., Johnson, R. & Simon, M., 2011. HIF1α and HIF2α: sibling rivalry in hypoxic tumour growth and progression. *Nature Reviews Cancer*, 12, pp.9 – 22.

Kessler, J. et al., 2010. HIF-1α inhibition by siRNA or chetomin in human malignant glioma cells: effects on hypoxic radioresistance and monitoring via CA9 expression. *BMC Cancer*, 10(605), pp.1 – 11.

Kim, J. et al., 2006. HIF-1-mediated expression of pyruvate dehydrogenase kinase: a metabolic switch required for cellular adaptation to hypoxia. *Cell Metabolism*, 3(3), pp.177–85.

Klimova, T. & Chandel, N.S., 2008. Mitochondrial complex III regulates hypoxic activation of HIF. *Cell Death and Differentiation*, 15(4), pp.660–6.

Koivunen, P. et al., 2007. Inhibition of hypoxia-inducible factor (HIF) hydroxylases by citric acid cycle intermediates: possible links between cell metabolism and stabilization of HIF. *The Journal of Biological Chemistry*, 282(7), pp.4524–32.

Kondo, A. et al., 2001. Hypoxia-induced enrichment and mutagenesis of cells that have lost DNA mismatch repair. *Cancer Research*, 61, pp.7603–7607.

Koo, D.H. et al., 2007. Adjuvant chemotherapy with 5-fluorouracil, doxorubicin and mitomycin-C (FAM) for 6 months after curative resection of gastric carcinoma. *European Journal of Surgical Oncology*, 33(7), pp.843 – 848.

Koshiba, T. et al., 2004. Structural basis of mitochondrial tethering by mitofusin complexes. *Science*, 305(5685), pp.858–62. Available at: http://www.ncbi.nlm.nih.gov/pubmed/15297672 [Accessed November 14, 2012].

Kroemer, Guido & Pouyssegur, J., 2008. Tumor cell metabolism: cancer's Achilles' heel. *Cancer Cell*, 13(6), pp.472–82.

Kuma, A. & Mizushima, N., 2010. Physiological role of autophagy as an intracellular recycling system: with an emphasis on nutrient metabolism. *Seminars in Cell & Developmental Biology*, 21(7), pp.683–90.

Kumar, A.P., Garcia, G.E. & Slaga, T.J., 2001. 2-Methoxyestradiol blocks cell-cycle progression at G2/M phase and inhibits growth of human prostate cancer cells. *Molecular Carcinogenesis*, 31, pp.111 – 124.

Kumar, R., Herbert, P.E. & Warrens, A.N., 2005. An introduction to death receptors in apoptosis. *International Journal of Surgery*, 3(4), pp.268–77.

Kuznetsov, A. V et al., 2011. Changes in mitochondrial redox state, membrane potential and calcium precede mitochondrial dysfunction in doxorubicin-induced cell death. *Biochimica et Biophysica Acta*, 1813(6), pp.1144–52.

Larsen, M. et al., 2008. Hypoxia-induced secretion of macrophage migration-inhibitory factor from MCF-7 breast cancer cells is regulated in a hypoxia-inducible factor-independent manner. *Cancer letters*, 265(2), pp.239–49.

Laughner, E. & Taghavi, P., 2001. HER2 (neu) signaling increases the rate of hypoxia-inducible factor 1α (HIF-1α) synthesis: novel mechanism for HIF-1-mediated vascular endothelial growth factor expression. *Molecular and Cellular Biology*, 21(12), pp.3995 – 4004.

LaVallee, T. M., Zhan, X.H. & Herbstritt, C.J., 2002. 2-Methoxyestradiol inhibits proliferation and induces apoptosis independently of estrogen receptors α and β. *Cancer Research*, 62, pp.3691–3697.

LaVallee, T. M., Zhan, X.H. & Johnson, M. S., 2003. 2-Methoxyestradiol up-regulates death receptor 5 and induces apoptosis through activation of the extrinsic pathway. *Cancer Research*, 63, pp.468–475.

Lawen, A., 2003. Apoptosis - an introduction. *BioEssays*, 25(9), pp.888–96.

Lee, M., 2009. Hypoxia targeting gene expression for breast cancer gene therapy. *Advanced Drug Delivery Reviews*, 61(10), pp.842–9.

Levine, B., Sinha, S. & Kroemer, G, 2008. Bcl-2 family members: dual regulators of apoptosis and autophagy. *Autophagy*, 4(5), pp.600–606.

Levy, J.M.M. & Thorburn, A., 2011. Targeting autophagy during cancer therapy to improve clinical outcomes. *Pharmacology & Therapeutics*, 131(1), pp.130–41.

Levy, V. et al., 2001. Evaluating treatment strategies in chronic lymphocytic leukemia: use of quality-adjusted survival analysis. *Journal of Clinical Epidemiology*, 54(7), pp.747 – 754.

Liang, X.H. et al., 1999. Induction of autophagy and inhibition of tumorigenesis by beclin 1. *Nature*, 402, pp.672–6.

Liu, X.W. et al., 2010. HIF-1α-dependent autophagy protects HeLa cells from fenretinide (4-HPR)-induced apoptosis in hypoxia. *Pharmacological Research*, 62(5), pp.416–25.

Liu, Z. & Zhu, B.T., 2004. Concentration-dependent mitogenic and antiproliferative actions of 2-methoxyestradiol in estrogen receptor-positive human breast cancer cells. *The Journal of Steroid Biochemistry and Molecular Biology*, 88(3), pp.265–75.

Lowe, S. & Lin, A., 2000. Apoptosis in cancer. *Carcinogenesis*, 21(3), pp.485–495.

Lum, J.J. et al., 2005. Growth factor regulation of autophagy and cell survival in the absence of apoptosis. *Cell*, 120(2), pp.237–48.

Lüpertz, R. et al., 2010. Dose- and time-dependent effects of doxorubicin on cytotoxicity, cell cycle and apoptotic cell death in human colon cancer cells. *Toxicology*, 271(3), pp.115–21.

Mabjeesh, N., Post, D. & Willard, M., 2002. Geldanamycin induces degradation of hypoxia-inducible factor 1α protein via the proteosome pathway in prostate cancer cells. *Cancer Research*, 62, pp.2478–2482. Available at: http://cancerres.aacrjournals.org/content/62/9/2478.short [Accessed December 5, 2012].

Mabjeesh, N.J. et al., 2003. 2ME2 inhibits tumor growth and angiogenesis by disrupting microtubules and dysregulating HIF. *Cancer Cell*, 3(4), pp.363–75.

Magagnin, M.G., Koritzinsky, M. & Wouters, Bradly G, 2006. Patterns of tumor oxygenation and their influence on the cellular hypoxic response and hypoxia-directed therapies. *Drug Resistance Updates*, 9(4-5), pp.185–97.

Maiuri, M. C. et al., 2010. Autophagy regulation by p53. *Current Opinion in Cell Biology*, 22(2), pp.181–5.

Maiuri, M. C. et al., 2007. Self-eating and self-killing: crosstalk between autophagy and apoptosis. *Molecular Cell Biology*, 8(9), pp.741–52.

Majeski, A.E. & Dice, J.F., 2004. Mechanisms of chaperone-mediated autophagy. *The International Journal of Biochemistry & Cell biology*, 36(12), pp.2435–44.

Matei, D. et al., 2009. Activity of 2 methoxyestradiol (Panzem NCD) in advanced, platinum-resistant ovarian cancer and primary peritoneal carcinomatosis: a Hoosier Oncology Group trial. *Gynecologic Oncology*, 115(1), pp.90–6.

Mathew, R. et al., 2009. Autophagy suppresses tumorigenesis through elimination of p62. *Cell*, 137(6), pp.1062–75.

Mathew, R. & White, E., 2011. Autophagy in tumorigenesis and energy metabolism: friend by day, foe by night. *Current Opinion in Genetics & Development*, 21(1), pp.113–9.

Mathiasen, I.S. & Jäättelä, M., 2002. Triggering caspase-independent cell death to combat cancer. *Trends in Molecular Medicine*, 8(5), pp.212–20.

Meijer, A.J. & Codogno, P., 2004. Regulation and role of autophagy in mammalian cells. *The International Journal of Biochemistry & Cell Biology*, 36(12), pp.2445–62.

Michalak, E. et al., 2005. Death squads enlisted by the tumour suppressor p53. *Biochemical and Biophysical Research Communications*, 331(3), pp.786–98.

Minotti, G., Menna, P. & Salvatorelli, E., 2004. Anthracyclines: molecular advances and pharmacologic developments in antitumor activity and cardiotoxicity. *Pharmacological Reviews*, 56(2), pp.185–229.

Mizushima, N., 2010. The role of the Atg1/ULK1 complex in autophagy regulation. *Current Opinion in Cell Biology*, 22(2), pp.132–9.

Mizushima, N. & Yoshimori, T, 2007. How to interpret LC3 immunoblotting. *Autophagy*, 3(6), pp.542–545.

Mole, D., Blancher, C. & Copley, R., 2009. Genome-wide association of hypoxia-inducible factor (HIF)-1α and HIF-2α DNA binding with expression profiling of hypoxia-inducible transcripts. *Journal of Biological Chemistry*, 284(25), pp.16767 – 16775.

Mooberry, S.L., 2003. Mechanism of action of 2-methoxyestradiol: new developments. *Drug Resistance Updates*, 6(6), pp.355–361.

Morse, S., 2003. For better or for worse, till the human development index do us part? *Ecological Economics*, 45(2), pp.281–296.

Morselli, E. et al., 2009. Anti- and pro-tumor functions of autophagy. *Biochimica et Biophysica Acta*, 1793(9), pp.1524–32.

Mosmann, T., 1983. Rapid colorimetric assay for cellular growth and survival: application to proliferation and cytotoxicity assays. *Journal of Imunological Methods*, 65(1-2), pp.55 – 63.

Mueck, A.O. & Seeger, H., 2010. 2-Methoxyestradiol - biology and mechanism of action. *Steroids*, 75(10), pp.625–31.

Mungai, P.T. et al., 2011. Hypoxia triggers AMPK activation through reactive oxygen species-mediated activation of calcium release-activated calcium channels. *Molecular and Cellular Biology*, 31(17), pp.3531–45.

Murphy, E.D., 1966. Characteristic Tumors. In *Biology of the Laboratory Mouse*. p. Chapter 27.

Nardinocchi, L. et al., 2009. Inhibition of HIF-1alpha activity by homeodomain-interacting protein kinase-2 correlates with sensitization of chemoresistant cells to undergo apoptosis. *Molecular Cancer*, 8, p.1.

Nguewa, P.A. et al., 2005. Poly(ADP-ribose) polymerases: homology, structural domains and functions. Novel therapeutical applications. *Progress in Biophysics and Molecular Biology*, 88(1), pp.143–72.

Notte, A., Leclere, L. & Michiels, C., 2011. Autophagy as a mediator of chemotherapy-induced cell death in cancer. *Biochemical Pharmacology*, 82(5), pp.427–34.

Oakman, C. et al., 2011. Uncovering the metabolomic fingerprint of breast cancer. *The International Journal of Biochemistry & Cell Biology*, 43(7), pp.1010–20.

Oberstein, A., Jeffrey, P.D. & Shi, Yigong, 2007. Crystal structure of the Bcl-XL-Beclin 1 peptide complex: Beclin 1 is a novel BH3-only protein. *The Journal of Biological Chemistry*, 282(17), pp.13123–32.

O'Donnell, J.L. et al., 2006. Oncological implications of hypoxia inducible factor-1alpha (HIF-1alpha) expression. *Cancer Treatment Reviews*, 32(6), pp.407–16.

Parks, M. et al., 2011. 2-Methoxyestradiol: new perspectives in colon carcinoma treatment. *Molecular and Cellular Endocrinology*, 331(1), pp.119–28.

Qu, X., Yu, J. & Bhagat, G., 2003. Promotion of tumorigenesis by heterozygous disruption of the beclin 1 autophagy gene. *Journal of Clinical Investigation*, 112(12), pp.1809–1820.

Rademakers, S.E. et al., 2008. Molecular aspects of tumour hypoxia. *Molecular Oncology*, 2(1), pp.41–53.

Rapisarda, A. & Melillo, G., 2009. Role of the hypoxic tumor microenvironment in the resistance to anti-angiogenic therapies. *Drug Resistance Updates*, 12(3), pp.74–80.

Raschi, E. et al., 2010. Anticancer drugs and cardiotoxicity: Insights and perspectives in the era of targeted therapy. *Pharmacology & Therapeutics*, 125(2), pp.196–218.

Razeghi, P. et al., 2001. Hypoxia in vivo decreases peroxisome proliferator-activated receptor alpha-regulated gene expression in rat heart. *Biochemical and Biophysical Research Communications*, 287(1), pp.5–10.

Razorenova, O. V. et al., 2011. VHL loss in renal cell carcinoma leads to up-regulation of CUB domain-containing protein 1 to stimulate PKCδ-driven migration. *Proceedings of the National Academy of Sciences*, 108(5), pp.1931–6.

Robey, I.F. et al., 2005. Hypoxia-Inducible Factor-1α and the Glycolytic Phenotype in Tumors. *Neoplasia*, 7(4), pp.324–330.

Rohwer, N. & Cramer, T., 2011. Hypoxia-mediated drug resistance: novel insights on the functional interaction of HIFs and cell death pathways. *Drug Resistance Updates*, 14(3), pp.191–201.

Roudier, E. & Perrin, A., 2009. Considering the role of pyruvate in tumor cells during hypoxia. *Biochimica et Biophysica Acta*, 1796(2), pp.55–62.

Salama, S. et al., 2011. 2-Methoxyestradiol, an endogenous estrogen metabolite, sensitizes radioresistant MCF-7/FIR breast cancer cells through multiple mechanisms. *International Journal of Radiation Oncology, Biology, Physics*, 80(1), pp.231–9.

Sanders, M.J. et al., 2007. Investigating the mechanism for AMP activation of the AMP-activated protein kinase cascade. *The Biochemical Journal*, 403(1), pp.139–48.

Schindl, M. & Schoppmann, S., 2002. Overexpression of hypoxia-inducible factor 1α is associated with an unfavorable prognosis in lymph node-positive breast cancer. *Clinical Cancer Research*, 8, pp.1831–1837.

Semenza, G. L., 2009. Regulation of cancer cell metabolism by hypoxia-inducible factor 1. *Seminars in Cancer Biology*, 19(1), pp.12–6.

Sessa, C. et al., 2008. Phase I clinical and pharmacokinetic study of trabectedin and doxorubicin in advanced soft tissue sarcoma and breast cancer. *European Journal of Cancer*, 45(7), pp.1153 – 1161.

Shimizu, S. et al., 2004. Role of Bcl-2 family proteins in a non-apoptotic programmed cell death dependent on autophagy genes. *Nature Cell Biology*, 6(12), pp.1221 – 1228.

Singh, M. N.et al, 2007. Tamoxifen: Important considerations of a multi-functional compound with organ specific properties. *Cancer Treatment Reviews*, 33, pp.91 – 100.

Solaini, G. et al., 2010. Hypoxia and mitochondrial oxidative metabolism. *Biochimica et Biophysica Acta*, 1797(6-7), pp.1171–7.

Solaini, G., Sgarbi, G. & Baracca, A., 2011. Oxidative phosphorylation in cancer cells. *Biochimica et Biophysica Acta*, 1807(6), pp.534–42.

Song, J. et al., 2009. Hypoxia-induced autophagy contributes to the chemoresistance of hepatocellular carcinoma cells. *Autophagy*, 5(8), pp.1131–44.

Sowter, H., Ratcliffe, P. & Watson, P., 2001. HIF-1-dependent regulation of hypoxic induction of the cell death factors BNIP3 and NIX in human tumors. *Cancer Research*, 61, pp.6669–6673.

Stander, B.A. et al., 2010. In vitro effects of 2-methoxyestradiol on morphology, cell cycle progression, cell death and gene expression changes in the tumorigenic MCF-7 breast epithelial cell line. *The Journal of Steroid Biochemistry and Molecular Biology*, 119(3-5), pp.149–60.

Steinbach, J.P. & Weller, M., 2006. Apoptosis Pathways and Chemotherapy. In *Handbook of Brain Tumor Chemotherapy*. pp. 141–154.

Sturm, I. et al., 2006. Loss of the tissue-specific proapoptotic BH3-only protein Nbk/Bik is a unifying feature of renal cell carcinoma. *Cell Death and Differentiation*, 13(4), pp.619–27.

Su, Y., Zhang, X. & Sinko, P., 2007. Exploitation of drug-induced Bcl-2 overexpression for restoring normal apoptosis function: a promising new approach to the treatment of multidrug resistant cancer. *Cancer Letters*, 253(1), pp.115–23.

Surveillance Research, 2012. Cancer facts & figures, 2012. *American Cancer Society*.

Sutherland, T.E. et al., 2007. 2-Methoxyestradiol - a unique blend of activities generating a new class of anti-tumour/anti-inflammatory agents. *Drug Discovery Today*, 12(13-14), pp.577–84.

Swift, L.P. et al., 2006. Doxorubicin-DNA adducts induce a non-topoisomerase II-mediated form of cell death. *Cancer Research*, 66(9), pp.4863–71.

Todde, V., Veenhuis, M. & Van der Klei, I.J., 2009. Autophagy: principles and significance in health and disease. *Biochimica et Biophysica Acta*, 1792(1), pp.3–13.

Trédan, O. et al., 2007. Drug resistance and the solid tumor microenvironment. *Journal of the National Cancer Institute*, 99, pp.1441–1454.

Twig, G. et al., 2008. Fission and selective fusion govern mitochondrial segregation and elimination by autophagy. *The EMBO Journal*, 27(2), pp.433–46.

Uchida, T. et al., 2004. Prolonged hypoxia differentially regulates hypoxia-inducible factor (HIF)-1alpha and HIF-2alpha expression in lung epithelial cells: implication of natural antisense HIF-1alpha. *The Journal of Biological Chemistry*, 279(15), pp.14871–8.

Vengellur, A. & LaPres, J.J., 2004. The role of hypoxia inducible factor 1alpha in cobalt chloride induced cell death in mouse embryonic fibroblasts. *Toxicological Sciences*, 82(2), pp.638–46.

Viola, R.J. et al., 2008. In vivo bioluminescence imaging monitoring of hypoxia-inducible factor 1α, a promoter that protects cells, in response to chemotherapy. *American Journal of Roentgenology*, 191(6), pp.1779–84.

Wang, F. et al., 2012. Common BRCA1 and BRCA2 mutations in breast cancer families: a meta-analysis from systematic review. *Molecular Biology Reports*, 39(3), pp.2109–18.

Wang, N. et al., 2011. Estrogen receptor positive operable breast cancer: Does menopausal status impact on HER2 and progesterone receptor status? *The Breast*, 20, pp.519 – 524.

Washbrook, E., 2006. Risk factors and epidemiology of breast cancer. In *Women's Health Medicine*. pp. 8–14.

Weljie, A.M. & Jirik, F.R., 2011. Hypoxia-induced metabolic shifts in cancer cells: moving beyond the Warburg effect. *The International Journal of Biochemistry & Cell Biology*, 43(7), pp.981–9.

Xiao, B. et al., 2011. Structure of mammalian AMPK and its regulation by ADP. *Nature*, 472(7342), pp.230–3.

Xue, L., Fletcher, G.C. & Tolkovsky, A.M., 2001. Mitochondria are selectively eliminated from eukaryotic cells after blockade of caspases during apoptosis. *Current Biology*, 11(5), pp.361–5.

Yamamoto, Y. et al, 2001. The Tamoxifen-responsive estrogen receptor α mutant D351Y shows reduced Tamoxifen-dependent interaction with co-repressor complexes. *Journal of Biological Chemistry*, 276, pp.42684 – 42691.

Yeo, E., Chun, Y. & Park, J., 2004. New anticancer strategies targeting HIF-1. *Biochemical Pharmacology*, 68(6), pp.1061–9.

Zakeri, Z., Melendez, A. & Lockshin, R.A., 2008. Detection of autophagy in cell death. In *Methods in Enzymology*. pp. 289–306.

Zhang, H. et al., 2008. Mitochondrial autophagy is an HIF-1-dependent adaptive metabolic response to hypoxia. *The Journal of Biological Chemistry*, 283(16), pp.10892–903.

Zhang, J. et al., 2010. Suppression of hypoxia-inducible factor 1α (HIF-1α) by tirapazamine is dependent on eIF2α phosphorylation rather than the mTORC1/4E-BP1 pathway. *PloS ONE*, 5(11), p.e13910.

Zhang, W. et al., 2007. Nuclear translocation of apoptosis inducing factor is associated with cisplatin induced apoptosis in LNCaP prostate cancer cells. *Cancer Letters*, 255(1), pp.127–34.

Zhong, H. et al., 1999. Overexpression of hypoxia-inducible factor 1α in common human cancers and their metastases. *Cancer Research*, 59, pp.5830–5835.

Van Zijl, C. & Lottering, M., 2008. In vitro effects of 2-• methoxyestradiol on MCF-• 12A and MCF-• 7 cell growth, morphology and mitotic spindle formation. *Cell Biochemistry and Function*, 2(April), pp.632–642.

Zundel, W. & Schindler, C., 2000. Loss of PTEN facilitates HIF-1-mediated gene expression. *Genes & Development*, 14, pp.391–396.

# APPENDIX A: PROTOCOLS

## *IN VITRO*

### SUBCULTURING/PASSAGING

The following aseptic culture procedures should be carried out in a microbiological safety cabinet under sterile conditions.

1. Remove the growth medium from the adherent cells of the culture flask using an aspirator.
2. Rinse the culture with $Ca^{2+}$ or $Mg^{2+}$-free PBS to remove any remaining serum that would inactivate the dissociating agent, trypsin.
3. Detach the cells from their anchor by the process of trypsinization. Trypsin is added at an amount which is sufficient enough to completely cover the surface of the monolayer. Pre-heating the trypsin to 37°C minimizes the exposure time of the cells to this potentially toxic agent.
4. Incubate the T-75 flask at 37°C for ~ 5 minutes without agitation as to avoid clumping. Frequently monitor the cell layer under an inverted microscope to ensure that at least 95% of cells have detached.
5. Terminate the lysis action of trypsin by adding an equal volume of serum-containing growth medium.
6. Transfer the cell suspension to a 15 mL conical Falcon tube. Separate the clumped cells by pipetting up and down several times with a serological pipette.
7. Count the cells using a Hemocytometer.
8. Spin the cell suspension down at 1500 rpm for 3 minutes at ambient temperature.
9. Discard supernatant and resuspended the pellet in the appropriate amount of growth medium.
10. A new culture flask containing the appropriate growth medium is then inoculated with this suspension. Cell growth is monitored using an inverted microscope. Microbial infection can be monitored by the colour change of the phenol red present in the growth medium.

### CELL COUNTING

1. Clean Hemocytometer and coverslip with 70% ethanol just prior to use.
2. Place the coverslip over the grooved calibrated grid until the rainbow-like pattern of Newton's rings become apparent.
3. Using a pipette, transfer ~20 µL of cell suspension to each chamber by touching the tip of the pipette at the edge of the coverslip-hemocytometer barrier.
4. Place the hemocytometer onto the mechanical stage of the inverted microscope and examine.
5. Using a tally counter, count the cells in four corners of the calibrated grid. The average is then multiplied by $10^4$ to obtain the number of cells per mL. Calculate the total amount of cells in the solution my multiplication with the dilution factor.

## CRYOPRESERVATION

Label cryogenic vials with the following information: cell line with passage number, date of freezing, cryoprotective medium used, and cell density.

1. Remove the growth medium from the almost confluent (~90%) cells of a T-75 flask using an aspirator.
2. Rinse the culture with $Ca^{2+}$ or $Mg^{2+}$-free PBS to remove any remaining serum that would inactivate the trypsin.
3. Detach the cells from its growth surface by the addition of trypsin, preheated to minimize exposure time and an amount sufficient enough to completely cover the surface of the monolayer.
4. Incubate the T-75 flask at 37°C for ~ 5 minutes without agitation as to avoid clumping. Monitor under an inverted microscope to ensure that at least 95% of cells have detached.
5. Terminate the lysis action of trypsin by adding an equal volume of serum-containing growth medium.
6. Transfer the cell suspension to a 15 mL conical Falcon tube.
7. Determine the concentration of cells in suspension using a Hemocytometer
8. Spin the cell suspension down at 1500 rpm for 3 minutes at ambient temperature.
9. Discard the supernatant and resuspend the pellet in appropriate amount of cryoprotective medium (FBS + 10% DMSO) so that the cell density is 1 x $10^6$ cells/1 mL. DMSO prevents mechanical injury from ice crystal formation during freezing.
10. Transfer 1ml of cell suspension into each cryogenic vial.
11. The following freezing rate should be followed: -20°C for an hour, -80°C for 24 hours and finally submerged in liquid nitrogen (-196°C) for permanent storage.

## MTT ASSAY

1. Freshly prepare a filtered 1% MTT solution and cover in aluminium foil to protect from light.
2. Remove the medium from the adherent cells in each well of the multi-well plate using an aspirator.
3. Add a prewarmed mixture of PBS: 1% MTT solution (3:1) to each well gently so as to avoid detachment of cells from the surface of the plate.
4. Maintain the plates in the dark at 37°C in a humidified 5% $CO_2$ atmosphere for ~2 hours to allow for colour development.
5. Remove the PBS: 1% MTT solution mixture from the adherent cells in each well of the multi-well plate using an aspirator.
6. Solubilize the formazan crystals by pipetting 1mL of an acidified isopropanol: triton-x (50:1) to each well. Solubilisation is increased by vigorous shaking at 300-500 rpm (~5 minutes).
7. Read the absorbance on a spectrophotometer at a wavelength of 540 nm using the acidified isopropanol: triton-x mixture as a blank.

## CASPASE-GLO® 3/7 ASSAY

1. Thaw the Caspase-Glo® Reagent to room temperature 45 minutes prior to start of the assay.
2. Remove the culture plate from the incubator and equilibrate to room temperature (~10 minutes).
3. Transfer 100 µL of the medium from the culture plate to the wells of a white-walled 96-well plate.
4. Add an equivalent amount (100 µL) of Caspase-Glo® Reagent to each well of a white-walled 96-well plate. Mix the plates at 300-500 rpm (~30 seconds).
5. Incubate the plates in the dark for 60 minutes at a constant room temperature.
6. Measure the luminescence in a luminometer.

## WESTERN BLOTTING

### HARVESTING CELLS/PREPARATION OF LYSATES

1. To avoid proteolysis and de-phosphorylation of proteins, the extraction steps are carried out in a walk-in freezer at 4°C.
2. Label conical tubes for each treatment group.
3. To harvest the detached population of cells that are suspended in the medium, transfer the medium of each treatment group to its respective pre-cooled conical tube.
4. Mechanistically harvest the adherent cells from the growth surface using a rubber spatula after the addition of ~1 mL of ice-cold PBS and transfer to its respective conical tube. Ensure sterilization of the rubber spatula with 70% ethanol between treatment wells. Pellet the cells by centrifuging at 1500 rpm for duration of 3 minutes at 4°C.
5. Resuspend the pellet in ~200 µL modified RIPA lysis buffer (freshly supplemented with 1 µg/1 mL PMSF), transfer to a micro-centrifuge tube and maintain for 10 minutes with gentle agitation.
6. Disrupt the cells using multiple short bursts of a sonicator by immersing the Microtip™ in the cell suspension. Rinse the probe with ethanol between samples to prevent cross-contamination.
7. Remove the insoluble cellular debris by centrifugation in a micro-centrifuge using a force of 8000 rpm for duration of 10 minutes at 4°C.
8. Transfer supernatant to fresh pre-cooled micro-centrifuge tube and store the lysates at -80°C until use.

### BRADFORD ASSAY – COLORIMETRIC ASSAY TO DETERMINE PROTEIN CONCENTRATION

1. Shortly prior to use, prepare a 200 µg/1 mL BSA working solution by diluting the 1 mg/1 mL stock in a 1:4 ratio with $dH_2O$ as the solvent.
2. Label micro-centrifuge tubes for each dilution standard, as well as the treatment group samples to be tested.
3. Prepare a standard curve by setting up a series of BSA dilutions as follows:

| Concentration (µg) | BSA (µL) | $dH_2O$ (µL) |
|---|---|---|
| 0 | 0 | 100 |
| 2 | 10 | 90 |
| 4 | 20 | 80 |
| 8 | 40 | 60 |
| 12 | 60 | 40 |
| 16 | 80 | 20 |
| 20 | 100 | 0 |

4. For each sample to be tested, pipette 5 µL of the supernatant to a microcentrifuge tube containing 95 µL of $dH_2O$. Vortex briefly.
5. Pipette 900 µL of Bradford working reagent to each microcentrifuge tube. Vortex briefly.
6. Incubate the dilution standards and samples for 10 minutes at ambient temperature.
7. Using a spectrophotometer, measure the absorbencies of the dilution standards and samples at a wavelength of 595 nm.
8. Plot a standard curve using the BSA serial dilution absorbencies and quantify the amount of protein in each sample by interpolation.

## SAMPLE PREPARATION

1. Label the desired amount of microcentrifuge tubes for each experimental group.
2. Fix the aliquoted sample in Laemmli sample buffer equal to a third of the final volume.
3. Pipette the amount of supernatant previously calculated to obtain desired protein yield for immunoblotting.
4. Boil the samples for five minutes in a heating block at 95°C. Ensure that pin-sized holes have been made in the microcentrifuge tubes so as to prevent pressure build-up.
5. Store at -80°C in a freezer.

## IMMUNOBLOTTING

*PREPARATION & LOADING OF MINI POLYACRYLAMIDE GELS*

1. Thoroughly clean short glass plates and spacer plates (1 mm thickness) with 70% ethanol and rinse with $dH_2O$.
2. Assemble the short glass plate to the spacer plate in the green casting frame. Complete the assembly by securing the clips and placing the casting frame onto the rubber gasket in the casting stand. Ensure a tight seal between the glass plates and rubber gasket so as to prevent leakage.

3. Make up a 6%/12% resolving polyacrylamide gel (see appendix B). The concentration of acrylamide used in the gel will depend on the size range of the proteins to be separated.
4. Using a plastic Pasteur pipette, immediately transfer the polyacrylamide solution between the glass plates in the assembly. Leave enough space for the stacking gel.
5. Overlay with isobutanol to prevent evaporation and exclude air. Allow resolving gel to polymerise for ~45 minutes. A sharp interface between the top of gel and bottom of isobutanol layer indicates a complete polymerisation.
6. Remove the isobutanol and rinse with $dH_2O$.
7. Make up a 5% stacking polyacrylamide gel (See appendix B).
8. Using a plastic Pasteur pipette, transfer the polyacrylamide solution between the glass plates in the assembly on top of the resolving gel. Gently align the comb (1 mm) in the correct position and allow gel to polymerise for ~10 minutes.
9. Gently remove the comb and rinse the wells out with $dH_2O$.

*SDS – FRACTIONATION OF PROTEIN EXTRACT*

1. Prepare an amount of migration buffer appropriate to the electrophoretic separation apparatus.
2. Retrieve prepared samples from -80°C freezer as well as the molecular weight marker from -20°C and allow to thaw.
3. Remove the glass plates from the casting stand and frame, and place in a U-shaped adapter cassette.
4. Place the assembled cassette into the electrophoresis tank
5. Fill the inner compartment with migration buffer so that it fills the wells
6. Place the yellow sample loading guide onto the top of the U-shaped adapter cassette between the glass plates.
7. The electrophoretic run is monitored by inclusion of 10 µL of molecular weight marker in the well of the first lane.
8. Thereafter, load an equivalent amount of sample protein per well starting from lane 2.
9. Fill the outer compartment with migration buffer
10. Attach the lid and connect the leads to the power supply.
11. An initial run of 100 V (constant) and 200 mA
12. Thereafter, the gel is run at 200 V (constant) and 200 mA.
13. Once the migration front reaches the end of gel, the power to the electrophoresis separation apparatus is switched off. Migration efficiency may be verified by the Coomassie stain (irreversible)

*ELECTROBLOTTING – TRANSFER EXACT REPLICA OF PROTEIN PATTERN FROM GEL TO MEMBRANE*

1. Prepare an amount of transfer buffer appropriate to the electrotransfer apparatus.
2. Cut the membrane/blotting pads/filter paper/foam pads to the correct size.
3. If using polyvinylidene fluoride (PVDF) membrane, activate by immersion in 100% methanol for ~ 5 minutes. Thereafter, rinse quickly in $dH_2O$ and soak in transfer buffer. Handle using tweezers avoiding as much contact as possible.
4. Submerge blotting pads/filter paper/foam pads briefly in transfer buffer.
5. Remove the polyacrylamide gel with fractionated protein pattern from the U-shaped cassette and equilibrate in transfer buffer with gentle agitation for ~10-15 minutes.
6. Construct the horizontal *semi-dry transfer* sandwich orientation: from the bottom electrode (anode), (1) a blotting pad, (2) the activated PVDF membrane, (3) the polyacrylamide gel, and another (4) blotting pad on top. Air bubbles must be removed using a test-tube as a roller otherwise they will reduce the efficiency of the transfer. Close the system and perform the semi-dry electrotransfer at 500 mA (constant) and 15 V for 1 hour.
7. Alternatively, the vertical *wet transfer* sandwich is constructed in the following orientation: open the holder cassette and lay flat. Then, from the cathode side (black electrode), place (1) a foam pad, (2) 2x filter papers, (3) the polyacrylamide gel, (4) the activated PVDF membrane, (5) 2x filter papers, and another (6) foam pad in contact with red surface. Air bubbles must be removed using a test-tube as a roller otherwise they will reduce the efficiency of the transfer. Close the latches of the cassette and place in the electrotransfer apparatus. A cooling brick unit is incorporated to minimize excessive heating. The wet transfer is performed at 200 mA (constant) and 200 V for 1 hour.
8. Upon completion of transfer, the membrane is washed three times in rinse buffer (1x TBS; 0.1% Tween-20) for 5 minutes each.
9. Transfer efficiency may be verified by the reversible Ponceau stain.

*IMMUNODETECTION*

1. Prevent non-specific binding to unoccupied sites on the membrane by incubation in 5% (w/v) non-fat dry milk blocking solution for 1 hour at room temperature. If the protein of interest is phosphorylated, a 3% (w/v) BSA blocking solution is used as milk contains the phosphorylated protein casein which will bind the antibody.
2. Wash the membrane three times in rinse buffer (1x TBS; 0.1% Tween-20) for 5 minutes each.
3. The blots are then incubated overnight at 4°C in primary antibody with gentle agitation using the recommended dilutions, typically 5 µL antibody in 5 mL rinse buffer (1x TBS; 0.1% Tween-20). Equal protein loading is confirmed using a primary antibody directed against beta-actin.
4. Wash the membrane three times in rinse buffer (1x TBS; 0.1% Tween-20) for 5 minutes each.

5. Incubate the blots for 1 hour at room temperature in HRP-linked secondary antibody with gentle agitation using the recommended dilutions, typically 1.25 µL antibody in 5 mL rinse buffer (1x TBS; 0.1% Tween-20).
6. Wash the membrane three times in rinse buffer (1x TBS; 0.1% Tween-20) for 5 minutes each.
7. Prepare a 1:1 ECL solution in a conical tube and protect from light by covering with foil.
8. For exposure, cover the section of the membrane containing the protein of interest with ~500 µL ECL and incubate for 1 minute.
9. The light produced is captured on photographic film in a dark room, or alternatively using the Chemidox MP Imager.

## LIVE CELL IMAGING

### PREPARATION & IMAGE ACQUISITION

1. Dilute the stock MitoTracker® Red CMXRos stock solution (1 mM) in serum-free growth medium.
2. Remove growth medium using an aspirator
3. Wash the cells 2X with PBS
4. Add prewarmed medium containing the selected MitoTracker® Red CMXRos probe at a final concentration of 100 nM, as well as the Hoechst 33342 (1:200). Staining is performed for at least 3 minutes prior to visualisation.
5. Ignite the Xenon burner ~10 minutes prior to visualisation.
6. Open Cell^R imaging software.
7. In *Illumination Control*, switch on main burner.
8. In the *Experiment Manager*, set up a new experimental plan using Image Acquisition icons and different command frames. Frames are drawn around the icons in the editor's display. The *Z-Stack Frame* enables multiple images at different focal planes to be recorded. The *Multi-Colour Frame* combines monochrome images each with different excitation wavelengths into a single multi-colour image.
9. Place a drop of oil on the 100x oil-immersion objective.
10. Select the eyepiece function in *Microscope Control*.
11. Select the specific excitation filter (*Illumination Control*). Begin by using DAPI to locate the focal plane.
12. Open the shutter to illuminate the specimen (*Illumination Control)*. Ensure to start with a low intensity setting so as to protect the eyes.
13. Focus on the specimen using the focus knobs of the microscope.
14. Once specimen is in focus, switch eyepiece to camera (*Microscope Control)* and select *live mode* to view image on screen.
15. For a *Z-Stack Frame*, the starting (lower) and ending (upper) limits of the focal plane, the number of layers and the desired step width between the images needs to be set.

16. Other parameters to be adjusted in the *Experiment Manager* include light intensity (*Illumination Control*) and exposure time (*Camera Control*). Optimise and save the settings in the *Experiment Manager*.
17. Close the shutter and turn off the *live mode.*
18. The feasibility, storage allocation and execution of the image acquisition is achieved by clicking on *verify, prepare, start* icons in the *Control Centre* toolbar, respectively.

### IMAGE PROCESSING

1. Open the cell^R imaging software and select the personal database under which the files were saved.
2. Select the *Navigate-Z* icon and overlay the different layers of the Z-stack by selecting *Maximum Intensity Projection.*
3. To remove stray light during Z-stack acquisition, go to the menu bar and select *Process*, *3-D Images*, and *3-D Deconvolution* from the list. Choose the *Nearest Neighbour* option under *Filter Selection* and 80% *Haze Removal Factor* under *Filter Parameters*. Click *Execute*.
4. To remove the background, select the *Define ROI* icon and choose the ellipse tool. Using the left mouse button, define the area to subtract and confirm selection by clicking with the right mouse button. Subsequently, the *Background Subtraction* icon is selected.
5. On the menu bar, select *Image*, *Image Display*, and *Adjust Display*. In the window that appears, each colour channel may be selected and the intensity and contract of the image adjusted with the aid of histograms.

## IN VIVO

### CANCER CELL INOCCULATION

1. Resuspend approximately 1250 cancer cells per µL of Hank's Buffered Salt Solution.
2. The mice that are to be inoculated are restrained by a firm grip of the animal's scruff.
3. Draw up the desired volume of the cancer cell suspension (200 µL/25 g mouse) using a syringe.
4. Inject the 200 µL of the cancer cell suspension into the left fourth mammary pad.

## TUMOUR PROCESSING/PREPARATION OF LYSATES

1. Retrieve the harvested tumour samples from the -80°C freezer.
2. Using a scalpel, slice the tumour into 1 $mm^2$ pieces
3. In a glass test tube, immerse one piece of tumour in 1 mL of RIPA buffer (freshly supplemented with 1 µg/1 mL PMSF).
4. Using a tissue homogeniser, disrupt the tumour until foam develops (~5 seconds).
5. Place the test-tube on ice for approximately 1 hour so as to allow the foam to settle
6. Transfer the contents to a micro centrifuge tube and pellet the insoluble debris by centrifugation at 8000 rpm for 10 minutes.
7. Transfer the supernatant to a fresh micro-centrifuge tube.
8. Store the lysate at -80°C.

# APPENDIX B: REAGENTS & SOLUTIONS

## *IN VITRO*

### CELL CULTURE

**GROWTH MEDIUM** - Tumorigenic MCF-7/E0771 breast epithelial cell line

| CONSTITUENT | FINAL VOLUME (%) | FINAL VOLUME (mL) |
|---|---|---|
| DMEM, High Glucose, GlutaMAX™, HEPES [Gibco®] | | 500 |
| Fetal Bovine Serum (FBS), Heat inactivated [Gibco®] | 10 | 50 |
| Penicillin-Streptomycin, liquid [Gibco®] | 1 | 5.5 |

Equilibrate the growth medium constituents to 37°C in a waterbath. Remove flocculence from FBS by centrifugation at 400 g, followed by filtration through 0.2 µm filters. Combine constituents as specified above while working in a microbiological safety cabinet under sterile conditions. Reconstituted growth medium is stored between 2-8°C. Protect from light.

**PHOSPHATE BUFFERED SALINE [PBS; 1L]**

**Materials:**

- Sodium Chloride [NaCl; Mr = 58.44 g/1 mol]| Merck Millipore 567440
- Potassium Chloride [KCl; Mr = 74.55 g/1 mol]| Merck Millipore 104936
- di-Sodium Hydrogen Phosphate di-Hydrate [$Na_2HPO_4$; Mr = 177.99 g/1 mol]| Merck Millipore 106580
- Potassium Dihydrogen Phosphate [$KH_2PO_4$; Mr = 136.08 g/1 mol]| Merck Millipore 104873
- $dH_2O$

**Methods:**

Dissolve the following in 500 mL of the following in 500 mL of $dH_2O$: 8 g NaCL, 0.2 g KCl, 1.44 g $Na_2HPO_4$, and 0.24 g $KH_2PO_4$. Mix thoroughly with the aid of a magnetic stirrer. Adjust the pH of the solution to 7.4. Fill up to 1 L with $dH_2O$. Sterilize by autoclaving. Store at room temperature.

## TREATMENT

### DOXORUBICIN STOCK SOLUTION [3.4 mM] – CHEMOTHERAPEUTIC AGENT

**Materials:**

- Doxorubicin Hydrochloride [Mr = 579.98 g/1 mol]| Sigma D1515| St Louis, USA
- Sterile reconstituted growth medium

**Method:**

Under sterile conditions, dissolve 10 mg Doxorubicin Hydrochloride in exactly 5071 µL reconstituted growth medium. Vortex the solution, filter-sterilize and store in aliquots at -20°C. Avoid freeze-thaw cycles. Protect from light by covering with foil.

### 2-METHOXESTRADIOL STOCK SOLUTION [33 mM] - HIF-1α INHIBITOR

**Materials:**

- 2-Methoxyestradiol [Mr = 302.4 g/1 mol]| Cayman Chemical 13021| Michigan, USA
- Sterile-filtered Dimethyl Sulfoxide Hybri-Max™ [DMSO]|Sigma D2650

**Methods:**

Under sterile conditions, dissolve 50mg 2-Methoxyestradiol in approximately 5010µL DMSO. Vortex the solution, filter-sterilize and store in aliquots at -20°C. Avoid freeze-thaw cycles.

### COBALT CHLORIDE STOCK SOLUTION [25 mM] – HIF-1α STABILIZER

**Materials:**

- Cobalt (II) Chloride Hexahydrate [Mr = 237.90 g/1 mol]| Merck 102539| Darmstadt, Germany
- Sterilized $dH_2O$

**Methods:**

Under sterile conditions, dissolve approximately 297.375 mg Cobalt (II) Chloride Hexahydrate in approximately 50 mL $dH_2O$ and mix thoroughly. Autoclave to sterilize and aliquot in practical amounts. Storage between 2-8°C.

**HIF-1α SILENCING STOCK SOLUTION [10 µM] – HIF-1α INHIBITOR**

**Materials:**

- Lyophilized siRNA duplex | Santa Cruz Biotechnology 35561| California, USA
- RNAse-free $H_2O$

**Methods:**

Under sterile conditions, dilute the 3.3 nmol of lyophilized siRNA duplex in 330 µL RNAse-free water. Store at -20°C. Avoid freeze-thaw cycles.

## BIOREDUCTIVE CAPACITY

**MTT WORKING SOLUTION [1%]**

**Materials:**

- MTT tetrazolium dye reagent [Mr = 414.32 g/1 mol]| Sigma M2128| St Louis, USA
- Sterile PBS

**Methods:**

Shortly prior to use, add 0.01 g MTT tetrazolium dye reagent for every 1 mL PBS and dissolve with vigorous vortexing. Pass through single filter. Protect from light.

**ACIDIFIED ISOPROPANOL [1% (w/v)]**

**Materials:**

- 2-Propanol [Mr = 60.1 g/1 mol]| Merck Millipore 109634| Darmstadt, Germany
- Hydrochloric Acid

**Methods:**

For every 1 mL of isopropanol, add 10 µL of hydrochloric acid. Mix thoroughly with aid of a vortex.

**TRITON-X [0.1%; 100 mL]**

**Materials:**

- Triton-X-100| BHD Laboratory Supplies| Midrand, South Africa
- $dH_2O$

- **Methods:**

Triton-X-100 is a viscous liquid so pipette at a slow pace. Dissolve 100 µL Triton-X-100 in $dH_2O$ and make up to 100 mL. Mix thoroughly and store at 2-8°C.

## CASPASE-GLO® 3/7 ASSAY

### CASPASE-GLO® REAGENT

**Materials:**

- Caspase-Glo® 3/7 Buffer| Promega G8091| Madison, USA
- Lyophilized Caspase-Glo® 3/7 Substrate| Promega G8091| Madison, USA

**Methods:**

Thaw assay constituents to room temperature. The buffer reagent is added to the lyophilized substrate and mixed vigorously by vortexing.

## PROTEIN EXTRACTION

### SODIUM DEOXYCHOLATE SOLUTION [10%; 100 mL]

**Materials:**

- Sodium Deoxycholate [$C_{24}H_{39}O_4$; Mr = 414.55 g/1 mol]| BDH Laboratories 430353D| Poole, England

**Methods:**

Dissolve 10 g of Sodium Deoxycholate in 80 mL of $dH_2O$. Adjust the pH to 9.0 using HCl. The solution is subsequently boiled and cooled and the pH adjusted to 9.0. This step is repeated until there is the solution becomes colourless. Fill up to 100 mL with $dH_2O$. Aliquot into practical amounts so as to avoid freeze-thaw cycles and store at -20°C. Protect from light.

### SODIUM FLUORIDE SOLUTION [200 mM; 500 mL]

**Materials:**

- Sodium Fluoride [NaF; Mr = 41.99]| Hopkins & Williams 7859| Essex, England
- Sterile $dH_2O$

**Methods:**

Weigh out 4.199 g of Sodium Fluoride and dissolve in 500 mL of $dH_2O$. Mix thoroughly with a magnetic stirrer. Store at -20°C. Inhibitor of serine and threonine phosphatases.

**SODIUM ORTHOVANADATE SOLUTION [200 mM; pH 9; 100 mL]**

**Materials:**

- Sodium Orthovanadate [$Na_3VO_4$; Mr = 183.91 g/1 mol]| Sigma S6508| St Louis, USA
- Sterile $dH_2O$

**Methods:**

Weigh out 3.678g of Sodium Orthovanadate and dissolve in 80 mL $dH_2O$. Boil until the solution is colourless. Set the pH to 9 using HCl. Fill up to 1 L with $dH_2O$. Aliquot the solution into practical amounts to avoid freeze-thaw cycles. Store at -20°C. Inhibitor of tyrosine phosphatases.

**ETHYLENE-DIAMINE-TETRAACETIC-ACID SOLUTION [EDTA; 100 mM; 100 mL]**

**Materials:**

- EDTA Salt Dihydrate [Mr = 372.24 g/1 mol]| Analar 10093| Lutterworth, UK
- Sterile $dH_2O$

**Methods:**

Weigh out 3.722 g EDTA Salt Dihydrate and dissolve in 80 mL $dH_2O$. Adjust the pH to 8.0. Fill up to 100 mL with dH2O. Mix thoroughly with magnetic stirrer. Store at room temperature. Inhibitor of metalloproteases.

**PHENYLMETHYLSULFONYL FLUORIDE [PMSF; 0.2 M; 50 mL]**

**Materials:**

- Phenylmethylsulfonyl fluoride [$C_7H_7O_2SF$; Mr = 174.2 g/1mol]| Roche| Mannheim, Germany
- 100% ethanol

**Methods:**

Weigh out 1.742 g PMSF and dissolve in 50 mL of 100% ethanol. Store at room temperature – stable for ~9 months. Inhibitor of serine and cysteine proteases.

**MODIFIED RADIO-IMMUNO-PRECIPITATION-ASSAY BUFFER [RIPA; 100 mL]**

**Materials:**

- 50 mM Tris-HCl [pH 7.4]
- Sterile $dH_2O$
- NaCl
- 10% NP-40
- 10% Sodium Deoxycholate
- 0.2 M PMSF
- 1M Benzamidine Hydrochloride Hydrate
- 100 mM EDTA [pH 7.4]
- 1 mg/1 mL Leupeptin
- 10 mg/1 mL Aprotonin
- 1 mg/1 mL Pepstatin
- 5 mg/1 mL Soy Bean Trypsin Inhibitor-1 (SBTI-1)
- 200 mM $Na_3VO_4$
- 200 mM NaF

**Methods:**

The following procedure should be carried out on ice. Working in a 100 mL beaker, prepare a 50 mM Tris solution by dissolving 790 mg Tris 75ml of $dH_2O$. Correct the pH to 7.4 using HCl and add the following constituents in the following order:

| **CONSTITUENTS** | **FINAL CONCENTRATION** | **VOLUME/WEIGHT OF STOCK** |
|---|---|---|
| NaCl | 150 mM | 876 mg |
| NP-40 | 1% | 10 mL |
| Sodium Deoxycholate | 0.25% | 2.5 mL |
| **Protease Inhibitors** | | |
| PMSF | 1 mM | 500 µL |
| Benzamidine | 1 mM | 100 µL |
| EDTA | 1 mM | 1 mL |
| Leupeptin | 1 µg/1 mL | 100 µL |
| Aprotonin | 2 µg/1 mL | 20 µL |
| Pepstatin | 1 µg/1 mL | 100 µL |
| SBTI-1 | 4 µg/1 mL | 80 µL |
| **Phosphatase Inhibitors** | | |
| $Na_3VO_4$ | 1 mM | 500 µL |
| NaF | 1 mM | 500 µL |

Make solution up to 100 mL with $dH_2O$ and mix thoroughly with a magnetic stirrer. Unwanted proteolysis and de-phosphorylation are slowed down by the addition of protease and phosphatase inhibitors. Aliquot the solution into practical amounts so as to avoid freeze-thaw cycles and store at -20°C. PMSF is unstable in aqueous solutions with a short half-life and thus should be added to RIPA buffer just prior to lysate preparation.

## PROTEIN CONCENTRATION DETERMINATION

### BRADFORD STOCK REAGENT [5X; 1 L]

**Materials:**

- Coomassie Brilliant Blue G [Mr = 854.02 g/1 mol]| Fluka 27815| Switzerland
- 95% ethanol
- Phosphoric acid
- Sterile $dH_2O$

**Method:**

Weigh out 500 mg of Coomassie Brilliant Blue G and dissolve in 95% ethanol (250 mL) and phosphoric acid (500 mL). Once the dye has dissolved, make the solution up to one litre with distilled water and pass through a single filter. Storage in amber bottle at 4°C. Protect from light.

### BRADFORD WORKING SOLUTION

**Materials:**

- 5X Bradford Stock Reagent
- Sterile $dH_2O$

**Method:**

Shortly prior to use, prepare a 1:4 Bradford working reagent by diluting the 5x stock in a 1:4 ratio with $dH_2O$ used as the solvent. Pass the solution through 2 filters simultaneously. Storage in amber bottle at 4°C. Protect from light.

### BOVINE SERUM ALBUMIN (BSA) STOCK SOLUTION [1mg/ml]

**Materials:**

- Bovine Serum Albumin Fraction V [Mr = 68 kDa]| Roche 10735
- Sterile $dH_2O$

**Method:**

Dissolve 10 mg of Bovine Serum Albumin Fraction V in 10 mL of $dH_2O$. Aliquot into practical amounts and store at -20°C.

## WESTERN BLOTTING

### LAEMELLI SAMPLE BUFFER [2X; 10 mL]

**Materials:**

- 0.5M Tris-HCl [pH 6.8]
- $dH_2O$
- Glycerol |Saarchem Analytics| Krugersdorp, South Africa
- 10% SDS
- 2-Mercaptoethanol [Mr = 78.13 g/1 mol]| Sigma M7154| St Louis, USA
- Bromophenol Blue [Mr = 669.99 g/1 mol]| Saarchem Analytics | Krugersdorp, South Africa

**Methods:**

Prepare a 125mM Tris solution by dissolving 1.514g Tris in 10mL $dH_2O$.

| CONSTITUENTS | FINAL CONCENTRATION (%) | AMOUNT OF STOCK |
|---|---|---|
| Glycerol | 20% | 2 mL |
| SDS | 4% | 4 mL |
| Bromophenol blue | 0.004% | 0.4 mg |
| 2-mercaptoethanol | 10% | 1 mL |

Bring the volume up to 10 mL with $dH_2O$.

### 1.5 M TRIS-HCL BUFFER [pH 8.8; 1 L]

**Materials:**

- Tris Base, Molecular Biology Grade [Mr = 121.1 g/1 mol]| EMD Millipore 648310
- Sterile $dH_2O$

**Methods:**

Weigh out 181.65 g of Tris Base and dissolve in 800 mL $dH_2O$. Adjust pH to 8.8 using HCl. Fill up to 1 L with $dH_2O$.

**50 mM TRIS-HCL BUFFER [pH 7.4; 1 L]**

**Materials:**

- Tris Base, Molecular Biology Grade [Mr = 121.1 g/1 mol]| EMD Millipore 648310
- Sterile $dH_2O$

**Methods:**

Weigh out 6.055 g of Tris Base and dissolve in 800 mL $dH_2O$. Adjust pH to 7.4 using HCl. Fill up to 1 L with $dH_2O$.

**0.5 M TRIS-HCL BUFFER [pH 6.8; 1 L]**

**Materials:**

- Tris Base, Molecular Biology Grade [Mr = 121.1 g/1 mol]| EMD Millipore 648310
- Sterile $dH_2O$

**Methods:**

Weigh out 60.55 g of Tris Base and dissolve in 800 mL $dH_2O$. Adjust pH to 6.8 using HCl. Fill up to 1 L with $dH_2O$.

**SODIUM DODECYL SULPHATE (SDS) SOLUTION [10% (w/v); 1 L]**

**Materials:**

- Sodium n-Dodecyl Sulfate, Molecular Biology Grade [Mr = 288.4 g/1 mol]| Merck Millipore 428023| Darmstadt, Germany
- Sterile $dH_2O$

**Methods:**

Weigh out 28.84g of SDS and dissolve in 800mL $dH_2O$. Place in heated waterbath to speed up the dissolving process. Fill up to 1 L.

**AMMONIUM PERSULPHATE (APS) [10% (w/v)]**

**Materials:**

- Ammonium Persulfate [APS]| Saarchem Analytics| Wadeville, South Africa
- Sterile $dH_2O$

**Methods:**

For every mL of $dH_2O$, dissolve 1 mg of APS by vigorous vortexing. Prepare immediately before use. Unstable and storage at -20°C should not exceed 1 week.

**TRIS-GLYCINE SDS-POLYACRYLAMIDE GELS**

**6% Resolving Gel**

| CONSTITUENTS | FINAL VOLUME [10 mL/2 gels] |
|---|---|
| $dH_2O$ | 5.3 |
| 40% Acrylamide Bis (37.5 : 1) | 2.0 |
| 1.5 M Tris (pH8.8) | 2.5 |
| 10% SDS | 0.1 |
| 10% Ammonium Persulfate | 0.1 |
| TEMED | 0.008 |

**12% Resolving Gel**

| CONSTITUENTS | FINAL VOLUME [10 mL/2gels] |
|---|---|
| $dH_2O$ | 3.3 |
| 40% Acrylamide Bis (37.5 : 1) | 4.0 |
| 1.5 M Tris (pH8.8) | 2.5 |
| 10% SDS | 0.1 |
| 10% Ammonium Persulfate | 0.1 |
| TEMED | 0.004 |

**5% Stacking Gel**

| CONSTITUENTS | FINAL VOLUME [2mL] |
|---|---|
| $dH_2O$ | 1.4 |
| 40% Acrylamide Bis (37.5 : 1) | 0.33 |
| 1.5 M Tris (pH6.8) | 0.25 |
| 10% SDS | 0.02 |
| 10% Ammonium Persulfate | 0.02 |
| TEMED | 0.002 |

As APS acts as a catalyst for the polymerization reaction, it should be added as the last component.

**TRIS BUFFERED SALINE BUFFER [TBS; 10x; 5 L]**

**Materials:**

- Tris Base, Molecular Biology Grade [Mr = 121.1 g/1 mol]| EMD Millipore 648310
- Sodium Chloride [NaCl; Mr = 58.44 g/1 mol]| Merck| Wadeville, South Africa
- $dH_2O$

**Methods:**

Weigh out 302.5 g Tris Base and 438.0 g Sodium Chloride, and dissolve in 5 L of $dH_2O$.

**MIGRATION BUFFER [25 mM TRIS, 192 mM GLYCINE, 0.1% (w/v) SDS, pH 8.3; 1 L]**

**Materials:**

- 10x premixed Tris/Glycine/SDS buffer| Bio-Rad 161-0772| Bio-rad, Johannesburg, South Africa
- Sterile $dH_2O$

**Methods:**

Dispense 100 mL of 10x premixed Tris/Glycine/SDS buffer into a 1 L measuring cylinder and make up to 1 L with $dH_2O$. Prepare just before electrophoresis.

**TRANSFER (TOWBIN'S) BUFFER [25 mM TRIS, 192 mM GLYCINE, pH 8.3]**

**Materials:**

- 10x premixed Tris/Glycine buffer | Bio-Rad 161-0771| Bio-rad, Johannesburg, South Africa

- Methanol| Merck| Darmstadt, Germany
- Sterile $dH_2O$

**Methods:**

Dispense 100 mL of 10x premixed Tris/Glycine buffer into a 1 L measuring cylinder. Add 200 mL methanol and make up to 1 L with $dH_2O$. Store at room temperature.

**RINSE BUFFER [1x TBS; 0.1% TWEEN-20; 1 L]**

**Materials:**

- 10x TBS
- Tween®20|Sigma P9416|St Louis, USA
- Sterile $dH_2O$

**Methods:**

Dispense 100 mL of 10x TBS stock solution into a 1 L measuring cylinder and make up to 1 L with $dH_2O$. Add 1 mL of Tween®20 and mix thoroughly. Store at room temperature.

**SODIUM HYDROXIDE [0.2 M; 1 L] - STRIPPING BUFFER**

**Materials:**

- Sodium Hydroxide pellets [NaOH; Mr = 40 g/1 mol]| Merck Millipore 106482| Midrand, South Africa
- Sterile $dH_2O$

**Method:**

Weigh out 8 g of NaOH pellets and dissolve in 1 L of $dH_2O$. Mix thoroughly with a magnetic stirrer. Store at room temperature.

**5% (w/v) NON-FAT DRY MILK BLOCKING SOLUTION**

**Materials:**

- Fat free instant milk powder
- Rinse Buffer [1x TBS; 0.1% Tween-20]

**Methods:**

Weigh out 5 g of fat-free instant milk powder and dissolve in 100 mL rinse buffer (1x TBS; 0.1% Tween®20). Make up fresh just prior to blocking of membranes.

**3% (w/v) BSA BLOCKING SOLUTION**

**Materials:**

- Bovine Serum Albumin Fraction V [Mr = 68 kDa]| Roche 10735
- Rinse Buffer [1x TBS; 0.1% Tween-20]

**Methods:**

Weigh out 3 g of Bovine Serum Albumin Fraction V and dissolve in 100 mL rinse buffer (1x TBS; 0.1% Tween®20). Make up fresh just prior to blocking of membranes.

## LIVE CELL IMAGING/FLUORESCENT MICROSCOPY

**HOECHST 33342 STOCK SOLUTION [1 mg/1 mL]**

**Materials:**

- bisBenzimide H 33342 trihydrochloride [Mr = 561.93 g/1 mol]| Sigma B2261| St Louis, USA
- Sterile-filtered Dimethyl Sulfoxide Hybri-Max™ [DMSO]|Sigma D2650

**Methods:**

For every mL of $dH_2O$, dissolve 1 mg of the yellow solid powder by vigorous vortexing. Protect from light by storage in an amber eppendorf tube. Storage at 2-8°C.

**MITOTRACKER RED® CMXROS [1 mM]**

**Materials:**

- Lyophilized MitoTracker Red® CMXRos [50 µg; Mr = 531.5236 g/1 mol]| Invitrogen M7512|
- Sterile-filtered Dimethyl Sulfoxide Hybri-Max™ [DMSO]|Sigma D2650

**Methods:**

Dissolve the 50 µg lyophilized solid in 100 µL DMSO. Protect from light. Storage at -20°C.

***IN VIVO***

**DOXORUBICIN STOCK SOLUTION [3.33 mg/1 mL]**

**Materials:**

- Doxorubicin Hydrochloride [Mr = 579.98 g/1 mol]| Sigma D1515| St Louis, USA
- Sterile reconstituted growth medium

**Methods:**

Dissolve 10 mg of the powder in 3 mL of reconstituted growth medium. Thorough solubilisation is achieved by vigorous vortexing. Store at 4°C. Protect from light.

**CARBOXYMETHYLCELLULOSE [0.5%]**

**Materials:**

- Carboxymethylcellulose sodium salt [CMC; Mr = 90kDa]| Sigma C5678| St Louis, USA
- Sterile $dH_2O$

**Methods:**

Weight out 4 g of carboxymethylcellulose sodium salt and add in portions to 100 mL $dH_2O$. Thorough solubilisation is achieved by gently mixing with a magnetic stirrer. Sterilize by autoclaving. Storage at room temperature.

**2-METHOXESTRADIOL [10 mg/1 mL]**

**Materials:**

- 2-Methoxyestradiol [2-ME; Mr = 302.4 g/1 mol]| Cayman Chemical 13021| Michigan, USA
- 0.5% Carboxymethylcellulose

**Methods:**

Dissolve 10 mg of 2-ME crystalline solid in 1 mL of 0.5% carboxymethylcellulose. Thorough solubilisation is achieved by vigorous vortexing. Store at 4°C.